Intense few-cycle laser fields: Frontiers of nonlinear optics

Thomas Brabec and Ferenc Krausz*

Institut für Photonik, Technische Universität Wien, Gusshausstrasse 27/387, A-1040 Wien, Austria

The rise time of intense radiation determines the maximum field strength atoms can be exposed to before their polarizability dramatically drops due to the detachment of an outer electron. Recent progress in ultrafast optics has allowed the generation of ultraintense light pulses comprising merely a few field oscillation cycles. The arising intensity gradient allows electrons to survive in their bound atomic state up to external field strengths many times higher than the binding Coulomb field and gives rise to ionization rates comparable to the light frequency, resulting in a significant extension of the frontiers of nonlinear optics and (nonrelativistic) high-field physics. Implications include the generation of coherent harmonic radiation up to kiloelectronvolt photon energies and control of the atomic dipole moment on a subfemtosecond ($1\ \mathrm{fs}=10^{-15}\ \mathrm{s}$) time scale. This review presents the landmarks of the 30-odd-year evolution of ultrashort-pulse laser physics and technology culminating in the generation of intense few-cycle light pulses and discusses the impact of these pulses on high-field physics. Particular emphasis is placed on high-order harmonic emission and single subfemtosecond extreme ultraviolet/x-ray pulse generation. These as well as other strong-field processes are governed directly by the electric-field evolution, and hence their full control requires access to the (absolute) phase of the light carrier. We shall discuss routes to its determination and control, which will, for the first time, allow access to the electromagnetic fields in light waves and control of high-field interactions with never-before-achieved precision.

CONTENTS

*Electronic addresses: brabec@tuwien.ac.at ferenc.krausz@tuwien.ac.at

I. INTRODUCTION

Lasers generating ultrashort light pulses have come of age. Their applications range from testing ultrahigh-speed semiconductor devices to precision processing of materials, from triggering and tracing chemical reactions to sophisticated surgical applications in opthalmology and neurosurgery. In the physical sciences, ultrashort light pulses enable researchers to follow ultrafast relaxation processes in the microcosm on never-before-accessed time scales and study light-matter interactions at unprecedented intensity levels.

Recent technological advances in ultrafast optics have permitted the generation of light wave packets comprising only a few oscillation cycles of the electric and magnetic fields. The spatial extension of these wave packets along the direction of their propagation is limited to a few times the wavelength of the radiation (≈ 0.5–$1\ \mu\mathrm{m}$ in the visible and near-infrared spectral range). The pulses are delivered in a diffraction-limited beam and hence focusable to a spot size comparable to the wavelength. As a consequence, radiation can be temporarily

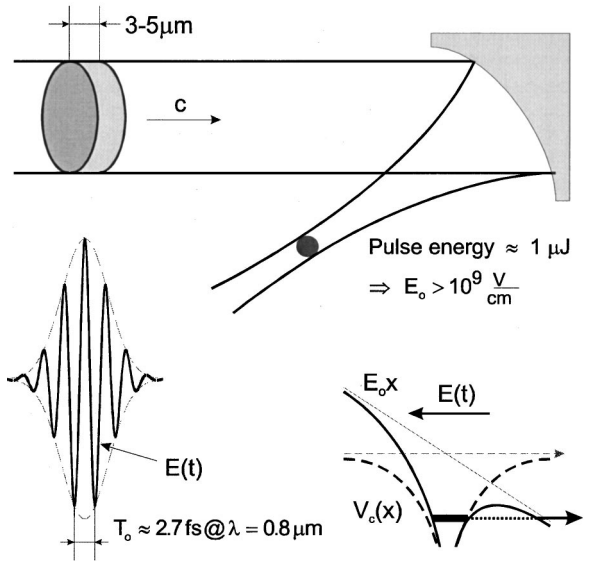

FIG. 1. Focusing of few-cycle ultrashort light pulses delivered in a collimated laser beam by a parabolic mirror, producing a "light bullet" with transverse and longitudinal dimensions of the order of a few microns. This extreme spatial and temporal confinement of light creates optical-field strengths sufficient to lower the Coulomb barrier of atoms and to tunnel-ionize an outer electron at moderate pulse energy levels.

confined to a few cubic micrometers at the focus of a parabolic mirror, forming a "light bullet," as shown in Fig. 1. Due to this extreme temporal and spatial confinement, moderate pulse energies of the order of one microjoule can result in peak intensities higher than 10^{15} W/cm^2. The amplitude of the electric field at these intensity levels approaches 10^9 V/cm. These field strengths exceed that of the static Coulomb field experienced by outer-shell electrons in atoms. As a consequence, the laser field is strong enough to suppress the binding Coulomb potential in atoms and triggers optical-field ionization (Keldysh, 1965).

This process temporarily enhances the nonlinear atomic polarization because the electron is far removed from the nucleus. Once the electron is set free, its response to the field becomes linear, terminating the nonlinear light-matter interaction (aside from a small residual nonlinearity originating from the ion polarizability). Significant new nonlinearities emerge only at substantially higher intensity levels by further ionization and/or when the free electrons become relativistic, both of which are beyond the scope of the present work. The nonlinear atomic polarization response culminates as the optical-field ionization rate peaks, shortly before the first weakly bound electron is detached. The intensity level at which this occurs strongly depends on the temporal evolution of the incident radiation.

Long laser pulses comprising many field oscillation cycles deplete the atomic ground state, i.e., detach an outer atomic electron with a probability approaching 100% at moderate intensity levels. In few-cycle laser fields high intensities can be "switched on" within a few optical periods lasting merely a few femtoseconds ($1\ \text{fs}=10^{-15}$ s). Hence detachment of the first electron is completed at substantially higher field strengths and the optical-field ionization rate becomes comparable to the laser field oscillation frequency. As a result, the electrons gain unprecedented kinetic energies (up to and beyond the keV level) during the first field oscillation cycle following their detachment, and a substantial fraction of the atoms is ionized during one laser oscillation period T_o. The implications are numerous and far reaching. Generally speaking, the nonlinear response of the ionizing atomic medium is extended to unprecedented irradiation intensity levels and the induced instantaneous nonlinear current densities reach unprecedented values. Previously inaccessible regimes of nonlinear optics and high-field physics are being entered.

Somewhat more specifically, circularly polarized intense few-cycle fields can inject an ultraintense jet of high-energy electrons with a rise time comparable to T_o into a plasma. This may open the way to the development of electron-pumped inner-shell x-ray lasers in the keV range (Kim *et al.*, 1999). The high temporal gradient of the pulse front allows neutral atoms to survive to intensities of the order of 10^{16} W/cm^2. The oscillation spectrum of the dipole moment of these atoms may extend to frequencies some thousand times higher than that of the linearly polarized few-cycle driving laser field, giving rise to the emission of (spatially) coherent harmonic radiation up to photon energies of 0.5 keV (Schnürer *et al.*, 1998). The extremely high optical-field ionization peaks impose appreciable modulation on the driving few-cycle pulse within T_o during propagation. The resulting nonadiabatic self-modulation is predicted to permit phase-matched high-harmonic emission at kiloelectronvolt photon energies (Tempea *et al.*, 1999b). Few-cycle-driven harmonic x-ray radiation may be temporally confined to a single burst of subfemtosecond duration, which may result in unprecedented peak intensities in the x-ray regime and a never-before-achieved time resolution in physics.

Temporal confinement of irradiation of atomic systems to a few cycles allows atom-field interactions induced by visible or near-infrared radiation to take place for the first time in the *strong-field regime* (characterized by the onset of optical-field ionization) without any notable preionization in the multiphoton regime. This implies that the nonlinear atomic polarization P_{nl} at instant t can be analytically expressed as a function of the driving electric field $E(t')$ with $t' \leqslant t$, which greatly facilitates theoretical analysis of the interaction of intense radiation with an extended atomic medium (propagation effects). Even more importantly, the explicit dependence of P_{nl} on E indicates that the evolution of the atomic dipole moment (or the electron wave function) is governed directly by the electric field, $E(t) = E_a(t)\cos(\omega t+\varphi_0)$; hence it depends not only on the intensity envelope $E_a^2(t)$, but also on the *carrier phase* φ of a few-cycle laser pulse. Strong-field processes driven by few-cycle wave packets hold promise for gaining ac-

cess to this parameter and thereby directly to the electric field in a light wave for the first time (Krausz *et al.*, 1998). Phase control will be one of the prerequisites for generating subfemtosecond extreme ultraviolet (xuv; 10–100 eV) /x-ray harmonic radiation in a reproducible manner. Generally, phase-controlled few-cycle light pulses will permit control of both the trajectories of freed electrons in strong-field interactions and bound-electron dynamics in atoms and molecules on a time scale of the light oscillation period.

This paper is devoted to the basic theoretical and experimental concepts underlying the generation of intense few-cycle laser pulses and high-field femtosecond light-atom interactions. Sections II and III review the underlying physics and evolution of ultrafast laser optics culminating in few-cycle pulse generation. Section IV addresses basic aspects of the nonlinear response of matter to intense radiation relevant to the generation of ultrashort light pulses (the perturbative regime) and their application to triggering optical-field ionization and concomitant phenomena (the strong-field regime). Section V introduces basic propagation equations for the above regimes. Section VI analyzes optical field ionization over a wide parameter range including the tunneling regime as well as the above-barrier regime. Section VII is devoted to few-cycle-driven high-order harmonic radiation, which can lead to the emission of single-attosecond xuv and x-ray pulses. Contrasting these phenomena with related processes driven by multicycle pulses beautifully shows the advantages of few-cycle drivers in the strong-field regime. In Sec. VIII it will be shown that the sensitivity of strong-field processes to the carrier phase of few-cycle light wave packets may open up access to the *absolute* phase of light for the first time. Finally, in Sec. IX we present some intriguing future prospects. In this paper we shall use units of the mksa system except for some cases, in which atomic units significantly simplify the treatment. Conversion between the two systems is given in Appendix A.

II. EVOLUTION OF ULTRASHORT-LIGHT-PULSE GENERATION

A. Basic concepts and early implementations

The development of ultrafast optics was triggered by the invention of *laser mode locking*, one of the most striking interference phenomena in nature (DiDomenico, 1964; Hargrove *et al.*, 1964; Yariv, 1965). Simultaneous oscillation of a vast number of highly coherent, phase-locked longitudinal modes in a laser yields a resultant field equal to zero most of the time except for very short intervals. The entire energy of the radiation field is concentrated within these short periods as a result of a short-lived constructive interference between the oscillating waves. Because the frequency spacing between adjacent phase-locked longitudinal modes is equal to $1/T_r$, where T_r is the resonator round-trip time, this temporary field enhancement is repeated periodically with a period T_r at a fixed position on the resonator axis. As a consequence, laser mode locking leads to the formation of a short light pulse circulating in the resonator. Each time the pulse hits a partially reflecting mirror, a small portion of its energy is coupled out of the oscillator, resulting in a train of ultrashort pulses at the output of the mode-locked laser, as illustrated in Fig. 2. Straightforward algebra relates the pulse duration and peak power to the number of phase-locked modes as summarized in Fig. 2.

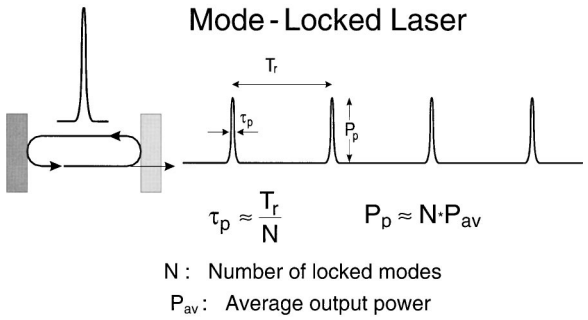

FIG. 2. Radiation power as a function of time at the output of a stationary mode-locked laser.

The large number of modes that can be locked using state-of-the-art mode-locking techniques give rise to light wave packets with unprecedented characteristics. In the rest of this section we shall survey the landmarks in the evolution of ultrashort-pulse laser physics and technology from the invention of laser mode locking up to the present day. When doing so we shall be able to cite only a tiny fraction of the relevant literature because of space limitations. Nevertheless, the referenced publications should provide a useful guide to the reader for finding further readings. Our apologies go to the numerous colleagues whose important contributions have not been credited. A comprehensive survey of the state of the art of primary (mode-locked laser) as well as secondary (frequency-converted) sources of ultrashort pulses is offered by conference proceedings, special issues of technical journals, and books.[1] The physics of the propagation, manipulation, and interaction of ultrashort laser pulses with matter (at low and moderate intensities) is thoroughly presented in two recent textbooks (Akhmanov *et al.*, 1992; Diels and Rudolph, 1996), whereas the physics and technology of the (most important) latest generation of ultrafast sources, namely, femtosecond solid-state lasers, have been reviewed by Krausz, Fermann *et al.* (1992), Keller (1994), Brabec *et al.* (1995), and French (1996).

The first generation of mode-locked lasers producing pulses of durations less than 100 ps used solid-state laser materials such as ruby, Nd:glass, or Nd:YAG as gain media. Mode locking was implemented either by active loss or frequency modulation driven by an external elec-

[1]These include Heritage and Nuss, 1992; Martin *et al.*, 1993; Barbara *et al.*, 1994; Krausz and Wintner, 1994; Barbara *et al.*, 1996; Zhang *et al.*, 1996; Keller 1997; Barty, White *et al.*, 1998; Elsässer *et al.*, 1998.

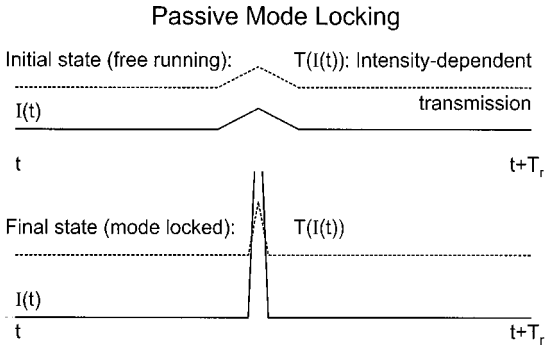

FIG. 3. Reliance of passive mode locking on a nonlinear element that exhibits an increased transmittivity for increased laser intensity. With such an element introduced in the oscillator, an initial amplitude fluctuation arising in the free-running laser (due to some mode beating, for instance) can grow upon repeated round trips in the cavity at the expense of the lower-intensity background. The resulting energy transfer continues until all the intracavity radiation energy is confined within a single pulse originating from the initial fluctuation. The steady-state pulse parameters are dictated by a balance between pulse-shortening and pulse-broadening effects. Saturable absorbers were the first (and for a long time the only) nonlinear optical elements employed for passive mode locking.

tronic oscillator (Deutsch, 1965; DiDomenico *et al.* 1966; Osterink and Foster, 1968; Kuizenga and Siegman, 1970a, 1970b), or by passive loss modulation with a fast-response saturable absorber (Mocker and Collins, 1965; DeMaria *et al.*, 1966). These techniques were termed active and passive mode locking, respectively. The principle of operation of the latter, which provides much more efficient pulse shaping and hence shorter pulses, is illustrated in Fig. 3. Nonlinear autocorrelation techniques needed to be developed for the temporal characterization of these pulses (Maier *et al.*, 1966; Armstrong, 1967; Weber, 1967). The passively mode-locked, flashlamp-pumped Nd:glass laser became the major ''workhorse'' for investigations in the field of nonlinear optics and opened up the entirely new field of time-resolved spectroscopy. The interested reader is referred to several excellent reviews devoted to these first-generation ultrafast sources and their characterization (DeMaria *et al.*, 1969; Bradley and New, 1974; Greenhow and Schmidt, 1974; Smith *et al.*, 1974).

The picosecond response time of organic saturable absorbers employed for passive mode locking has set a limit to the pulse duration. Continuous-wave operation (Peterson *et al.*, 1970) of an organic dye laser (Schäfer *et al.*, 1966; Sorokin and Lankard, 1966) and its mode locking by a saturable absorber (Ippen *et al.*, 1972) in a specifically designed cavity (Kogelnik *et al.*, 1972) triggered the development of the second generation of mode-locked lasers. In contrast with solid-state lasers, the response time of the absorber no longer constituted a limitation to the achievable pulse duration, owing to the active role of gain saturation in pulse formation (New, 1972, 1974; Haus, 1975a). As a result, optical pulses shorter than 1 ps could be produced for the first time (Ruddock and Bradley, 1976) and subsequent improvements in the cavity design allowed the breaking of the 100-fs barrier by utilizing a new concept, colliding-pulse mode locking (Fork *et al.*, 1981, 1983). Intracavity dispersion control by means of low-loss Brewster-angled prism pairs (Fork *et al.*, 1984; Martinez *et al.*, 1984) was the next major breakthrough, which together with improved insight into the relevant physical processes and limitations (Kühlke *et al.*, 1983; Stix and Ippen, 1983; De Silvestri *et al.*, 1984; Martinez, Fork, and Gordon, 1984; Diels *et al.*, 1985; Martinez *et al.*, 1985) allowed reproducible generation of sub-100-fs pulses and the demonstration of pulses as short as 27 fs directly from a laser oscillator (Valdmanis *et al.*, 1985; Valdmanis and Fork, 1986). This progress was achieved by using the organic dye Rhodamine 6G (Rh6G) as a gain medium emitting at around 620 nm. The dispersion-controlled colliding-pulse mode-locked Rh6G laser was the major workhorse for femtosecond spectroscopy until the late 1980s. Nevertheless, a number of other cw dye lasers have also been successfully mode locked to produce femtosecond pulses in the visible and near-infrared spectral range (French *et al.*, 1987, 1989; French and Taylor, 1988). For comprehensive reviews of ultrafast dye lasers see French (1985) and Shank (1988).

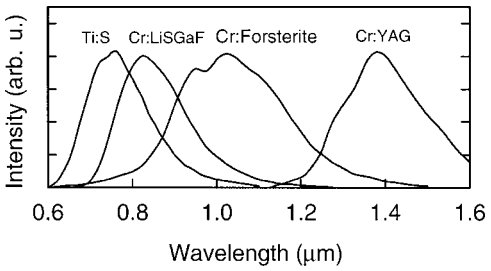

FIG. 4. Fluorescence emission spectra of some transition-metal-doped broadband solid-state laser crystals.

B. Continuous-wave passively mode-locked solid-state lasers

In the 1980s, continued work on the development of solid-state laser materials gave rise to the emergence of a number of new laser media. Various host crystals (YAG, sapphire, forsterite, LiSAF, etc.) doped with transition-metal (titanium, chromium) ions now provide laser transitions with enormous bandwidths on the order of 100 THz in the near-infrared wavelength range, as shown in Fig. 4 (Moulton, 1982, 1986; Petricevic *et al.*, 1989; Borodin *et al.*, 1992; Smith *et al.*, 1992). The development of novel techniques and devices suitable for passive mode locking of lasers with long gain relaxation and their application in these broadband solid-state systems led to the emergence of the third generation of ultrafast laser sources. Continuous-wave passive mode locking of broadband solid-state laser oscillators was accomplished by exploiting resonant (Keller, Knox, and 't Hooft 1992) and nonresonant (Krausz, Fermann, *et al.*, 1992) optical nonlinearities. The most successful devices for implementing the former technique have been semiconductor

saturable absorber mirrors, referred to as SESAMs, and saturable Bragg reflectors (Keller *et al.*, 1990; Feldmann *et al.*, 1991; Keller, Miller, *et al.*, 1992; Rizvi *et al.*, 1993; Tsuda *et al.*, 1995; for reviews see Keller, Knox, and 't Hooft, 1992; Keller *et al.*, 1996; Tsuda *et al.*, 1996; Keller, 1999). The simultaneous exploitation of a solitonlike interplay between negative intracavity group delay dispersion (GDD) and self-phase modulation (SPM) induced by the nonresonant Kerr effect allowed the generation of optical pulses significantly shorter than the pico- or subpicosecond absorber recovery time (Kärtner and Keller, 1995; Kärtner *et al.*, 1996).

Because of the inability of long-relaxation-time solid-state gain media to participate in ultrashort pulse formation, fast-response "artificial" saturable absorbers based on nonresonant optical nonlinearities were devised by several researchers. The first attempt dates back to the early 1970s (Dahlström, 1972) and was followed by a number of proposals based on third-order $\chi^{(3)}$ type (Sala *et al.*, 1977; Ouellette and Piché, 1986) and second-order $\chi^{(2)}$ type (Stankov and Jethwa, 1988; Barr *et al.*, 1991) nonlinearities [for a definition of $\chi^{(2)}$ and $\chi^{(3)}$, see Eq. (19)]. The first breakthrough occurred when reseachers recognized that coupled cavities containing a Kerr nonlinearity [see Eq. (30)] introduced by a single-mode fused silica fiber that can be used for mode locking. This concept was first employed in the soliton laser (Mollenauer and Stolen, 1984; Mitschke and Mollenauer, 1986, 1987) and subsequently was shown to introduce a fast saturable-absorber effect over a wide wavelength range irrespective of fiber dispersion (Blow and Wood, 1988; Blow and Nelson, 1988; Kean *et al.*, 1989; Mark *et al.*, 1989). The technique was called coupled-cavity or additive-pulse mode locking (Ippen *et al.*, 1989; Morin and Piché, 1990; Haus *et al.*, 1991) because coherent superposition of the intracavity pulse with its self-phase-modulated replica introduced the saturable-absorber effect. Additive-pulse mode locking allowed cw self-starting passive mode locking (Ippen *et al.*, 1990; Krausz *et al.*, 1991) in a wide range of solid-state lasers. Implementing additive-pulse mode locking in all-fiber lasers (Duling 1991; Hofer *et al.*, 1991 1992; Richardson *et al.*, 1991; Tamura *et al.*, 1993; Fermann *et al.*, 1994) led to the development of compact turnkey femtosecond sources; for recent reviews see Duling and Dennis (1995) and Fermann (1995).

C. Kerr-lens and solitary mode locking: Routine generation of femtosecond pulses

The discovery of self-mode-locking (Spence *et al.*, 1991) in a titanium-doped sapphire (Ti:S) laser (Moulton, 1982, 1986) revolutionized ultrafast laser technology. Subsequent experimental (Keller *et al.*, 1991; Spinelli *et al.*, 1991) and theoretical (Piché, 1991; Salin *et al.*, 1991; Brabec, Spielmann, Curley *et al.*, 1992; Haus *et al.*, 1992) work revealed that an intracavity aperture translates self-focusing (Zakharov and Shabat, 1972; Marburger, 1975) introduced by the Kerr nonlinearity of the laser crystal into an ultrafast saturable-absorber-like

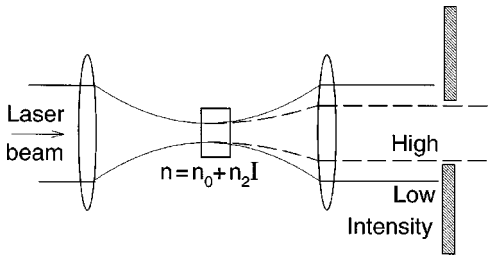

FIG. 5. Self-focusing-induced changes in the transmittivity of an aperture: the ultrafast-response saturable-absorber effect results in Kerr-lens mode locking.

self-amplitude-modulation (SAM), and the technique has been termed Kerr-lens mode locking (KLM). The operational principle of KLM is illustrated schematically in Fig. 5. The optical Kerr effect in the laser host crystal results in a fast-response intensity-induced change,

$$\Delta n(\mathbf{r},t)=n_2 I(\mathbf{r},t), \tag{1}$$

of the refractive index. Here n_2 [cm^2/W] is the nonlinear index of refraction and I [W/cm^2] is the cycle-averaged laser intensity. This effect transforms the radial intensity profile of a laser beam in a lensing effect, which tends to more strongly focus more intense temporal "slices" of the laser beam. An aperture of suitable size placed at a suitable position in the cavity can thus transmit a larger fraction of the laser beam at instants of higher intensity. The consequence is reduced loss for increased intensity, which constitutes a fast saturable-absorber effect (similar to additive-pulse mode locking). This ultrafast SAM effect can initiate and sustain the formation of an ultrashort pulse in Ti:S and other solid-state lasers. Simultaneously, $\Delta n(\mathbf{r},t)$ directly modulates the phase, which is termed self-phase-modulation (SPM).

The effect of SAM and SPM on the laser pulse circulating in the resonator can be simply described by the change they cause in the complex amplitude envelope $\tilde{E}_a(\tau)$, where the time τ is measured in a frame of reference retarded such that the pulse peaks at $\tau=0$ at any time [for definition see Eq. (14)] upon each round trip in the cavity:

$$\Delta\tilde{E}_a(\tau)=k_{SAM}p(\tau)\tilde{E}_a(\tau) \tag{2}$$

and

$$\Delta\tilde{E}_a(\tau)=ik_{SPM}p(\tau)\tilde{E}_a(\tau), \tag{3}$$

respectively. Here $p(\tau)\propto|\tilde{E}_a(\tau)|^2$ is the cycle-averaged time-dependent radiation power carried by the laser beam and k_{SAM}, k_{SPM} [W^{-1}] stand for the SAM and SPM coefficients, respectively. In KLM lasers, calculation of the intensity-dependent beam radius in the frame of the quadratic approximation[2] allows us to determine the coefficient k_{SAM} analytically. A more complete list of related literature is given in a recent paper of Kalosha

[2]See, for example, the calculations of (Piché, 1991; Salin *et al.*, 1991; Brabec, Spielmann, Curley *et al.*, 1992; Georgiev *et al.*, 1992; Haus *et al.*, 1992; Chilla and Martinez, 1993; Cerullo *et al.*, 1994; Herrmann, 1994; Agnesi, 1995; Lin *et al.*, 1995).

et al. (1998), which presents a comprehensive numerical analysis of Kerr-lens mode locking. For the SPM coefficient, straightforward algebra leads to

$$k_{SPM}=\gamma_{SPM}L, \quad \gamma_{SPM}=\frac{2n_2}{\lambda_0 w_0^2}. \tag{4}$$

Here λ_0 is the carrier wavelength of the laser pulse, L is the length of the Kerr medium, which is assumed to be shorter than the confocal parameter $2z_0=2\pi w_0^2/\lambda_0$, and w_0 is the $1/e^2$ beam radius.

In a typical KLM Ti:S laser, the SPM coefficient is on the order of $k_{SPM}\geqslant 10^{-6}\,\mathrm{W}^{-1}$, whereas SAM is weaker by more than an order of magnitude: $k_{SAM}\leqslant 10^{-7}\,\mathrm{W}^{-1}$ (Krausz, Fermann *et al.*, 1992). Typical intracavity pulse peak powers of the order of 10^5–10^6 W in the subpicosecond and femtosecond regimes hence introduce an amplitude modulation of merely a few percent by means of the KLM artificial saturable absorber. This comparatively weak modulation is incapable of overcoming the pulse broadening caused by dispersion of the laser medium in the femtosecond regime, which stops pulse shortening far from the limit set by the gain bandwidth in the Ti:S laser.

Accessing the regime well below 100 fs in the Ti:S laser becomes feasible when we introduce negative group delay dispersion (GDD) and exploit a highly efficient pulse-shortening mechanism resulting from an interplay between Kerr-induced SPM (e.g., in the laser crystal) and a net negative cavity GDD introduced, for example, by a pair of prisms (Fork *et al.*, 1984). This interplay is referred to as solitary mode locking (Brabec *et al.*, 1991) and will be discussed as the key technique for the generation of few-cycle light pulses in a broader context in the next section.

Because $k_{SPM}/k_{SAM}\gg 1$, solitary pulse shaping dominates pulse shortening in the presence of a net negative intracavity GDD and determines the steady-state pulse duration in the KLM Ti:S laser. In the frame of the weak pulse-shaping approximation, $|\Delta\tilde{E}_a(t)/\tilde{E}_a(t)|\ll 1$, which defines the range of validity of the powerful analytic master-equation approach of Haus *et al.* (1991, 1992), and in the limit $k_{SPM}/k_{SAM}\gg 1$, the master equation yields a steady-state pulse of the form $\tilde{E}_a(\tau)=E_0\mathrm{sech}(\tau/\tau_0)$ with

$$\tau_0=\frac{2|D|}{k_{SPM}W_p} \tag{5}$$

and a pulse duration of $\tau_p=1.76\tau_0$ [full width at half maximum of $p(\tau)\propto|\tilde{E}_a(\tau)|^2$]. Here W_p is the intracavity pulse energy and $D(<0)$ [fs^2] denotes the net intracavity GDD [for a definition, see Eq. (8)]. Further, Eq. (5) is valid under the assumption that D is independent of frequency, i.e., that high-order dispersion is negligible. This latter approximation tends to fail increasingly for decreasing pulse durations, which rely on smaller and smaller values of $|D|$ according to Eq. (5), and this eventually sets a limit to pulse shortening. The lowest-order perturbation to a constant GDD is a small linear dependence on frequency, $D(\omega)=D+D_3(\omega-\omega_0)$, where $D=D(\omega_0)$, ω_0 is the center frequency of the mode-locked laser, and D_3 [fs^3] is referred to as third-order dispersion, because it is equal to the third derivative of the phase with respect to frequency, as will be revealed by Eq. (8). Computer simulations yielded the explanation that mode locking becomes increasingly perturbed and eventually unstable as $\tau_p\to|D_3/D|$, setting a limit to the minimum pulse width achievable with solitary mode locking in the presence of third-order dispersion (Brabec, Spielmann, Curley, *et al.*, 1992). Overcoming this limitation would result in a mode-locked spectrum extending into a wavelength regime, where the cavity GDD $D(\omega)$ becomes positive, preventing stable solitary pulse formation (Spielmann *et al.*, 1994).

In the absence of high-order dispersion and limitations due to the finite high-reflectivity bandwidth of mirrors, the separate action of negative GDD and SPM is predicted to limit pulse shortening well before attainment of the gain-bandwidth limit of Ti:S, which would permit pulse durations approaching 1 fs at low cavity losses. Discrete solitary pulse shaping is a consequence of the Kerr-induced phase shift $k_{SPM}p(t)$ approaching (or even exceeding) unity at the pulse peak for decreasing $|D|$, leading to pulse shortening below 10 fs. As a result, the weak pulse-shaping approximation breaks down and a correction term proportional to $k_{SPM}W_p$, which is negligible for large values of $|D|$, appears on the right-hand side of Eq. (5) (Brabec *et al.*, 1991; Krausz *et al.*, 1992). This correction term is dependent on the position in the resonator, predicting a periodic pulse evolution in the (sub-)10-fs regime.

These findings resulted in a rapid evolution of prism-dispersion-controlled KLM Ti:S lasers, driven by the search for prism materials characterized by the smallest ratio of third-order dispersion to GDD. Fused silica was found to be the best choice and, as a result, fused-silica-prism-controlled KLM Ti:S lasers were the first laser oscillators producing pulses in the 10-fs regime (Asaki *et al.*, 1993; Curley *et al.*, 1993; Proctor and Wise, 1993; Spielmann *et al.*, 1994; Zhou *et al.*, 1994). Just as in femtosecond dye lasers (De Silvestri *et al.*, 1984; Salin *et al.*, 1990), high-order dispersion of the prisms limited the pulse duration (Lemoff and Barty, 1993a; Spielmann *et al.*, 1994). These technological limitations were to be overcome with the discovery of chirped multilayer dielectric mirrors (Szipöcs *et al.*, 1994, 1995), which will be treated below. With these devices, resonators providing high reflectivity and approximately constant negative GDD over the entire gain band of Ti:sapphire ($\approx$600–1000 nm) can be constructed.

Compact mirror-dispersion-controlled (MDC) KLM Ti:S laser oscillators now routinely generate high-quality sub-10-fs pulses (Stingl *et al.*, 1995; Kasper and Witte, 1996) with peak powers exceeding 1 MW (Xu *et al.*, 1997, 1998; Beddard *et al.*, 1999). Recently, hybrid dispersion control using prisms and chirped mirrors yielded pulses below 6 fs from Ti:S lasers (Gallmann *et al.*, 1999; Morgner *et al.*, 1999; Sutter *et al.*, 1999). Combining the concept of mirror dispersion control with extension of the laser cavity by a telescope (Cho *et al.*, 1999; Libertun

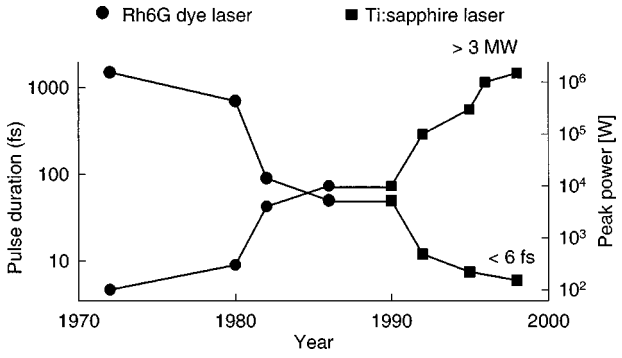

FIG. 6. Evolution of the passively mode-locked Rh6G dye laser and the passively mode-locked Ti:sapphire laser in terms of pulse duration and peak power from the mid 1960s to date. A comparison of the shortest pulse durations achieved with Kerr-lens mode locked, mirror-dispersion-controlled Ti:sapphire lasers with the round-trip time $T_r = 10-15$ ns reveals that more than one million phase-locked longitudinal resonator modes are oscillating in these systems (see Fig. 2).

et al., 1999) resulted in the generation of stable sub-10-fs pulses with peak powers exceeding 3 MW for the first time directly from a laser oscillator (Poppe, Lenzner, *et al.*, 1999). These technological advances led to a rapid evolution of femtosecond Ti:S lasers since the first demonstration of passive mode locking in a Ti:sapphire laser (French, Williams, *et al.*, 1989) and gave rise to an improvement of the pulse duration and peak power by more than two and four orders of magnitude, respectively, within the last 30 years, as depicted in Fig. 6. Due to the absence of intracavity components other than the gain medium in KLM/MDC Ti:S lasers, the noise performance of femtosecond sources could also be improved substantially (Poppe *et al.*, 1998). The KLM Ti:S laser is now commercially available with both prism and mirror dispersion control and has become the major workhorse for ultrafast time-resolved spectroscopy and nonlinear optics. More recently, it was also demonstrated as a promising tool for metrology applications in high-resolution spectroscopy (Udem *et al.*, 1999a; 1999b).

D. Chirped pulse amplification: Boosting the peak power to unprecedented levels

Many intriguing applications of ultrashort pulses call for intensities requiring peak powers far exceeding the power levels that can be directly obtained from cw mode-locked oscillators. To this end, the pulses delivered by mode-locked lasers need to be amplified. Femtosecond pulse amplification was first demonstrated by using dye cells or jets pumped by Q-switched Nd:YAG and copper-vapor lasers (Fork *et al.*, 1982; Sizer *et al.*, 1983; Koroshilov *et al.*, 1984; Knox *et al.*, 1985); for a review see Knox, 1988). The maximum pulse energy that can be practically achieved in dye amplifiers is restricted to less than ≈ 1 mJ. This limitation relates to the fact that the maximum possible energy that can be extracted per unit beam cross-sectional area without significant temporal distortion of the amplified pulse is given by the saturation fluence

$$F_{sat} = \hbar \omega_l / \sigma_e , \tag{6}$$

where ω_l and σ_e are the center frequency and the peak stimulated-emission cross section of the laser transition, respectively. The above limit is set by the low saturation fluence implied by the high emission cross section σ_e of dye lasers and the maximum dye volume that can be uniformly pumped in practice. The fundamental relationship

$$\tau_f \sigma_e \Delta \nu_l = k \frac{\lambda_l^2}{n^2} \tag{7}$$

connecting the characteristics of a laser transition ($\Delta \nu_l$ is the gain bandwidth, n is the refractive index of the gain medium, and k is a numerical factor of the order of unity that depends on the emission line shape) reveals that the high σ_e also implies a short fluorescence lifetime τ_f (Koechner, 1996). The related short energy-storage time and strong amplified spontaneous emission constitute further drawbacks of dye amplifiers. Excimer amplifiers have similar characteristics but offer significantly larger uniformly inverted apertures, allowing amplification up to hundreds of millijoules in the ultraviolet spectral range at pulse durations of the order of 100 fs (Glownia *et al.*, 1987; Szatmári *et al.*, 1987; Watanabe *et al.*, 1988; Taylor *et al.*, 1990; Mossavi *et al.*, 1993; for a review see Szatmári, 1994). Owing to their high peak power, of the order of 1 TW, excellent beam quality, and short wavelength, these pulses can be focused to a spot size below 1 μm, resulting in peak intensities in excess of 10^{18} W/cm^2 (Szatmári, 1994).

Novel solid-state gain media developed in the 1980s held promise for producing even higher peak powers due to their far higher energy fluences and broader bandwidths (see Fig. 4). However, amplification of femtosecond pulses in these media gives rise to catastrophic effects due to an accumulated intensity-dependent phase shift induced by the optical Kerr effect long before the saturation fluence can be reached (see, for example, Koechner, 1996). This limitation has been overcome by the ingenious concept of chirped pulse amplification (Strickland and Mourou, 1985; Maine *et al.*, 1988), the principle of which is illustrated in Fig. 7. By the early 1990s, chirped pulse amplification implemented with diffraction-grating-based pulse compressors (Treacy *et al.*, 1969) and stretchers (Martinez, 1987) had made it possible to generate pulses in the 100-fs range with peak powers of several terawatts from laboratory-scale systems based on Ti:S and Cr:LiSAF (Sullivan *et al.*, 1991; Beaud *et al.*, 1993; Ditmire and Perry, 1993), and the use of large-aperture Nd:glass power amplifiers resulted in ≈ 1-ps pulses having peak powers of tens of TW (Patterson and Perry, 1991; Sauteret *et al.*, 1991; Yamakawa *et al.*, 1991; Rouyer *et al.*, 1993; Blanchot *et al.*, 1995).

Advances in Ti:S seed oscillators (Asaki *et al.*, 1993; Curley *et al.*, 1993; Stringl *et al.*, 1995) and stretcher/compressor design (Lemoff and Barty, 1993b; Zhou

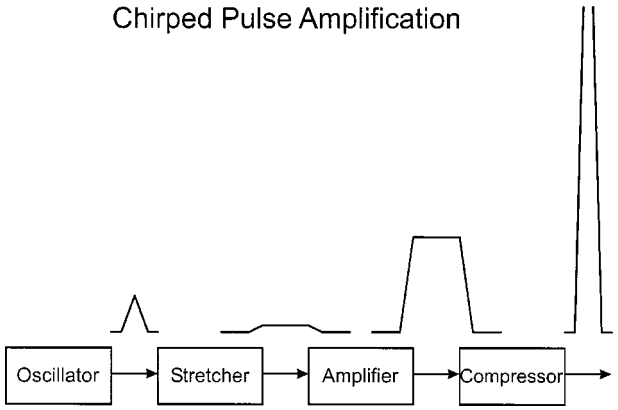

FIG. 7. Principle of chirped pulse amplification (Strickland and Mourou, 1985). A low-energy ultrashort seed pulse is temporally stretched before amplification and recompressed after amplification to avoid high peak powers in the amplifier system.

et al., 1995; Cheriaux *et al.*, 1996) led to the development of Ti:S chirped pulse amplification systems generating multiterawatt pulses in the 20-fs regime at 10 Hz (Barty *et al.*, 1994; Zhou *et al.*, 1995) and triggered a subsequent rapid evolution of these systems (Chambaret *et al.*, 1996; Yamakawa *et al.*, 1998a) to a peak power of 100 TW (Yamakawa *et al.*, 1998b) and (expected) peak intensities at focus in excess of 10^{20} W/cm^2. The evolution of laboratory chirped pulse amplification systems is depicted in Fig. 8 (for recent reviews see Perry and Mourou, 1994; Morou, 1997). This and similar laboratory-scale chirped pulse amplification architectures based on Ti:sapphire or Yb:glass (Nees *et al.*, 1998) are expected to be scalable to petawatt peak power levels, which could be demonstrated with a large laser system at Lawrence Livermore National Laboratory, Livermore (Perry *et al.*, 1999). Peak powers in excess of 10^{21} W/cm^2 can now be attained from both large-scale (Perry *et al.*, 1999 and lab-scale lasers (Patterson *et al.*, 1999). The excellent thermal conductivity and favorable thermo-optic properties of Ti:sapphire and the availability of kHz-rate Q-switched solid-state pump sources opened the way to implemeting chirped pulse amplification at kHz repetition rates. Related research recently culminated in the demonstration of kHz sources of sub-20-fs pulses with peak powers of several hundred gigawatts (Backus *et al.*, 1997; Nibbering *et al.*, 1997; Nabekawa *et al.*, 1998; for a review see Backus *et al.*, 1998) and suggest the feasibility of kHz-repetition-rate terawatt sources (Durfee *et al.*, 1998) in the near future.

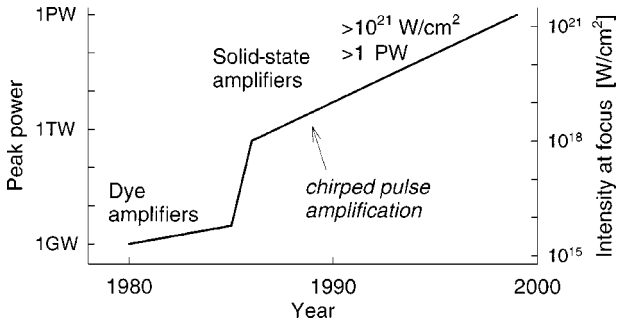

FIG. 8. Evolution of ultrashort-pulse amplification in terms of peak power and achievable peak intensity.

E. Chirped multilayer mirrors: Paving the way towards the single-cycle regime

In the preceding subsections we have addressed how optical nonlinearities can be efficiently exploited for the generation of femtosecond laser pulses in broadband solid-state oscillators and how they can be efficiently avoided when their energy is boosted in solid-state amplifiers. Apart from optical nonlinearities, dispersion becomes increasingly important as ever shorter pulses are sought. In fact, generating bandwidth-limited pulses of decreasing duration calls for controlling the frequency-dependent group delay over increasing bandwidth with increasing precision. Hence precision broadband dispersion control is a prerequisite for approaching the few-cycle regime in ultrashort pulse generation.

Dispersion can be quantified by expanding the group delay, which is equal to the first derivative of the phase retardation $\phi(\omega)$ of the optical system with respect to frequency, about the center of the pulse spectrum ω_0 in the form

$$T_g(\omega)=\phi'(\omega)=\phi'(\omega_0)+\phi''(\omega_0)(\omega-\omega_0)+\frac{1}{2}\phi'''(\omega_0)(\omega-\omega_0)^2+\frac{1}{6}\phi''''(\omega-\omega_0)^3+\cdots . \quad (8)$$

Here $\phi'(\omega_0)$ gives the time it takes for the peak of the pulse to traverse the dispersive medium. The higher-order terms in the expansion describe the frequency dependence of the group delay and hence are responsible for dispersive effects. $\phi''(\omega_0)$ is the lowest-order (linear) group delay dispersion or second-order phase dispersion, most frequently referred to as group delay dispersion (GDD) in the literature and denoted by D, a convention that we also adopt in this work; $\phi'''(\omega_0)\equiv D_3$ and $\phi''''(\omega_0)\equiv D_4$ are termed third-order and fourth-order dispersion, respectively. Critical values of the dispersion coefficients, above which dispersion causes a substantial change of the pulse, obey the simple scaling $\phi^{(n)}=\tau_p^n$. For instance, a GDD of $\phi''=\tau_p^2$ results in a pulse broadening by more than a factor of 2. This scaling reveals a dramatic increase in susceptibility to dispersion-induced broadening and distortion for decreasing pulse durations.

Most laser and optical materials exhibit some *positive* GDD, implying a group delay that increases with frequency and hence imposing a positive frequency sweep or chirp on a pulse passing through the medium. Pulses tens of fs in duration tend to broaden significantly even upon passage through transparent optical media (such as quartz or sapphire) of merely a few mm in length. This broadening even gets accelerated at high intensities, leading to self-phase-modulation due to the optical Kerr

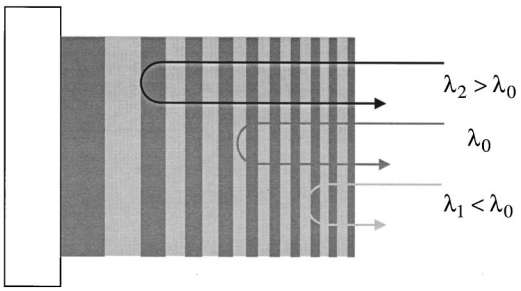

FIG. 9. Schematic illustration of the origin of dispersion in a chirped multilayer mirror. Quasimonochromatic wave packets carried at different wavelengths penetrate to different depths before being reflected, as a consequence of a modulation of the multilayer period across the layer stack. In the illustrated example, the increasing multilayer period with increasing distance from the mirror surface implies that radiation with increasing wavelength has to penetrate deeper before being reflected as a result of constructive interference of the partial waves reflected from the interfaces between the low- and high-index layers. The result is a group delay that increases with increasing wavelength, i.e., decreasing frequency, giving rise to negative group delay dispersion.

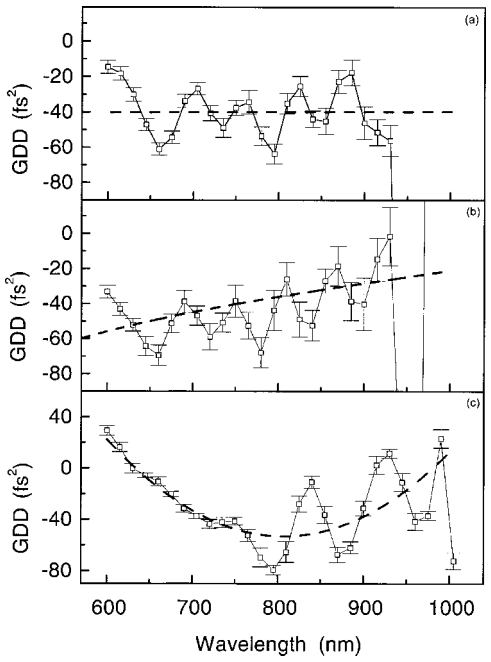

FIG. 10. Group delay dispersion (GDD) vs wavelength of ultrabroadband chirped mirrors aiming at introducing GDD as well as higher-order dispersion control in sub-10-fs Ti:sapphire-based systems: □, measured data (restricted to the range 600–1000 nm) obtained from white-light interferometry; dashed curves, nominal (averaged) or target GDD curves. The quasiperiodic fluctuation of the measured dispersion is inherent to chirped mirrors consisting of discrete layers and can be efficiently (by more than 50%) suppressed by complementary mirrors with opposite fluctuations. (a) Chirped mirror designed for nominally constant negative GDD of $-40\,\mathrm{fs}^2$. (b) Chirped mirror designed for compensating the dispersion introduced by fused silica up to (and including) fourth order over the wavelength range 580–930 nm; dashed line, dispersion introduced by fused silica (with reversed sign) over a 1-mm propagation length: $D=-36\,\mathrm{fs}^2$, $D_3=-27\,\mathrm{fs}^3$, and $D_4=-11\,\mathrm{fs}^4$ at $\lambda_0=800\,\mathrm{nm}$. (c) Chirped mirror designed for compensating high-order dispersion up to (and including) fourth-order dispersion over the wavelength range 560–1000 nm; dashed line, least-squares fit to the data yielding $D=-53\,\mathrm{fs}^2$, $D_3=9\,\mathrm{fs}^3$, and $D_4=400\,\mathrm{fs}^4$ at $\lambda_0=800\,\mathrm{nm}$. The high reflectivity ($>99\%$) range of these mirrors extends over more than 200 THz, exceeding the bandwidth of standard quarterwave mirrors by more than a factor of two.

effect, which broadens the spectrum by imposing a positive temporal chirp. Clearly, restoring the duration of pulses passed through optical materials calls for negative GDD, just as does compressing pulses spectrally broadened by self-phase-modulation.

Treacy (1969) was the first to demonstrate negative GDD by passing light pulses through a pair of diffraction gratings, successfully achieving pulse compression with such a system. The Brewster-angled prism pairs of Fork *et al.* (1984) were the first low-loss sources of negative GDD, which have been extensively employed for dispersion control inside laser oscillators since their discovery. In both cases, negative GDD is accompanied by significant amounts of intrinsic high-order dispersion, which cannot be lowered or adjusted independently of the (useful) lowest-order dispersion (GDD), limiting the bandwidth over which adequate dispersion control can be provided. This drawback was overcome, to lowest order, by combining prism and grating pairs exhibiting third-order dispersion of opposite sign, thus allowing pulse compression to 6 fs in the mid 1980s (Fork *et al.*, 1987) and recently to less than 5 fs (Baltuska *et al.*, 1997a). Nevertheless, this approach cannot be used for few-cycle pulse generation either in oscillators (because of the high losses of gratings) or in external compressors at high power levels (because of unwanted nonlinearities in the prisms).

Recently, modulation of the multilayer period of dielectric laser mirrors was demonstrated to result in a wavelength-dependent penetration depth of the incident radiation (Szipöcs *et al.*, 1994). This implies a corresponding dependence of the group delay on frequency (see Fig. 9), which can be tailored to yield—within certain limits—required amounts of GDD as well as higher-order dispersion over almost the entire high-reflectivity band of the mirror, which can be substantially broader than that of a standard quarterwave stack. These devices have been referred to as chirped multilayer mirrors (Szipöcs *et al.*, 1994). Recent advances in the design and manufacturing of such structures have led to chirped mirrors exhibiting high reflectivity and approximately constant negative GDD over unprecedented bandwidths (Matuschek, 1998; Tempea, Krausz, *et al.*, 1998).

Figure 10 depicts the GDD versus wavelength for several chirped mirrors designed for second- and higher-order dispersion control in Ti:sapphire-based sub-10-fs systems. These results demonstrate the power of this technique for controlling dispersion over unprecedented bandwidths with unprecedented precision. The chirped mirrors' current capability of exhibiting high reflectance

over a bandwidth >200 THz and controlling dispersion over a spectral range as broad as >150 THz has allowed the generation of sub-6-fs pulses directly from laser oscillators (Gallmann *et al.*, 1999; Morgner *et al.*, 1999; Sutter *et al.*, 1999) sub-5-fs pulses from optical parametric amplifiers (Shirakawa *et al.*, 1999), and pulse compression at high (subterawatt) power levels down to 4 fs (Cheng *et al.*, 1998). The latter pulses are carried at a wavelength of $\lambda_0 \approx 0.8\,\mu$m, implying a laser oscillation cycle of $T_o \approx 2.6$ fs. Hence chirped mirrors are able to provide adequate dispersion control for the generation of light pulses comprising merely one and a half field oscillation cycles within their intensity half maximum and hold promise for pushing the limits of ultrafast optics into the single-cycle regime in the near future.

III. GENERATION OF INTENSE LIGHT PULSES IN THE FEW-CYCLE REGIME

In this section we briefly review the key physical mechanisms and techniques that allow the generation of powerful light pulses with durations approaching the light oscillation period T_o and peak intensities penetrating far into the strong-field regime (see Fig. 24 below). After presenting the status of few-cycle optical pulse generation, we address a parameter that has not received attention until recently: the *absolute phase* of light wave packets becomes important in the interaction of intense few-cycle radiation with matter, and its control in ultrabroadband mode-locked laser oscillators will also benefit precision measurements of the frequency of light as well as atomic transitions.

A. Principles of optical pulse compression

The nonlinear refractive index n_2, as defined in Eq. (1), was recognized as a source of new frequency components during propagation of an intense short light pulse through a Kerr medium. The time-dependent nonlinearly induced phase shift $\Delta\varphi_{nl}(\tau) = (2\pi/\lambda_0) n_2 I(\tau) L$, where $I(\tau)$ is the intensity, τ the retarded time as defined in the previous section, and L the propagation length, manifests itself as a *self-phase-modulation* (SPM) and tends to broaden the spectrum of an initially bandwidth-limited pulse (Shimizu, 1967; Fisher *et al.*, 1969; Laubereau, 1969; Laubereau and von der Linde, 1970; Alfano and Shapiro, 1970). In high-power laser systems, this effect is undesirable because the dependence of I on the transverse space coordinates introduces phase aberrations leading to a degradation of the laser beam. However, under specific experimental conditions $\Delta\varphi_{nl}$ can be utilized for the generation of ultrashort pulses.

The feasibility of pulse compression arises from the sequential emergence of new redshifted and blueshifted spectral components at different positions of the pulse envelope. As a consequence, subsequent passage of the pulse through a delay line, introducing shorter group delay for the new spectral components riding on the trailing edge of the pulse, as compared to the delays suffered by the components emerging on the front edge, translates the pulse carrying $\Delta\varphi_{nl}$ into a temporally compressed pulse, as illustrated in Fig. 11. The frequency sweep (or chirp) $d\Delta\varphi_{nl}/d\tau$ is linear to good accuracy in the vicinity of the pulse center ($\tau=0$), where most of the energy is concentrated, particularly if $\Delta\varphi_{nl}$ emerges in the presence of GDD of the same sign as $\Delta\varphi_{nl}$ (Tomlinson *et al.*, 1984). As a consequence, optimum temporal compression calls for a group delay $T_g(\omega)$ exhibiting a near-linear dependence on frequency in the dispersive delay line. The nonlinear index n_2 is generally positive far from resonances, hence a negative group delay dispersion $(dT_g/d\omega)_{\omega_0} < 0$ is required for pulse compression.

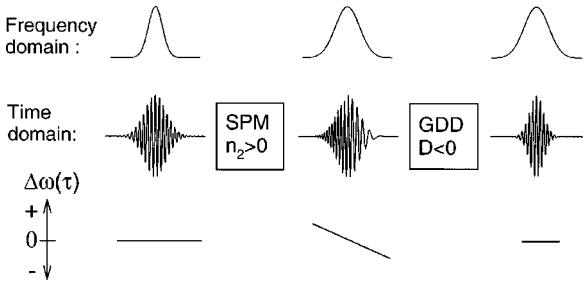

FIG. 11. Schematic representation of optical pulse compression. The graphs depict qualitatively the spectral intensity distribution (frequency domain), and evolution of the electric field $E(t)$ and change in instantaneous frequency with respect to the carrier frequency $\Delta\omega(\tau) = \omega_{\text{inst}}(\tau) - \omega_0$ (time domain). The bandwidth-limited $[\Delta\omega(\tau)=0]$ input pulse propagates from the left to the right. The positive frequency sweep $\Delta\omega(\tau) = (d/d\tau)\Delta\varphi_{nl}(\tau)$ imposed on the intense light pulse by self-phase-modulation induced by the optical Kerr effect upon passage through a transparent optical medium can be removed by subsequently passing the pulse through a dispersive delay line with negative group delay dispersion, resulting in a temporal compression.

This interplay between Kerr-induced self-phase-modulation and negative GDD forms the basis of all pulse compression schemes that have been demonstrated to date. At low (nanojoule) pulse energy levels, compression can be most efficiently implemented by passing the pulse through a single-mode fiber and subsequently through a grating pair (Grischkowski and Balant, 1981; Johnson *et al.*, 1984), and somewhat later, through gratings and prisms for improved high-order dispersion control, resulting in nanojoule-energy 6-fs pulses at 620 nm (Fork *et al.*, 1987). This long-standing record has recently been improved by using a single-mode-fiber/chirped-mirror compressor seeded with 15-fs pulses generated by a cavity-dumped KLM Ti:sapphire laser (Ramaswamy *et al.*, 1993; Pshenichnikov *et al.*, 1994). This compact all-solid-state system is capable of generating nanojoule pulses down to 4.5 fs in duration at MHz repetition rates (Baltuska *et al.*, 1997a; 1997b; Pshenichnikov *et al.*, 1998), constituting a powerful tool for ultrafast spectroscopy with unprecedented temporal resolution.

Nanojoule-energy few-cycle pulses with durations between 5 and 6 fs have more recently been directly avail-

able from KLM Ti:S oscillators employing chirped multilayer resonator mirrors (Gallmann *et al.*, 1999; Morgner *et al.*, 1999; Sutter *et al.*, 1999). For restoring these pulse durations after amplification to millijoule energy levels, the implementation of self-phase-modulation in a gas-filled multimode hollow waveguide (Nisoli *et al.*, 1996) and subsequent temporal compression in chirped mirrors (Nisoli, De Silvestri, *et al.*, 1997; Nisoli, Stagira, *et al.*, 1997; Sartania *et al.*, 1997) have been proposed and successfully demonstrated. The formation of few-cycle pulses in Ti:S oscillators and hollow-fiber-based compressors is the consequence of the same physical mechanisms (SPM-GDD interplay) exploited in distinctly different parameter regimes. In the following subsections we provide a unified treatment of the formation of few-cycle pulses in solitary (bulk) laser oscillators and in multimode-waveguide/chirped-mirror-based compressors (at low and high energy levels, respectively) and present the state of the art of few-cycle pulse generation.

B. Self-phase-modulation in free space and guided-wave propagation

Self-phase-modulation (SPM) of ultrashort laser pulses and related spectral broadening can be most simply induced by focusing into a bulk nonlinear medium. If the length L of the medium is short compared to the confocal parameter of the beam, the wave front is approximately planar and the radial intensity distribution approximately constant in the nonlinear medium. Yet the radial intensity variation produces a spatially varying $\Delta\varphi_{nl}$, giving rise to self-focusing (for $n_2>0$) and small-scale instabilities (Campillo *et al.*, 1969). In addition, the extent of spectral broadening depends on the radial coordinate, frustrating a spatially uniform pulse compression. Creating a near-flat-top intensity profile in a thin nonlinear medium by beam truncation and suppressing small-scale instabilities by spatial filtering is one possible way of circumventing these problems (Rolland and Corkum, 1988). The penalty to be paid in this approach is very high losses.

Spatially uniform spectral broadening can be achieved much more efficiently by guiding the self-phase-modulated beam and distributing $\Delta\varphi_{nl}$ over an extended propagation length. To shed light on the crucial role of wave guiding and of a slow accumulation of $\Delta\varphi_{nl}$ we decompose the laser beam into transverse eigenmodes of the propagation medium and perform coupled-mode analysis to contrast nonlinear propagation in a multimode waveguide with that in free space. A unified theoretical treatment of these phenomena becomes feasible by replacing the transverse eigenmodes of the waveguide with the Hermite-Gaussian solutions of the paraxial wave equation (Haus, 1984) in the coupled-mode analysis of nonlinear wave propagation.

In most practical cases, the fundamental propagation mode is excited at the entrance of the nonlinear medium. The nonlinear index n_2 has two major implications in this scenario: (i) a spatially uniform phase shift $\Delta\varphi_{nl}(\tau)$ is imposed on the fundamental mode and (ii) a fraction of its energy is coupled to higher-order modes during propagation. Self-focusing and related beam deterioriation are consequences of the latter effect. It was recently shown that the coupled-mode equations can be solved analytically in the limit of small depletion of the fundamental mode for nonlinear light-pulse propagation in a multimode (hollow) waveguide (Tempea and Brabec, 1998b) as well as in free space (Milosevic *et al.*, 1999). In what follows we summarize the major results of these analyses and draw important conclusions for implementing few-cycle pulse generation.

First, we address free-space propagation. If the fundamental TEM_{00} mode is focused into a nonlinear medium, the nonlinear polarization response of the medium couples energy from the incident fundamental into higher-order TEM_{mn} modes. The upper diagram of Fig. 12 depicts qualitatively the fractional energy coupled from the TEM_{00} into the TEM_{01} mode during propagation in a bulk nonlinear medium of length L positioned between $z=-L/2$ and $z=L/2$, where $z=0$ is the position of the beam waist. A useful scale parameter for the nonlinear interaction is the nonlinear length, defined as

$$L_{nl}=\frac{1}{\gamma_{SPM}p_0}, \tag{9}$$

where γ_{SPM} is defined in Eq. (4) and p_0 stands for the peak power of the pulse. If $L_{nl}\gg z_0$, where $z_0=\pi w_0^2/\lambda_0$ denotes the Rayleigh range and w_0 is the $1/e^2$ radius at the beam waist, only a small fraction of the energy of the light pulse fed into the medium in the fundamental transverse mode is coupled to higher-order modes, and for a medium of length $L\gg z_0$ a perturbative approach allows us to solve the coupled-mode equations analytically.

From this solution we can obtain the fractional power $\Gamma(z)$, coupled from the fundamental TEM_{00} mode to the lowest-order higher transverse mode TEM_{01}, to which coupling due to n_2 is strongest, and the evolution of the peak nonlinear phase shift $\Delta\varphi_{nl}(z,r,\tau)$ imposed on the propagating beam. In the limit of $L_{nl}\gg z_0$, the fractional energy extracted temporarily from the TEM_{00} mode is small and the energy coupled to higher-order modes is fed back to the fundamental mode behind the beam waist in a lossless and dispersion-free medium. As a consequence, the output pulse is delivered in a Gaussian beam and carries a spatially uniform phase shift (i.e., $\Delta\varphi_{nl}$ is independent of the radial coordinate r). $\Gamma(z)$ (solid line) and $\Delta\varphi_{nl}(z,\tau=0)$ (dashed line) calculated under these conditions are plotted qualitatively in the upper diagram of Fig. 12. The energy flow between the TEM_{00} and TEM_{mn} modes decreases with increasing mode order and changes its sign an increasing number of times for increasing mode order between the fundamental and higher-order modes.

The maximum energy transferred to the mode TEM_{01} at the beam waist and the peak nonlinear phase shift carried by the pulse exiting the medium are given by (Tempea and Brabec, 1998b)

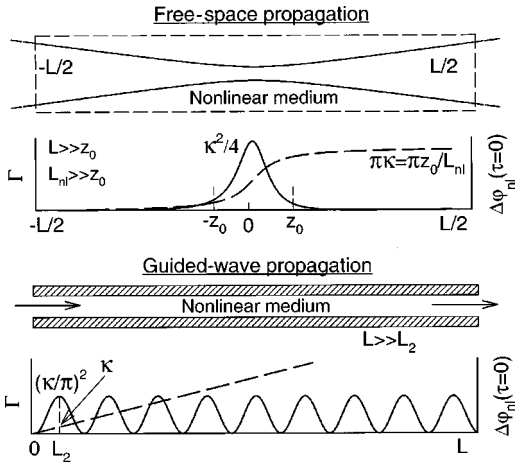

FIG. 12. Schematic of pulse evolution in a Kerr nonlinearity without and with guiding. Upper graphs, free space propagation in a Kerr nonlinear medium with a length L much longer than the nonlinear length L_{nl}, which in turn is assumed to be much longer than the Rayleigh range z_0 of the beam (for definitions see text) and the signal coupled from the fundamental (TEM_{00}) Gaussian mode into the next higher-order TEM_{01} mode vs propagation distance: solid curve, the fractional energy transfer $\Gamma(z)$ from the TEM_{00} into the TEM_{01} mode in the limit of $\Gamma(0)=\kappa^2/4\ll 1$. Under this condition coupling to higher-order modes may be neglected. Dashed curve, the nonlinear phase shift at the peak of the pulse, which is independent of the transverse coordinates as long as the condition of weak coupling, $\Gamma(0)\ll 1$, is met. The dominant contribution to the nonlinear phase shift $\Delta\varphi_{nl,out}(\tau=0)$, which determines Kerr-induced spectral broadening, originates from the region $-z_0<z<z_0$. Lower graphs, guided-wave propagation in a hollow fiber filled with some noble gas to introduce a Kerr nonlinearity. Here $\Gamma(z)$ represents the fraction of the energy of the pulse carried in the fundamental LP_{01} mode that is transferred into the next higher-order LP_{02} mode by means of n_2. In the limit of $\Gamma(L_2)=(\kappa/\pi)^2\ll 1$, only a small amount of energy is coupled from the fundamental into the next higher mode, which oscillates between the two modes with a periodicity equal to twice the coherence length L_2. Under this condition a spatially uniform nonlinear phase shift can grow to lengths much longer than the coherence length. This is in contrast with propagation in a bulk nonlinear medium and results from confinement of the beam, keeping the intensity high over propagation lengths far beyond z_0.

$$\Gamma(0)=\frac{\kappa^2}{4}=\left(\frac{p_0}{p_{c,fs}}\right)^2 \quad \text{and} \quad \Delta\varphi_{nl,out}(\tau=0)=\pi\kappa, \tag{10}$$

respectively, where

$$\kappa=\frac{z_0}{L_{nl}} \quad \text{and} \quad p_{c,fs}=\frac{\lambda_0^2}{\pi n_2}. \tag{11}$$

The requirement of small depletion of the fundamental mode can be formulated as $\kappa^2/4\ll 1$, which can be rewritten in terms of $(p_0/p_{c,fs})^2\ll 1$, where $p_{c,fs}$ determines the power at which self-focusing tends to introduce severe distortions to the laser beam propagating in free space. This power identified by coupled-mode analysis is in reasonable agreement with the well-known critical power for self-focusing in a bulk medium $p_c=\alpha_{fs}\lambda_0^2/(8\pi n_2)$, where $\alpha_{fs}\approx 3.8$–6.4 is a correction factor acquired from numerical investigations (Sheik-Bahae *et al.*, 1984).

The requirement of $\kappa^2/4\ll 1$, which is to be fulfilled for spatially uniform self-phase-modulation and weak beam deterioration, implies that $\Delta\varphi_{nl,out}(\tau=0)$ can at maximum be equal to $\approx\pi$. Such an SPM-induced peak nonlinear phase shift, when carried by a near-bandwidth-limited pulse, can induce relative spectral broadening by a factor of 2 (Agrawal, 1995), which determines the maximum compression factor in spatially uniform temporal compression that is achievable after a single pass through a bulk nonlinear medium. For generating a larger spatially uniform nonlinear phase shift, the process needs to be repeated several times by refocusing the beam with a suitable array of lenses or mirrors. For large compression factors requiring many passes, the resultant discrete ''guiding'' configuration tends to become impractical.

Guiding of high-power laser pulses can be implemented much more conveniently and efficiently in a hollow waveguide (Marcatili and Schmeltzer, 1964). Filling the waveguide with some gas can introduce a Kerr (or other) nonlinearity required for spectral broadening of high-power laser pulses and their subsequent temporal compression (Nisoli *et al.*, 1996). In the limit of small depletion, the energy transferred from the fundamental linearly polarized mode LP_{01}, which can be excited at the waveguide entrance by a Gaussian input beam with near-100% efficiency (Nisoli *et al.*, 1998), into the higher-order modes LP_{mn} ($m=0$ and $n\geqslant 2$, where for $m\geqslant 1$ the mode-coupling constant is zero) is fully returned to the fundamental mode over a propagation length comparable to z_0 of the input beam (Tempea and Brabec, 1998b).

The lower part of Fig. 12 depicts qualitatively the evolution of the energy coupled into the LP_{02} mode during propagation through the waveguide. The energy oscillation period is twice the mutual coherence length between LP_{01} and LP_{0n}, $L_n=\pi/|\beta_0^{(n)}-\beta_0^{(1)}|$. Under optimum input coupling conditions for exciting the fundamental mode, which is achieved for $w_0\approx(2/3)a$, where a is the bore radius of the hollow waveguide and w_0 is the beam waist of the incoming beam (Nisoli *et al.*, 1998), the coherence length between the two lowest-order modes L_2 can be approximately expressed as $L_2\approx 1.1z_0$. The propagation constant of the LP_{0n} mode, $\beta_0^{(n)}$, defined in Eq. (27), decreases with increasing mode order and so does the maximum transferred energy, which is proportional to L_n^2.

The bottom diagram of Fig. 12 depicts the periodic energy exchange between the fundamental mode and the LP_{02} mode, for which the oscillating energy is maximum, as a function of the propagation length in the waveguide. For low depletion of the fundamental mode, the maximum fractional energy coupled to the LP_{02} mode and the evolution of the peak nonlinear phase shift, which is uniform across the beam, can be written as

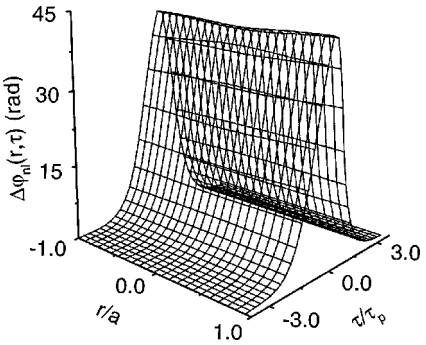

FIG. 13. Phase shift $\Delta\varphi_{nl}(z=L,r,\tau)$ imposed by the Kerr nonlinearity of argon gas at a pressure of 4 bars ($n_2=4\times10^{-19}$ cm/W) in a fused-silica hollow waveguide having a channel diameter of 140 μm and a length of $L_{nl}=29L_2\approx29$ cm upon a pulse of peak power $p_0=3.5$ GW injected into the fundamental LP_{01} mode at the entrance of the waveguide (Tempea and Brabec, 1998b). For these parameters, the pulse peak power is lower than the critical power for self-focusing, $p_{c,wg}\approx8$ GW. Under this condition, the power coupled into higher modes remains small ($\Gamma\approx0.25$), allowing the accumulation of spatially uniform self-phase-modulation on the pulse propagating primarily in the fundamental mode. This self-phase-modulation grows linearly with propagation distance until propagation losses become significant.

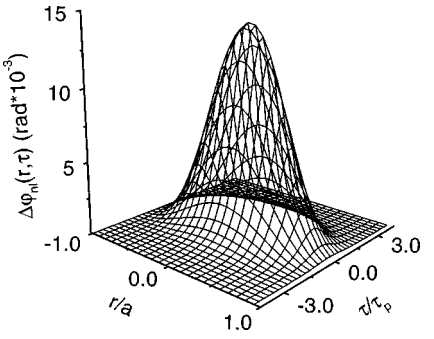

FIG. 14. Self-phase-modulation-induced phase $\Delta\varphi_{nl}(z,r,\tau)$ imposed by the Kerr nonlinearity on a pulse in a hollow waveguide as a function of the radial and the temporal coordinates under conditions described in the caption of Fig. 13 for a propagation length of $z=L_2/50$ (Tempea and Brabec, 1998b). For $z\ll L_2$, the signals coupled into different higher-order modes are comparable; therefore all coupling channels must be taken into account, resulting in a spatially varying phase shift that follows the transverse intensity profile of the fundamental LP_{01} mode. For pulse peak powers p_0 approaching $p_{c,wg}$ this phenomenon causes self-focusing of the beam, destroying propagation in the fundamental mode.

$$\Gamma(L_2)=\left(\frac{\kappa}{\pi}\right)^2=\left(\frac{p_0}{p_{c,wg}}\right)^2$$

and

$$\Delta\varphi_{nl}(z,\tau=0)=\kappa\frac{z}{L_2}\approx\kappa\frac{z}{z_0}, \tag{12}$$

respectively (see Fig. 12), where

$$p_{c,wg}=\frac{\lambda_0^2}{2n_2} \tag{13}$$

is the critical power for self-focusing in the multimode hollow waveguide and $p_{c,wg}\approx1.5p_{c,fs}$, i.e., self-focusing in waveguides and in free space sets in at comparable power levels (Milosevic *et al.*, 1999). For $w_0\approx\frac{2}{3}a$ the coupling coefficient κ is approximately defined by Eqs. (11), (9), and (4) with w_0 replaced by a (Tempea and Brabec, 1998b). Most importantly, meeting the requirement of weak depletion, $(\kappa/\pi)^2\ll1$, implies the feasibility of accumulating a spatially uniform SPM-induced phase shift over many times the Rayleigh range z_0 of the incident Gaussian beam. As a matter of fact, Fig. 13 reveals that a spatially uniform phase shift of $\Delta\varphi_{nl}\approx\pi$ can be imposed on the pulse over a propagation length of $2L_2$ without the onset of self-focusing, implying a spectral broadening of a factor of ≈10 over $L\approx20z_0$. Enhancing SPM-induced spectral broadening by increasing the propagation length is limited only by the propagation loss suffered by the fundamental mode in the leaky waveguide and/or by distortion of the temporal pulse shape.

It is instructive to look at $\Delta\varphi_{nl}(z,r,\tau)$ in the opposite limit, $L\ll L_2$, which is shown, under the same experimental conditions, in Fig. 14. The plot in Fig. 14 is the result of superimposing an infinite number of high-order modes, many of which with $L_n>L$ have comparable amplitudes, on the fundamental LP_{01} mode. For propagation lengths much shorter than the coherence length L_2, the nonlinear phase shift mimics not only the temporal shape of the pulse but also the transverse intensity distribution of the fundamental mode. It is this latter effect that gives rise to self-focusing if the peak power becomes so high that κ/π approaches unity and depletion of the fundamental mode becomes appreciable. Analogously, strong self-focusing emerges in a bulk nonlinear medium as $p_0\to p_{c,fs}$. In order to avoid catastrophic effects, L must be significantly shorter than z_0.

These are the experimental conditions relevant to passively mode-locked femtosecond Ti:sapphire and other solid-state laser oscillators. These systems are capable of delivering ultrashort pulses in the fundamental TEM_{00} mode, which is in apparent contradiction to coupling an appreciable amount of energy from the fundamental into higher-order transverse modes by the radially varying nonlinear phase shift $\Delta\varphi_{nl}(r,\tau)$ induced by the nonlinear index of the gain medium. This paradox can be resolved by considering the spatial filtering action of a laser resonator, which efficiently suppresses the emerging high-order modes and can lead to a TEM_{00} output beam even in the presence of strong nonlinearities in the cavity.

We may therefore conclude that the same nonlinear optical process in strongly different parameter regimes, $L<z_0$ and p_0 comparable to p_c on the one hand, and $L\gg z_0$ and $p_0\ll p_c$ on the other hand, is responsible, in combination with broadband GDD control, for the generation of low-energy few-cycle light pulses in laser oscillators and for the generation of few-cycle pulses at much higher power levels by guided-wave compression following amplification.

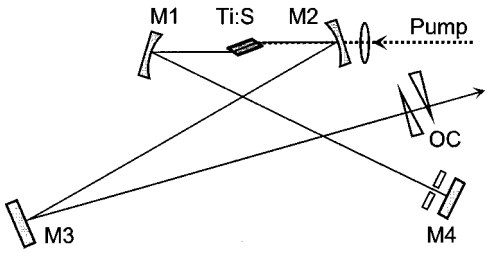

FIG. 15. Schematic of a mirror-dispersion-controlled Ti:sapphire laser made up of chirped mirrors (M1-M4), a broadband output coupler (OC), and a thin, highly doped Ti:sapphire crystal (Ti:S); for more details see, for example, Xu *et al.* (1997).

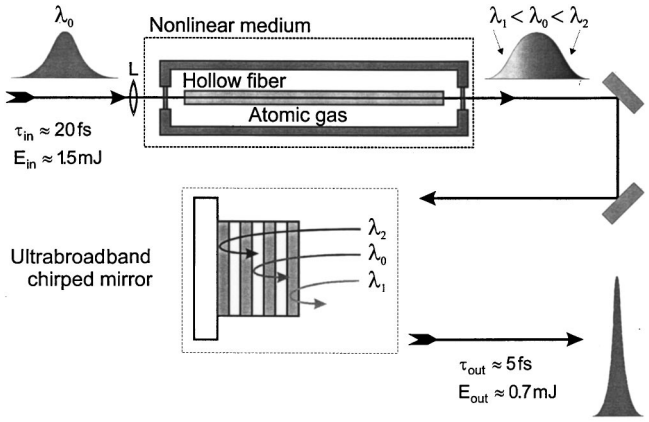

FIG. 16. Schematic experimental setup of a hollow-fiber chirped-mirror high-energy pulse compressor. The input pulse is coupled into a gas-filled hollow fiber, where its spectrum is broadened by self-phase-modulation imposed by the optical Kerr effect in the gas. Subsequently, the chirp of the broadened pulse is removed upon reflection off broadband chirped mirrors [see diagrams (a) and (b) in Fig. 10], which leads to a temporal compression of the laser pulse (courtesy of A. Poppe).

C. Few-cycle pulse generation: Current state of the art

Optical pulse compression based on the interplay between self-phase-modulation induced by the optical Kerr effect and negative group delay dispersion is the key concept for light-pulse generation in the few-cycle regime. Currently it is most efficiently implemented in mirror-dispersion-controlled (MDC) Kerr-lens mode-locked (KLM) Ti:sapphire laser oscillators and hollow-fiber chirped-mirror compressors.

In the former systems, schematically illustrated in Fig. 15, SPM in the laser crystal and negative GDD in the chirped mirrors M1–M4 act alternately many thousand times before the stationary pulse duration in the sub-10-fs regime is reached. The pulse is moderately chirped and spectrally broadened upon passage through the Ti:S crystal, which is converted in a temporal compression in the broadband chirped resonator mirrors. In the steady state this pulse, shortening process is stopped by the finite bandwidth over which nearly constant negative GDD can be introduced by the mirrors and/or balanced by the finite gain and resonator bandwidth.

Solitary pulse formation *inside* a laser oscillator needs to be assisted by a fast saturable-absorber-like self-amptitude modulation (SAM), which is introduced by KLM in the Ti:S oscillator, as described in the previous section. The role of this SAM action is (i) to initiate and support the formation of a short pulse in the cavity and (ii) to stabilize the SPM/GDD-dominated shortening process and eventually the stationary state against low-intensity noise. This noise arises inherently due to gain and positive feedback in the pulse wings and can be efficiently filtered by SAM outside the short interval comprising the mode-locked pulse (see Fig. 3).

When pulse compression external to a laser oscillator is implemented, both SPM and GDD usually act only once and in this sequence, as illustrated in Fig. 16. Hence spectral broadening in the Kerr medium is much stronger than in the case of intracavity solitary pulse formation. The absence of quasiperiodic pulse evolution and gain in extracavity pulse compression implies that instabilities and noise cannot grow. Hence filtering by SAM is not absolutely necessary. Summing up, both SPM and GDD tend to impose a much stronger modification on the light pulse in extracavity compressors than does compression inside the oscillator. In addition, intra- and extracavity spectral broadening in a KLM Ti:S laser and a multimode hollow waveguide take place in entirely different physical regimes, as described at the end of the previous subsection. Table I contrasts the parameter regimes of KLM/MDC Ti:S oscillators and multimode-hollow-waveguide/chirped-mirror compressors by listing typical values of the parameters relevant to few-cycle pulse formation.

KLM/MDC Ti:S laser oscillators routinely generate sub-10-fs pulses at typical pulse energy levels of a few nanojoules and multi-MHz repetition rates. The simplest embodiment of this system is depicted in Fig. 15. It is capable of producing pulses down to 7 fs in duration with peak powers up to 1 MW (Xu *et al.*, 1997; 1998; Beddard *et al.*, 1999) and exhibits unparalleled noise characteristics in the sub-50-fs regime while being pumped with a low-noise diode-pumped solid-state laser (Poppe *et al.*, 1998). Incorporating a pair of low-dispersion prisms as a source of adjustable GDD in addition to the chirped mirrors and employing specially designed output couplers in KLM/MDC Ti:S lasers recently pushed the record below 6 fs in laser oscillators (Morgner *et al.*, 1999; Sutter *et al.*, 1999). Figure 17 shows the intensity envelope and phase of sub-6-fs pulses (Gallmann *et al.*, 1999) obtained from a SPIDER measurement (spectral phase interferometry for direct electric-field reconstruction; Walmsley and Wong, 1996). The pulses are generated by a self-starting KLM/MDC Ti:S laser developed by U. Keller and co-workers at the Eidgenössische Technische Hochschule (ETH) Zurich with energies of 2–4 nJ at peak power levels of approximately 0.5 MW (Sutter *et al.*, 1999).

The pulse energy can be enhanced by extending the cavity with a telescope and reducing the repetition rate (Cho *et al.*, 1999; Libertun *et al.*, 1999). Implementing this technique in a KLM/MDC Ti:S laser has yielded

TABLE I. Parameter ranges for few-cycle pulse generation in Kerr-lens-mode-locked/mirror-dispersion-controlled Ti:S oscillators at low energy levels and in hollow-waveguide/chirped-mirror compressors at high energy levels.

Systems parameters	KLM/MDC Ti:sapphire oscillator	Multi-mode hollow-waveguide/ chirped-mirror compressor
Nonlinear interaction length	$<z_0$	$\gg z_0$
p_0/p_c	$\geqslant 1$	$\ll 1$
p_c	≈ 2.5 MW	10 GW–1 TW
$\Delta\varphi_{nl}(\tau=0)$	$0.1\pi-0.5\pi$	$5\pi-10\pi$
Spectral broadening/pass	1.1–1.3	5–10
Net negative group delay dispersion $\lvert D\rvert$	10–30 fs^2	10–30 fs^2
Compression factor/pass	1.1–1.3	5–10
Self-amplitude modulation depth	1–3 %	—
Output pulse energy	3–30 nJ	0.01–1 mJ
Output pulse duration	5–8 fs	4–7 fs
Output peak power	0.3–3 MW	1 GW–0.2 TW
Peak intensity in focus	up to 10^{14} W/cm^2	up to 10^{18} W/cm^2

sub-10-fs pulses with energies in excess of 30 nJ, giving rise to peak powers of >3 MW at a repetition rate of 25 MHz (Poppe, Lenzner, *et al.*, 1999). This value approaches peak power levels which until recently could only be attained with cavity-dumped Ti:S lasers at high (>1 MHz) repetition rates (Ramaswamy *et al.*, 1993; Pshenichnikov *et al.*, 1994). The lower repetition rate (as compared to 80–100 MHz typically) of extended-cavity and cavity-dumped Ti:S oscillators not only enhances the peak power to levels allowing further pulse compression below 5 fs (Baltuska *et al.*, 1997a, 1997b; Pshenichnikov *et al.*, 1998), but also reduces thermal load to the sample in ultrafast spectroscopy.

The highest peak intensities that can be expected from oscillators in the few-cycle sub-10-fs regime approach 10^{14} W/cm^2 (Xu *et al.*, 1998; Jasapara and Rudolph, 1999; Poppe, Lenzner, *et al.*, 1999). Although strong-field effects may arise at these intensity levels in some systems, the exploration (and possibly exploitation) of a wide range of strong-field phenomena calls for substantially higher pulse energies, which can only be achieved by external amplification. This process is incapable of preserving the duration of few-cycle seed pulses even if laser media with the broadest amplification band available to date (see Fig. 4) are used. Gain narrowing is inherently coupled to a high gain, limiting the relative bandwidth $\Delta\omega/\omega_0$ of the amplified pulses typically to a few percent or less. Because wave packets comprising just a few field oscillation cycles are characterized by $\Delta\omega/\omega_0>0.1$, the generation of intense few-cycle light pulses requires pulse compression after amplification.

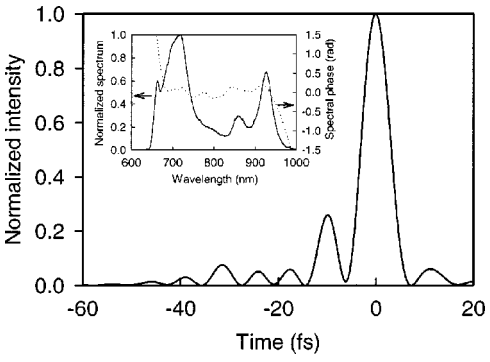

FIG. 17. Spectral intensity and phase (insert) and intensity envelope of sub-6-fs pulses produced by a semiconductor-saturable-absorber-initiated Kerr-lens mode-locking mirror-dispersion-controlled Ti:S laser (Sutter *et al.*, 1999). The data have been evaluated from a SPIDER (spectral phase interferometry for direct electric-field reconstruction) measurement (Gallmann *et al.*, 1999).

This can be implemented by spectral broadening in a multimode gas-filled hollow fiber (Nisoli *et al.*, 1996; Nisoli, De Silvestri, *et al.*, 1997; Nisoli, Stagira, *et al.*, 1997) followed by temporal compression upon reflection off chirped mirrors (Sartania *et al.*, 1997; Tempea and Brabec, 1998a), as illustrated schematically in Fig. 16. In strong contrast with pulse shortening in the oscillator, broadening of the laser-pulse spectrum can be effected dramatically upon one single passage through the nonlinear medium, owing to guided-wave propagation as explained above and shown in Fig. 18. Seeded with pulses of 20–25 fs in duration and 1.5–1.7 mJ in energy, the system described in the caption of Fig. 16 produces 5-fs pulses of energy of 0.7–0.8 mJ, implying a peak power of some 0.15 TW, at a repetition rate of 1 kHz. The technique is expected to be scalable to peak powers approaching the terawatt level. The pulses are delivered in a diffraction-limited beam and have recently been focused to intensities approaching 10^{18} W/cm^2. Figure 19 shows the temporal intensity envelope and the phase (Cheng *et al.*, 1999) as evaluated from a frequency-resolved optical gating measurement (Kane and Trebino, 1993; Trebino *et al.*, 1997) with φ_0 arbitrarily chosen to be zero. The clean front edge of the pulse is of prime importance for strong-field experiments. The time it takes for the intensity to rise from 10 to 90% of the peak is less than 5 fs and hence less than two field oscillation periods.

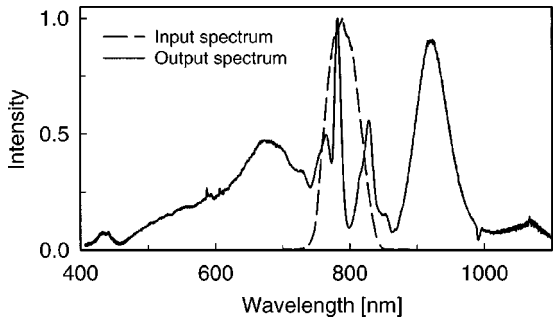

FIG. 18. Typical spectrum before (dashed line) and after (solid line) propagation through a hollow fiber having a channel diameter of 250 μm and a length of approximately 1 m. The waveguide is seeded with 25-fs, 1.5-mJ input pulses and filled with neon at a pressure of $\approx$1 bar.

To test the limits of currently available chirped mirror technology, sub-6-fs pulses from the compressor have been gently focused in atmospheric air at reduced energy levels and slightly broadened temporally (resulting in some positive chirp) such that the nonlinear index of air broadened the spectrum by some 30% uniformly across the laser beam, as predicted by the coupled-mode analysis reviewed in the previous subsection. Subsequent reflection off a few ultrabroadband chirped mirrors [see diagrams (a) and (b) in Fig. 10] compensated for the GDD and third-order dispersion of air and the SPM-induced chirp and resulted in the interferometric autocorrelation (Diels, Fontaine, *et al.*, 1985) depicted by the solid line in Fig. 20. The dotted line is calculated from the inverse Fourier transform of the measured spectrum (corrected for the spectrograph and detector response) under the assumption of no spectral phase modulation, yielding a pulse duration of 4 fs at a peak power of 30 GW (Cheng *et al.*, 1998). These are the shortest electromagnetic pulses demonstrated to date, comprising some one and a half field oscillation cycles within the full width at half maximum of their intensity envelope. These unique characteristics have far-reaching impacts on strong-field physics, some of which will be addressed in the remaining part of this paper.

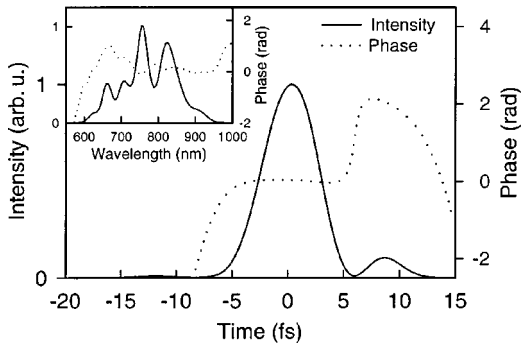

FIG. 19. Millijoule-scale pulses exiting the hollow-fiber chirped-mirror compressor: solid curve, intensity envelope; dotted curve, phase, with φ_0 chosen arbitrarily to be equal to zero; inset, spectrum. The data were retrieved from a frequency-resolved optical gating measurement (Cheng *et al.*, 1999). The pulse duration evaluated is $\tau_p = 5.3$ fs.

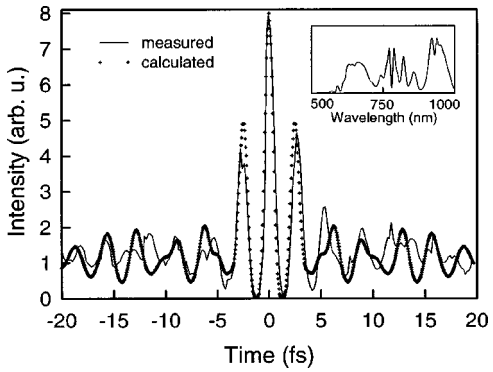

FIG. 20. Intense pulses originating from double-stage pulse compression, as described in the text and reported by Cheng *et al.* (1998): solid curve, measured interferometric autocorrelation; dotted curve, calculation from the inverse Fourier transform of the measured spectrum in the absence of a frequency-dependent phase, yielding a FWHM pulse duration of $\tau_p = 4$ fs; inset, spectrum.

D. Approaching the light oscillation period: Does the absolute phase of light matter?

Generating ultrashort pulses with durations approaching the light oscillation period $T_o = 2\pi/\omega_0 = \lambda_0/c$ brings up several questions for experimentalist and theorist alike: Are the techniques used for characterization in the multicycle regime still adequate and do they provide complete information about the characteristics of few-cycle wave packets? Does the description of ultrashort pulses in terms of carrier and envelope remain valid as the pulse duration τ_p approaches T_o? These questions are not quite independent of each other, given the fact that the determination of τ_p, defined as the full width at half maximum of the intensity envelope, relies on a physically meaningful definition of the intensity envelope.

First let us address the latter question, in order to provide a convenient mathematical framework for addressing the former. The complex amplitude (envelope) $\tilde{E}_a(t)$ of pulsed radiation permits the electric field $E(t)$ to be expressed as

$$E(t) = \tilde{E}_a(t) e^{-i\omega_0 t + i\varphi_0} + \text{c.c.} \tag{14}$$

For multicycle pulses, $\tilde{E}_a(t)$ can be derived from $E(t)$ by introducing the complex field $\tilde{E}(t) = (2\pi)^{-1/2} \int_0^\infty \tilde{E}(\omega) e^{-i\omega t} d\omega$, in which $\tilde{E}(\omega) = (2\pi)^{-1/2} \int_{-\infty}^\infty E(t) e^{i\omega t} dt$. This obeys $E(t) = \tilde{E}(t) + \text{c.c.}$, and hence $\tilde{E}_a(t)$ can be determined from $\tilde{E}(t) = \tilde{E}_a(t) e^{-i\omega_0 t + i\varphi_0}$, provided that ω_0 and φ_0 are known. The tilde represents a complex quantity throughout the paper. In order to avoid fast oscillations in $\tilde{E}_a(t)$, the reference frequency ω_0 must be roughly at the center of the spectrum of the wave packet. The precise choice of ω_0 is not critical for describing pulse propagation on the basis of Eq. (14). There are several possible definitions of ω_0, one of which,

$$\omega_0 = \overline{\omega} = \frac{\int_0^\infty \omega |\tilde{E}(\omega)|^2 d\omega}{\int_0^\infty |\tilde{E}(\omega)|^2 d\omega}, \tag{15}$$

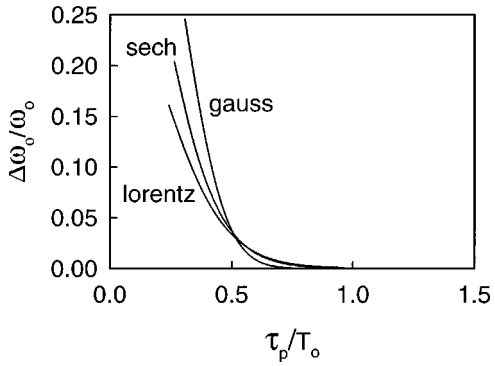

FIG. 21. Relative change $\Delta\omega_0/\omega_0$ in the carrier frequency, as defined in Eq. (15), caused by modifying the carrier phase by $\Delta\varphi=\pi/2$ as a function of the pulse duration for the following analytic pulse shapes: Gaussian, $A_g=\exp[-(1.17t/\tau_p)^2]$; Sechant hyperbolic, $A_s=\mathrm{sech}(1.76t/\tau_p)$; and Lorentzian, $A_l=1/[1+(1.29t/\tau_p)^2]$.

stands out for its minimization of the intensity-weighted phase variation of $\tilde{E}_a(t)$ (Diels and Rudolph, 1996). In spite of this important characteristic, there is some arbitrariness in the above definition of ω_0. Therefore it is important to stress that the major conclusions from the following considerations are not affected by the specific choice of a definition for ω_0. Now with ω_0 defined and φ_0 chosen arbitrarily so that the imaginary part of $\tilde{E}_a(t)$ is zero at the reference instant $t=0$ (which is, for practical reasons, often adjusted to coincide with the center of gravity of $|E(t)|^2$), the route to determining $\tilde{E}_a(t)$ from $E(t)$ is unambiguously prescribed.

The above definition of the complex amplitude envelope of a transient wave form (wave packet) is apparently valid irrespective of the duration of the wave packet. However, to legitimize the concept of carrier and envelope we must require that ω_0 and $\tilde{E}_a(t)$ remain *invariant* under a change of φ_0, the physical significance of which is confined to determining the relative position of the carrier wave with respect to the envelope. A shift of φ_0 by some $\Delta\varphi$ yields the new wave form $\tilde{E}'(t)=\tilde{E}_a(t)e^{-i\omega_0 t+i(\varphi_0+\Delta\varphi)}$, i.e., translates the carrier with respect to the envelope. In order that the definition of $\tilde{E}_a(t)$ and ω_0 be self-consistent, the modified wave $\tilde{E}'(t)=\tilde{E}(t)e^{i\Delta\varphi}$ must yield $\omega_0'=\omega_0$, which also implies $\tilde{E}_a'(t)=\tilde{E}_a(t)$. Intuitively, one expects the concepts of carrier and envelope to fail as the temporal extension of the transient wave form becomes comparable to the oscillation cycle of the wave.

In order to develop some feel for the parameter range in which one can rely on the carrier-envelope concept, we have computed ω_0 for $E(t)=E_{\mathrm{anal}}\sin(\Omega t)$ and ω_0' for its phase-translated counterpart $\tilde{E}'(t)=\tilde{E}(t)e^{i\Delta\varphi}$ for some of the most important analytic pulseforms. $\Delta\varphi=\pi/2$ was chosen to maximize the expected difference between ω_0' and ω_0 for short pulses. Figure 21 depicts $|\omega_0'-\omega_0|/\omega_0$ as a function of the pulse duration normalized to the oscillation period $T_{\mathrm{osc}}=2\pi/\Omega$. As anticipated, the requirement of phase invariance of carrier frequency and hence that of the envelope is met with a high accuracy for pulse durations that are long compared to T_{osc}. It is, however, somewhat surprising that this requirement is still well satisfied for extremely short wave forms with durations comparable to the carrier oscillation period T_{osc} and tends to be increasingly violated only as the pulse duration τ_p [full width at half maximum (FWHM)] of the intensity envelope $|\tilde{E}_a(t)|^2$) becomes shorter than the carrier period. It can be seen by inspection that this finding applies irrespective of the precise choice of either ω_0 or the temporal profile of (bell-shaped) wave packets.

In the multicycle regime the complex envelope $\tilde{E}_a(t)$ can also be used to calculate the cycle-averaged radiation intensity $I(t)\propto|\tilde{E}_a(t)|^2$, which yields the energy fluence $F=\int I(t)dt$. To what extent this approach remains accurate for $\tau_p\to T_o$ can be assessed when we calculate the energy fluence by integrating the instantaneous energy density flow proportional to $E^2(t)$ over the pulse and investigate its phase dependence. For a Gaussian pulse, the maximum relative variation of F upon varying φ_0 can be expressed as $\Delta F/F=\exp[-\pi\tau_p/T_{\mathrm{osc}}\ln 2)]$ (Reichert *et al.*, 1999), justifying the use of the cycle-averaged intensity from the envelope down to pulse durations approaching the carrier oscillation cycle. As a consequence, *the description of pulsed electromagnetic radiation in terms of carrier and envelope is self-consistent, unambiguous, and hence legitimate, for FWHM pulse durations down to the carrier oscillation cycle*, $\tau_p\geqslant T_o$ (Brabec and Krausz, 1997). This finding allows the powerful mathematical and physical concepts based on the envelope and carrier [developed originally for pulses that obey $\partial|\tilde{E}_a(t)|/\partial t\ll|\tilde{E}_a(t)|/T_o$] to be extended into a new regime of nonlinear optics, in which the interaction time is limited to the order of the optical cycle.

The violation of the phase invariance of ω_0 and hence $\tilde{E}_a(t)$ for $\tau_p<T_o$ is found to correlate with a rapid increase in the variation of the spectral intensity $|\tilde{E}(\omega)|^2$ with φ_0 at low frequencies near $\omega=0$. This finding sheds light on the mathematical origin of the failure of the carrier-envelope concept: the amplitude of the low-frequency ($\omega\ll\omega_0$) spectral components of pulsed radiation are not invariant under the transformation $\tilde{E}'(t)=\tilde{E}(t)e^{i\Delta\varphi}$, but sensitively depend on φ_0. For sufficiently broadband signals, the fractional weight of the low-frequency components becomes significant, causing ω_0, and hence $\tilde{E}_a(t)$, to become dependent on φ_0. The low-frequency components also have important implications for laterally confined (three-dimensional) wave-packet propagation, because they suffer from a stronger diffraction when carried in a laserlike beam. As a result, the low-frequency components are subject to increased attenuation on the beam axis with increasing z, giving rise to a truncation of the low-frequency part of the pulse spectrum, i.e., to a deformation of the wave packet. This effect was recently observed in the propagation of single-cycle THz pulses (Hunsche *et al.*, 1999).

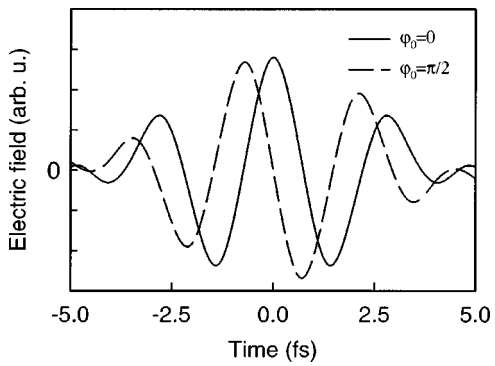

FIG. 22. Possible evolutions of the electric field in the 4-fs pulse obtained in the experiment summarized in Fig. 20 carried at a wavelength of 750 nm for two different pulse phases ($\phi_0 = 0, \pi/2$) with all other parameters $[\omega_0, \tilde{E}_a(t)]$ left unchanged. Variation of the absolute carrier phase ϕ_0 leaves the interferometric autocorrelation unchanged in Fig. 20.

We now return to the first question raised at the beginning of this subsection. Figure 22 depicts two (out of an infinite number of) possible evolutions of the electric field which yield the autocorrelation trace shown by the dotted line in Fig. 20. These evolutions are obtained by varying the absolute carrier phase φ_0 and leaving all other parameters of the pulse $[\omega_0, \tilde{E}_a(t)]$ unchanged. Clearly, the interferometric autocorrelation is invariant under changes of the absolute carrier phase and so are all other measurement techniques used for the characterization of ultrashort light pulses, including FROG (frequency-resolved optical gating) and SPIDER. This implies that none of the currently available techniques provides access to the absolute carrier phase φ_0, nor does a technique exist for controlling this parameter. In the multicycle regime of light-matter interactions, failure to gain access to φ_0 does not impair our ability to control nonlinear optical processes, because all known processes are insensitive to φ_0 for $\tau_p \gg T_o$. Hence *nonlinear optics may be fully controlled in terms of the amplitude envelope and frequency of intense light pulses in the regime of many cycle pulses*.

This situation changes dramatically as the interaction time between a light wave and atoms is confined to a period approaching the oscillation cycle of the light field, particularly for the strong-field regime (see Sec. IV), where the electric (and, at relativistic intensities, also the magnetic) field takes control over the evolution of nonlinear light-matter interactions. Under these conditions, interactions lasting merely a few optical cycles are greatly sensitive to the absolute phase φ_0 rather than only to the envelope $\tilde{E}_a(t)$ and frequency ω_0 of the incident radiation, as will be shown in Sec. VIII. As a consequence, gaining access to and controlling φ_0 in addition to $\tilde{E}_a(t)$ becomes indispensible for precise control of physical measurables originating from strong-field interactions in the few-cycle regime.

The issue of the absolute phase of few-cycle light pulses was first addressed by Xu *et al.* (1996). The experiments of Xu *et al.* revealed that the position of the carrier relative to the envelope is generally rapidly varying in the pulse train emitted from a mode-locked laser oscillator. This phenomenon arises because the carrier wave of the laser pulse gets shifted upon each round trip in the cavity, and the shift makes the carrier slide underneath the envelope in the output pulse train. To understand the origin of this carrier phase shift, we recall that initiating plane-wave propagation of the field given in Eq. (14) along the z axis from the plane $z=0$ in a linear medium results in a wave packet propagation that can be described by

$$E(z,t) = \tilde{E}_a(z, t-\beta_1 z) e^{i\beta_0 z - i\omega_0 t + i\varphi_0} + \text{c.c.}, \tag{16}$$

which can be obtained by solving the wave Eq. (29) in the absence of nonlinearities. Here $\beta_0 = \omega_0 n_0/c$ and $n_0 = \mathrm{Re}[n(\omega_0)]$ is the real part of the refractive index at $\omega = \omega_0$ and $\beta_1 = (\omega_0/c)\mathrm{Re}[(\partial n/\partial\omega)_{\omega_0}]$. The time retardation in the argument of the envelope indicates that the center of the wave packet propagates at a velocity of $v_g = \beta_1^{-1}$, which is referred to as the group velocity. It is therefore convenient to introduce a coordinate system moving with the pulse at the group velocity and following pulse evolution in this system. This can be simply done by performing the coordinate transformation $\tau = t - z/v_g$ and $\xi = z$. Equation (16) in this moving frame of reference can then be rewritten as

$$E(\xi,\tau) = \tilde{E}_a(\xi,\tau) e^{-i\omega_0 t + i\varphi(\xi)} + \text{c.c.},$$

where

$$\varphi(\xi) = \varphi_0 + \omega_0 \left(\frac{1}{v_{ph}} - \frac{1}{v_g} \right) \xi \tag{17}$$

and $v_{ph} = \omega_0/\beta_0$ represents the phase velocity.

By inspecting $\varphi(\xi)$, which determines the position of the carrier relative to the envelope, we can identify the difference between the phase delay $(\omega_0\xi/v_{ph})$ and the group delay $(\omega_0\xi/v_g)$ as the reason that the carrier slides under the envelope as the pulse circulates in the mode-locked laser. The difference between phase and group delay in transparent optical materials originates from the wavelength dependence of the (real) refractive index, which becomes obvious when we express the change in the carrier phase shift upon passage through a medium of length L as $\Delta\varphi(\xi) = 2\pi(\partial n/\partial\lambda)_{\lambda_0}\xi$, from which the dephasing length (Xu *et al.*, 1996)

$$L_{\text{deph}} = \frac{1}{2} \left| \frac{\partial n}{\partial \lambda} \right|_{\lambda_0}^{-1} \tag{18}$$

can be introduced. Here L_{deph} is the propagation length over which the carrier is offset by a phase of π with respect to the envelope. It can be as short as 29 and 19 μm in quartz and sapphire, respectively. As a consequence, $\varphi(\xi)$ is shifted by several dozen times 2π upon a full round trip of the laser pulse in a KLM/MDC Ti:S laser. The round-trip carrier phase shift (relative to the envelope) $\Delta\varphi_r = \varphi_{n+1} - \varphi_n$ causes a shift of the carrier with respect to the envelope by $\Delta\varphi_r - 2\pi m = \Delta\varphi_r'$ (where m is an integer chosen to yield $0 < \Delta\varphi_r' < 2\pi$)

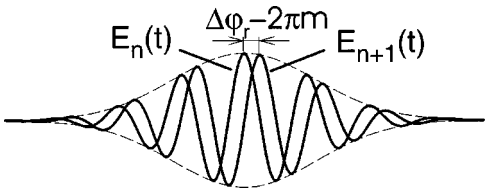

FIG. 23. Evolution of electric fields in two adjacent pulses in the pulse train emitted by a mode-locked laser. The phase shift $\Delta\varphi_r - 2\pi m$ can be measured by interferometric cross correlation (Xu *et al.*, 1996).

between any two laser pulses following one another in the output pulse train, as illustrated in Fig. 23. This shift can be measured by interferometric cross correlation (Xu *et al.*, 1996). It was recently pointed out that the physically relevant (relative) carrier shift $\Delta\varphi_r'$ offsets by $f_0=(\Delta\varphi_r'/2\pi)T_r^{-1}$ the frequency comb emitted by the mode-locked laser, resulting in locked frequencies that can be written as $f_m=f_0+mf_r$, where m is a (large) positive integer and $f_r=1/T_r$ is the pulse repetition rate (Reichert *et al.*, 1999).

By introducing adjustable dispersion with a pair of thin quartz wedges in the cavity (Xu *et al.*, 1996), $\Delta\varphi_r$ can be set equal to an integer multiple of 2π. Unfortunately, the carrier cannot be "locked" to the envelope in the output pulse train by this measure for an extended period. This is because intensity-dependent contributions to both the round-trip phase delay and the round-trip group delay translate small energy fluctuations into a rapidly accumulating jitter of φ, destroying phase stabilization on a time scale of microseconds (a few hundred to a few thousand round trips) in the KLM/MDC Ti:S laser (Xu *et al.*, 1996).

Measuring and subsequently stabilizing the absolute phase of few-cycle light generated by a mode-locked laser might become feasible by exploiting the phase sensitivity of some strong-field processes, which will be discussed in detail in Sec. VIII. Unfortunately, well-known and well-understood candidates such as optical-field ionization (Sec. VI) and high-order harmonic generation (Sec. VII) in atomic gases come into play only at intensity levels ($I>10^{14}\,\mathrm{W/cm^2}$) that are difficult to attain with pulses from an oscillator without subsequent amplification. Amplification can only be performed at strongly reduced repetition rates (every hundred-thousandth pulse or so), which would not allow carrier phase stabilization in the oscillator by a servo loop, if dephasing occurs during a few hundred or thousand round trips in the oscillator.

Replacing the atomic gas by a metal as the nonlinear medium and inducing photoemission from the surface of a metal in the tunneling regime (Sommerfeld, 1967) might provide low-energy oscillator pulses direct access to strong-field optics (Poppe, Fürbach, *et al.*, 1999). As a matter of fact, optical tunneling from a gold photocathode is predicted to occur (Toth *et al.*, 1991) and to be phase dependent at intensity levels (see Fig. 47 below) that can be reached by state-of-the-art sub-10-fs Ti:S oscillators (Xu *et al.*, 1998; Beddard *et al.*, 1999; Poppe, Lenzner, *et al.*, 1999). Once a phase-sensitive physical measurable (such as the photocurrent in the previous example) can be acquired, a servo loop for stabilizing φ_n can be constructed.

An entirely different approach to controlling the evolution of φ_n in the output pulse train was recently proposed (Telle *et al.*, 1999) and demonstrated (Reichert *et al.*, 1999) in the frequency domain. By locking different modes of the mode-locked lasers to different harmonics of a narrow-line reference source (Udem *et al.*, 1999a; Reichert *et al.*, 1999) or locking a mode to a frequency derived from another mode of the mode-locked laser by nonlinear conversion techniques (Telle *et al.*, 1999), the offset frequency $f_0=(\Delta\varphi_r'/2\pi)T_r^{-1}$ could be measured (with a much higher accuracy than is feasible with the previously demonstrated interferometric cross-correlation technique) and could be controlled with suitable cavity adjustments (Reichert *et al.*, 1999). It could, in principle, also be set equal to zero, implying phase stabilization. However, the actual stabilized value of the absolute carrier phase cannot be acquired by these techniques. Exploiting some strong-field process that is field dependent seems to be imperative to achieve this objective. Because precise control of individual optical frequencies is highly developed in frequency-domain metrology, a combination of the above-described time-domain (strong-field) and frequency-domain techniques appears to be the most promising route to realizing phase-controlled few-cycle pulse generation. Our ability to measure the absolute phase at the output of a mode-locked laser will also allow us to test field-dependent nonlinearities *inside* the laser oscillator for achieving phase-stable (strong-field) mode locking.

The generation of phase-stabilized few-cycle light pulses from a mode-locked laser will have major impact on both precision frequency-domain spectroscopy and high-field physics. For the former, a precisely known comb of harmonics of the laser repetition rate (each being a frequency standard once one single laser mode is locked to a reference frequency) spanning an unprecedented spectral range will become available. In the latter, the evolution of atomic and molecular systems as well as plasmas will become controllable directly with the electric (and magnetic) fields. Gaining access to the absolute phase of light and developing viable techniques for its control is undoubtedly one of the major challenges facing researchers in modern optics in the coming years.

IV. NONLINEAR RESPONSE OF ATOMS TO STRONG LASER FIELDS

The nonlinear response of matter to intense radiation manifests itself in a nonlinear dependence of the induced polarization (atomic dipole moment times density of atoms) on the electric (and possibly magnetic) field of the incident radiation. The nonlinearity can originate from distinctly different processes, depending on the intensity. At low and moderate intensities, the external laser field is much weaker than the static atomic Cou-

lomb field. As a consequence, the laser field only slightly perturbs the atomic quantum states under nonresonant excitation conditions. The energy levels suffer only a faint shift proportional to E_a^2, which is referred to as the ac Stark shift (Landau and Lifshitz, 1977). The atoms remain, with a high probability, in their ground state and the extension of the wave function of the ground state remains on the order of the Bohr radius a_B. Nonlinear interactions taking place under these conditions can be well described by a perturbative approach, and hence we refer to this parameter range as the *regime of perturbative nonlinear optics*.

If the electric-field strength becomes comparable to (or higher than) the binding atomic Coulomb field experienced by the outer-shell electrons, an electron can escape with a substantial probability from its bound state (via tunneling or above-barrier detachment) before the laser electric field reverses its sign. The electron wave packet liberated by optical-field ionization subsequently wiggles in the linearly polarized electric field. The amplitude of the wiggle exceeds the Bohr radius by several orders of magnitude and the cycle-averaged kinetic energy of the electron exceeds the binding energy W_b. The parameter range giving rise to these processes is referred to as the *strong-field regime* of nonlinear optics. The atomic polarization response is dominated by the ionization process and the contribution from the bound electrons is negligible.

Nonlinear polarization induced by optical-field ionization emerges only as long as the electron remains in close proximity to its parent ion. Once the electron is set free, its trajectory is governed by the Newtonian equations of motion, resulting in a linear response (with a small remaining nonlinearity originating from the parent ion's reduced polarizibility). A strong nonlinearity arises only at intensities order(s) of magnitude higher due to optical-field ionization stripping the next electron and/or to the wiggle energy of free electrons becoming comparable to their rest energy mc^2, indicating the onset of *relativistic nonlinear optics*.

Figure 24 assigns the relevant intensity regions to the above regimes of nonlinear optics for visible and near-infrared radiation. Here we focus on nonrelativistic light-matter interactions. We shall (i) review how exploitation of processes in the perturbative regime allows generation of intense light pulses in the few-cycle regime and (ii) demonstrate that these pulses are capable of significantly extending the frontiers of strong-field nonlinear optics. Whereas in the perturbative regime the intensity envelope governs the evolution of nonlinear optical processes, in the strong-field regime the electric (and at relativistic intensities also the magnetic) fields take control. Because the generation of ultrashort light pulses relies on perturbative processes, the phase φ_0 [see Eq. (14)] is unknown, and the electric field of these pulses is indefinite. The light fields are expected to become accessible when strong-field processes with few-cycle wave packets are induced (see Sec. VIII). In Secs. IV. A-IV.C, we analyze the polarization response of an atomic medium irradiated with strong laser fields and

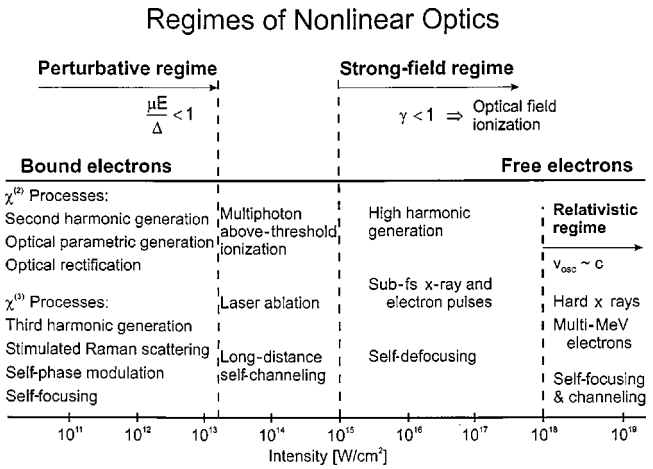

FIG. 24. Regimes of nonlinear optics. Only nonresonant interactions have been considered by assuming the detuning $\Delta\hbar$ to be larger than the photon energy (≈ 1 eV). The boundaries between different regimes are not sharply defined. In the strong-field regime, the intensity scale applies to the visible and near-infrared spectral range.

introduce field-strength scale parameters that roughly define the borders of the above regimes. The relation of the induced medium polarization to the incident fields is indispensable for describing the propagation of intense radiation in atomic media, i.e., for the interaction of intense light with matter in a macroscopic volume.

A. Perturbative nonlinear optics

At low and moderate intensities the polarization, P [$\mathrm{As/m^2}$] (where As represents Ampere seconds), of an atomic ensemble can be expanded into a Taylor series with respect to the electric field and can be given as the superposition of the linear and nonlinear responses $P = \varepsilon_0 \chi^{(1)} E + P_{nl}$, where

$$P_{nl} = \varepsilon_0 \chi^{(2)} E^2 + \varepsilon_0 \chi^{(3)} E^3 + \varepsilon_0 \chi^{(4)} E^4 + \cdots, \tag{19}$$

$\varepsilon_0 = 8.85 \times 10^{-12}$ As/V m is the vacuum permeability, and $\chi^{(k)}$ [$(\mathrm{m/V})^{k-1}$] is the kth-order susceptibility (Bloembergen, 1965). It is implicit in Eq. (19) that the atomic polarization instantly follows the change of the field, which is usually a good approximation even on a time scale of a few femtoseconds. This is because the induced atomic dipole moment is of purely electronic origin with a response time on the order of $1/\Delta$, where $\Delta = |\omega_{ik} - \omega_0|$, ω_{ik} represents the transition frequency from the initial (usually ground) quantum state i into some excited state k for which $|\omega_{ik} - \omega|$ is the minimum and the dipole transition matrix element μ_{ik} is nonzero, and ω_0 is the laser carrier frequency [see Eq. (14)]. Since the typical transition frequency from the atomic ground state to the lowest excited state significantly exceeds the laser frequency in the visible and near-infrared range, $1/\Delta$ is typically less than 1 fs. In molecules and condensed matter, nuclear motion may also provide a significant contribution to the induced dipole moment. This contribution has a response time of hundreds of femto-

seconds to several picoseconds, leading to a more complicated expression for P_{nl} (Shen, 1984; Boyd, 1992). Moreover, the polarization response is generally anisotropic, with $\chi^{(k)}$ being a kth-rank tensor connecting the Cartesian components of E and P_{nl} (Shen, 1984; Boyd, 1992).

When we disregard bound-free transitions, the quantum theory of linear and nonlinear optical susceptibilities yields the simple approximate expression

$$\frac{\chi^{(k+1)}E^{k+1}}{\chi^{(k)}E^{k}} \approx \frac{\mu_{ik}E_a}{\hbar\Delta} \approx \frac{eE_a a_B}{\hbar\Delta} = \alpha_{bb} \tag{20}$$

for the ratio of the successive terms in Eq. (19), where E_a is the (time-dependent) amplitude of the (linearly polarized) radiation, which is related to the complex amplitude defined in Eq. (14) as $E_a = 2|\tilde{E}_a|$, carried at the angular frequency ω_0, $\hbar = 1.06\times10^{-34}$ Js is Planck's constant, and a_B is the Bohr radius. For $\alpha_{bb} \ll 1$ bound-bound transitions are sufficiently weak to allow the expansion in Eq. (19) to converge.

For bound-free transitions the analysis of Keldysh (1965) yielded the scale parameter

$$\frac{1}{\gamma} = \frac{eE_a}{\omega_0\sqrt{2mW_b}} = \frac{eE_a a_B}{\hbar\omega_0} = \alpha_{bf}, \tag{21}$$

where $m = 9.11\times10^{-31}$ kg is the electron rest mass, $e = -1.6\times10^{-19}$ C is the charge, and $W_b \gg \hbar\omega_0$ is the binding energy of the most weakly bound electron, i.e., the ionization potential of the atom. For the derivation of the second expression we utilized the general connection $a_B = \hbar/\sqrt{2mW_b}$, which can be used as a "generalized" Bohr radius for atomic number >1 in expressions (20) and (21). If $\alpha_{bf} \ll 1$ bound-free transitions (i.e., ionization) can also be described perturbatively. In conclusion, *the regime of perturbative nonlinear optics is defined by* $\alpha_{bb}, \alpha_{bf} \ll 1$. A comparison of Eqs. (20) and (21) reveals that it is simply the ratio of detuning to laser frequency Δ/ω_0 that determines whether a bound-bound or bound-free transition violates the perturbative approximation for increasing field strengths.

In this paper we focus on the latter case, i.e., we assume $\Delta > \omega_0$, which is generally fulfilled in the interaction of visible and near-infrared radiation with atoms. In this spectral range the perturbative approach provides an adequate description of nonlinear processes up to intensities of around 10^{13} W/cm^2. Here we have also utilized the connection between intensity and electric field strength $I[\mathrm{W/cm^2}] = (1/2Z_0)E_a^2[\mathrm{V/cm}]$, where $Z_0 = \sqrt{\mu_0\varepsilon_0} = 377V/A$ is the vacuum impedance. In the above intensity range, Eq. (19) constitutes a good approximation, describing a wide range of nonlinear phenomena, a few of which are listed in Fig. 24. These include self-focusing and self-phase-modulation, which are the responsible nonlinear processes for femtosecond pulse generation in solid-state lasers (see Sec. II) and pulse compressors (see Sec. III).

For intensities of the order of 10^{13} W/cm^2, multiphoton ionization by simultaneous absorption of $N, N+1, N+2$, etc. photons comes into play (N being the smallest number of photons needed to reach the continuum), with the multiphoton channels of different order becoming comparable for increasing intensity. This is the phenomenon of above-threshold ionization (Agostini *et al.*, 1979; for a review, see Freeman *et al.*, 1992; Muller *et al.*, 1992). In this intensity regime the contributions of the electrons freed by multiphoton ionization and the induced atomic dipoles become comparable. One remarkable implication is that self-focusing due to the optical Kerr effect and self-defocusing due to free electrons tend to balance each other over long distances, resulting in self-channeling of intense femtosecond pulses over hundreds of meters (Braun *et al.*, 1995; Nibbering *et al.*, 1996; Wöste *et al.*, 1997). Unfortunately, in this intermediate regime between perturbative and strong-field nonlinear optics, the polarization response cannot be given analytically, and generally sophisticated numerical codes are needed for solving the time-dependent Schrödinger equation either directly (for a review see Kulander *et al.*, 1992) or indirectly by the Floquet ansatz (for a review, see Potvliege and Shakeshaft, 1992).

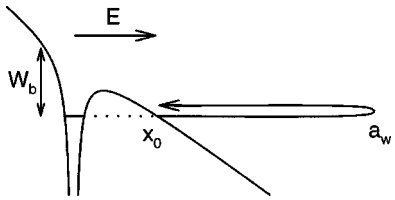

FIG. 25. Resultant (quasistatic) potential felt by the most weakly bound electron in the presence of a strong laser field. The electron can tunnel through the barrier. It is born at the position x_0 with some drift velocity (Corkum *et al.*, 1989) and follows the periodic motion of the laser field. The maximum amplitude during the first excursion is denoted by a_w.

B. The strong-field regime

For $\gamma^{-1} > 1$, the laser field suppresses the Coulomb potential so strongly that the wave function of the (most weakly bound) electron of energy $-W_b$ penetrates the barrier and reaches its outer side at x_0, as illustrated in Fig. 25, within a fraction of the laser oscillation cycle T_o (Keldysh, 1965). As a consequence, the resultant escape rate adiabatically follows the variation of the optical field, giving rise to a "quasistatic" ionization rate $w(E)$ that is dependent only on the instantaneous electric field and the ground state from which the electron tunnels out. This process is generally termed optical-field ionization and will be addressed in more detail in Sec. VI.

Using classical mechanics to describe the evolution of the electron wave packet ejected into the continuum (Corkum *et al.*, 1989; Corkum, 1993) and neglecting the Coulomb field of the source ion, we obtain for the amplitude of the wiggling motion of an electron $a_w = eE_a/m\omega_0^2$ in the linearly polarized field and the release position of the electron $x_0 \approx W_b/eE_0$. The cycle-averaged kinetic energy of the wiggling electron is given by $U_p = e^2E_a^2/4m\omega_0^2$, which is referred to as the *pon-*

deromotive potential ($U_p = 93$ eV and $a_w = 12.4$ nm at $I = 10^{15}$ W/cm^2 and $\lambda_0 = 1$ μm). The Keldysh parameter can be reexpressed with these quantities as $1/\gamma^2 = a_w/2x_0 = 2U_p/W_b$. Consequently, for $1/\gamma > 1$, the freed electron is substantially removed from the position of its birth and acquires a large kinetic energy within a fraction of T_o. This indicates that the external field becomes dominant and the influence of the static Coulomb field becomes small immediately after ionization. These circumstances define the *strong-field regime of nonlinear optics*.

On the time scale of T_o, classical mechanics provides a quantum-mechanically meaningful and correct description of the evolution of the center of gravity of the liberated electron wave packet, because its extension grows at a rate of typically less than 1 nm/fs due to quantum diffusion (Delone and Krainov, 1991; Dietrich *et al.*, 1994). Thus it remains small as compared to the wiggle amplitude in the strong-field regime. The drift motion of the ejected wave packet is correctly accounted for by classical mechanics on essentially unlimited time scales. In fact, combining the quasistatic tunneling rate $w(E)$ obtained from quantum mechanics with a classical approach to tracing the motion of the center of mass of the electron wave packet, released from the atom with zero initial velocity provides an accurate description of strong-field phenomena including above-threshold-ionization electron spectra (Corkum *et al.*, 1989; Corkum, 1993) and high-order harmonic generation (Corkum, 1993; Lewenstein *et al.*, 1994; Spielmann *et al.*, 1998).

Here we use the same approach to derive the constitutive law for the *nonrelativistic* strong-field regime. The trajectory of the center of mass of the freed electron wave packet $x(t)$ fulfills $|x(t)| \gg a_B$; hence the first time derivative of the macroscopic polarization $P(t)$ of an atomic ensemble is dominated by the current density of the freed electrons, which for a linearly polarized strong electric field is given by $\dot{P} \approx \dot{P}_{nl} = J_{free} = en_e\dot{x} + e\dot{n}_e x_0$. The dot represents the first partial time derivative and n_e is the density of free electrons. The second term originates from the appearance of electrons outside the Coulomb barrier, whereas the first term accounts for the contribution of free electrons moving away from the source atoms. This motion is governed by $m\ddot{x} = eE$. The relative weight of the second "localized" contribution to the current tends to decrease with respect to the first "plasma" contribution with increasing field strength due to the reversed scaling of x_0 and $\dot{x}$ with E. From $v_0 \approx 0$, it follows that the term $e\dot{n}\dot{x}$ vanishes in the expression of the second time derivative of the polarization, which therefore simplifies to

$$\ddot{P}_{nl}(t) = \frac{e^2}{m} n_e(t) E(t) + W_b \frac{\partial}{\partial t}\left(\frac{\dot{n}_e(t)}{E(t)}\right), \tag{22}$$

where

$$n_e(t) = n_a\left(1 - \exp\left[-\int_{-\infty}^{t} dt' w\{E(t')\}\right]\right), \tag{23}$$

n_a is the density of atoms, and $w(E)$ is the optical-field ionization rate (see Sec. VI). Equations (22) and (23) in combination with the optical-field ionization rate provide an explicit constitutive law for field-ionizing media. The first term in Eq. (22) predominantly modifies the phase of the propagating strong light wave, giving rise to a blueshift and broadening of its frequency spectrum. This is the only term showing up in previous work (Brunel, *et al.*, 1990; Gildenburg *et al.*, 1990; 1995; Wood *et al.*, 1991; Kan *et al.*, 1997). Our derivation yields an additional contribution proportional to W_b, giving proper account for the loss of light energy due to ionization. It will be shown in the next section that this term can be significant in regimes of practical importance. The same formalism can be used for deriving the constitutive law for arbitrary polarization. In deriving Eq. (22) we have neglected possible recombination of the electron into its original bound state approximately an optical cycle after its detachment, because this process occurs with a rather low probability and contributes negligibly to the medium polarization in the spectral range of an incident light field. Nevertheless, this recombination process plays a central role in high-order harmonic generation and hence will be discussed in detail in Sec. VII.

Whether or not Eq. (22) is energy conserving can be checked by calculating the change in field energy density due to interaction of the light pulse with the ionizing medium $\delta\rho_E = \int_{-\infty}^{\infty} dt\, E\dot{P}$. Using Eq. (22) we obtain

$$\delta\rho_E = -\frac{e^2}{2m}\int_{-\infty}^{\infty} dt_0 A^2(t_0)\dot{n}_e(t_0) - n_{ef}W_b, \tag{24}$$

where $A(t)$ is the vector potential defined by the relation $E = -\dot{A}$ and by the boundary condition $A(t \to \pm\infty) = 0$ and $n_{ef} = \lim_{t\to\infty} n_e(t)$. The second term in Eq. (24) is the energy density that needs to be transferred to the medium for producing free electrons with zero kinetic energy. Hence, for energy conservation, the first term must account for the kinetic energy of the free electrons. This results from a drift motion at a velocity $v_d = \lim_{t\to\infty}\dot{x}(t)$, which remains after the light pulse has left the (infinitesimal) interaction volume. Simple solution of $m\ddot{x} = eE$ by imposing the initial condition $v_0 = 0$ results in $v_d = (e/m)A(t_0)$ (Brunel, 1990). Therefore the first term in Eq. (24) totals the kinetic energy $mv_d^2/2$ of the free electrons ejected at all possible instants t_0, as required by energy conservation.

So far we have assumed that the polarization response of the atomic medium is *local*, i.e., at a fixed position in space $P(t)$ depends only on the electric-field evolution $E(t')$ for $t' \leq t$ at the same location. Therefore the spatial coordinate was dropped from the arguments of P and E for simplicity. This is the electric dipole approximation, which applies to good accuracy even after the onset of strong ionization as long as the interaction is nonrelativistic. For electric-field strengths sufficiently high to accelerate free electrons to velocities approaching c, this approximation breaks down, because the

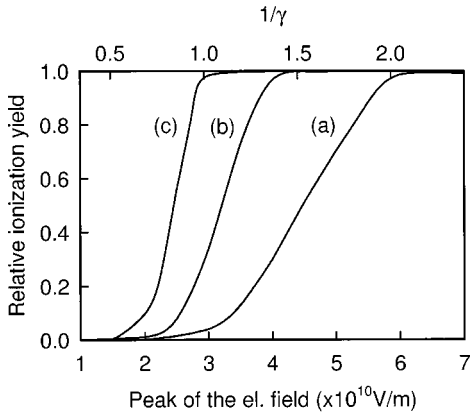

FIG. 26. Ionization yield in hydrogen after the laser pulse defined by Eq. (33) vs peak electric-field strength for laser pulses of durations of (a) $\tau_p = 10$ fs, (b) $\tau_p = 100$ fs, and (c) $\tau_p = 1000$ fs carried at $\lambda_0 = 0.8\,\mu$m. Ionization was calculated by numerical solution of the time-dependent nonrelativistic Schrödinger equation.

magnetic component of the Lorentz force becomes comparable to the electric component and free electrons travel distances comparable to the wavelength during T_o. As a consequence, the polarization response becomes a *nonlocal* function of the fields. Light-matter interactions become relativistic as the parameter

$$\alpha_{rel} = \frac{eE_0}{mc\omega_0} = \sqrt{\frac{4U_p}{mc^2}} \tag{25}$$

approaches or exceeds unity (Sarachick and Schappert, 1970). In the visible and near-infrared spectral range, this condition is fulfilled for intensities on the order of 10^{18} W/cm^2 and higher ($\alpha_{rel} \approx 0.9$ for $I = 10^{18}$ W/cm^2 at $\lambda = 1\,\mu$m), giving rise to a number of striking phenomena including relativistic self-channeling (Pukhov and Meyer-ter-Vehn, 1996), the generation of collimated multi-MeV electron jets (Modena *et al.*, 1995; Umstadter *et al.*, 1996), and nonlinear Thomson scattering (Chen *et al.*, 1998).

C. The role of the pulse duration in strong field physics

Before we leave this section, a brief comment on the role of the pulse duration τ_p in strong-field interactions is in order. Because the intensity $I(t)$ starts from zero in each laser pulse, nonlinear interaction always comes into play in the perturbative regime first, which is possibly turned into a strong-field process at higher intensities on the leading edge of the pulse. Clearly, the extent to which the overall interaction occurs in the strong-field regime sensitively depends on τ_p. Figure 26 depicts the fraction of hydrogen atoms left behind ionized by laser pulses of different duration as a function of the electric field amplitude at the pulse peak E_0. The inverse Keldysh parameter γ^{-1} [defined by Eq. (21)], corresponding to this field strength, is also depicted. The results shown in Fig. 26 reveal that in the visible/near-infrared spectral range ionization is essentially completed before the strong-field regime ($\gamma^{-1} > 1$) is entered for pulse durations of 1 ps or longer. Even for pulse durations as short as 100 fs, a significant fraction of the atoms is ionized in the intermediate region between the perturbative and strong-field regimes [Fig. (24)] via multiphoton channels of comparable magnitude (Agostini *et al.*, 1979). Only in the 10-fs regime does multiphoton preionization become negligible and optical-field ionization fully take over. As a consequence, *in the visible/near-infrared spectral range pure strong-field interactions can only be induced by few-cycle laser pulses*.

Figure 26 also reveals that the shorter the pulse, the stronger the laser field the electron experiences at the instant of its detachment. As a direct consequence, with a few-cycle laser pulse (i) the atom can be driven much more strongly before its dipole moment drops dramatically due to ionization and (ii) the detached electron can be ejected with a much higher drift velocity into the surrounding plasma. In addition, these processes can be confined temporally to a small fraction of T_o. Hence few-cycle light pulses open up previously inaccessible parameter regimes in high-field physics.

V. PROPAGATION OF INTENSE LIGHT PULSES

The constitutive laws derived in the previous section relate the induced nonlinear polarization P_{nl} to the driving electric field. The Fourier transform of $P_{nl}(t)$ generally contains frequency components within and around the spectral range of the incident light pulse. It may also contain frequency components far from ω_0, giving rise to high-order harmonics of the laser field, which will be addressed in Sec. VII. Here, we consider the components near ω_0, which modify the light pulse upon propagation through an extended interaction volume.

In the nonrelativistic regime, i.e., within the frame of the dipole approximation, a first-order propagation equation, which contains only the first-order derivative with respect to the propagation coordinate, can be derived. The significance of the first-order propagation equation lies in the fact that it can be solved with substantially less computational effort than can Maxwell's wave equation (Ziolkowski and Judkins, 1993), which is of second order in the propagation coordinate. In its most universal, although not directly usable, form the first-order propagation equation can be formally given in the complex Fourier domain as

$$[\partial_z - ik(\omega)]\tilde{E}(\mathbf{r},\omega) = \frac{i}{2k(\omega)}\nabla_\perp^2 \tilde{E}(\mathbf{r},\omega) - \frac{i\omega}{2\varepsilon_0 n(\omega) c}\hat{F}[\tilde{P}_{nl}(\mathbf{r},t)]; \tag{26}$$

for a derivation see Appendix B. The first-order propagation equations applying specifically to the perturbative and strong-field regimes will be derived from Eq. (26) below. Here, $\tilde{E}(\mathbf{r},\omega) = \hat{F}[E(\mathbf{r},t)]$, the Fourier transform is defined by $\tilde{f}(\mathbf{r},\omega) = \hat{F}[f(\mathbf{r},t)] = \int dt\, f(\mathbf{r},t)\exp(i\omega t)$. Here the tilde again represents complex quantities. Fur-

ther, the light wave is assumed to propagate along the z direction, $k(\omega)=\omega n(\omega)/c$ is the (generally complex) propagation constant, $n(\omega)$ is the linear refractive index, $\nabla_\perp=\partial_x^2+\partial_y^2$ is the transverse Laplace operator, and ∂_i stands for partial derivation with respect to coordinate i.

Two approximations lead to Eq. (26). First, the electric field is assumed to be slowly varying (i.e., exhibiting little variation over a distance of one wavelength) in the transverse dimensions, $|\partial_{x,y}\tilde{E}(\mathbf{r},\omega)|\ll\beta_0 E$, where $\beta_0=2\pi/\lambda_0$. This assumption allows wave propagation to be described with the *scalar wave equation* (Yariv and Yeh, 1984). Second, the wave packet is assumed to be subject to little change along a propagation distance equal to the wavelength, which has been referred to as the *slowly-evolving-wave approximation* (Brabec and Krausz, 1997).

It is generally rather inconvenient (in some cases impossible) to handle the Fourier transform of P_{nl}; therefore a transformation of Eq. (26) into the time domain is desirable. Fortunately, this is feasible in both the perturbative and the strong-field regimes of nonlinear optics, but for entirely different physical and mathematical reasons. Hence, starting from Eq. (26), different routes must be followed to reach the first-order propagation equation applicable to the respective parameter ranges.

A. Perturbative nonlinear optics

In the perturbative regime (assuming nonresonant interaction), the nonlinear response is usually much weaker than the linear one, $|P_{nl}|\ll|\varepsilon_0\chi^{(1)}E|$; hence dispersive effects resulting from the frequency dependence of the linear response tend to significantly affect femtosecond pulse propagation. Proper description of dispersive effects in the time domain relies on an expansion of $k(\omega)$ in a power series about the carrier frequency ω_0, which requires a physically meaningful definition of ω_0. This is feasible even for pulse durations approaching the carrier oscillation period T_o, as concluded in Sec. III, permitting a decomposition of wave packets into carrier and envelope,

$$E(\mathbf{r},t)=\tilde{E}_a(\mathbf{r},t)e^{i(\beta_0 z-\omega_0 t+\varphi_0)}+\text{c.c.} \tag{27}$$

Here $\tilde{E}_a$ is the complex envelope decribing both the amplitude envelope and possible phase modulation, $\beta_0=\mathrm{Re}[k(\omega_0)]=\omega_0 n_0/c$ and $n_0=\mathrm{Re}[n(\omega_0)]$. Owing to the simple power law connecting P_{nl} to E, as given by Eq. (19), the induced nonlinear polarization wave carried at ω_0 can be expressed as

$$P_{nl}(\mathbf{r},t)=\tilde{B}(\mathbf{r},t,\tilde{E}_a)e^{i(\beta_0 z-\omega_0 t+\varphi_0)}+\text{c.c.} \tag{28}$$

in the perturbative regime. These circumstances allow one to derive from Eq. (26) a time-domain first-order propagation equation for $\tilde{E}_a(\mathbf{r},t)$ that is free from the fast-oscillating component of E and P_{nl} (Appendix B):

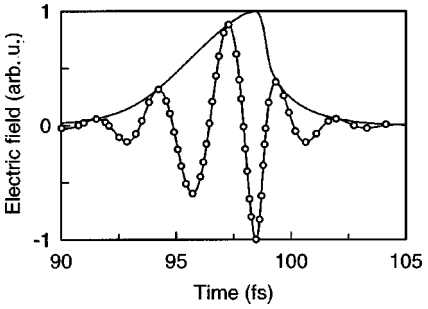

FIG. 27. Solution of the first-order propagation (FOP) equation [Eq. (29)] in a nonlinear Kerr medium, characterized by Eq. (30) in arbitrary units, vs propagation time: solid curve with circles, electric-field strength; solid curve without circles, the field envelope. The FOP equation was solved by a split-step Fourier method (Agrawal, 1995). ○, the electric field obtained from a solution of the Maxwell equation. In advancing the coupled Maxwell equations in space, a leapfrog method was used; the time derivatives were calculated by utilizing a fast Fourier transform. The initial pulse has a sech shape and the parameters are $I_0=4\times10^{13}\,\mathrm{W/cm^2}$, $n_2=3\times10^{-16}\,\mathrm{cm^2/W}$, $\omega_0=2.35\,\mathrm{fs}^{-1}$ ($\lambda_0=0.8\,\mu\mathrm{m}$, $T_0=2.67\,\mathrm{fs}$), $\tau_p=T_0=2.67\,\mathrm{fs}$ (one optical cycle within the FWHM width of the pulse), $n_0=1.45$, $dn/d\omega|_{\omega_0}=0$ (no dispersion), propagation distance $z=20\,\mu\mathrm{m}$, and propagation time $t=96.7\,\mathrm{fs}$. In the absence of dispersion, self-steepening due to the Kerr nonlinearity creates an optical shock wave at the trailing edge of the pulse. The critical distance for self-steepening is 23.26 μm, which is close to the chosen propagation distance. Even along the shock front, where the change of the envelope is comparable to the carrier frequency, the two solutions are virtually identical.

$$\begin{aligned}(\partial_z+\beta_1\partial_t)\tilde{E}_a(\mathbf{r},t)&=-\frac{\alpha_0}{2}\tilde{E}_a+i\hat{D}\tilde{E}_a+\frac{i}{2\beta_0}\hat{T}^{-1}\nabla_\perp^2\tilde{E}_a\\&\quad+\frac{\beta_0}{2\varepsilon_0 n_0^2}i\hat{T}\tilde{B}(\mathbf{r},t,\tilde{E}_a),\end{aligned} \tag{29}$$

where $\hat{T}=1+(i/\omega_0)\partial_t$, $\hat{D}=-(\alpha_1/2)\partial_t+\Sigma_{m=2}^{\infty}(\beta_m+i\alpha_m/2)m!^{-1}(i\partial_t)^m$, $\beta_m=\mathrm{Re}[(\partial^m k/\partial\omega^m)_{\omega_0}]$, and $\alpha_m=\mathrm{Im}[(\partial^m k/\partial\omega^m)_{\omega_0}]$. The lowest-order and hence dominant contribution to $\tilde{B}$ is introduced by the optical Kerr effect:

$$\tilde{B}=2\varepsilon_0\Delta n\tilde{E}_a=\frac{4\varepsilon_0 n_0}{Z_0}n_2|\tilde{E}_a|^2\tilde{E}_a, \tag{30}$$

where Δn is given by Eq. (1) and the relationship $I=(2n_0/Z_0)|\tilde{E}_a|^2$ connecting the cycle-averaged intensity with the complex envelope of the electric field was used. Because the optical Kerr effect represents the dominant nonlinear effect in the perturbative regime, Eq. (29) in combination with Eq. (30) covers a wide range of phenomena, including those of central importance for the generation and manipulation of ultrashort pulses (see Sec. III). The results presented in Fig. 27 confirm that the first-order propagation Eq. (29) works well down to the single-cycle regime, and recent investi-

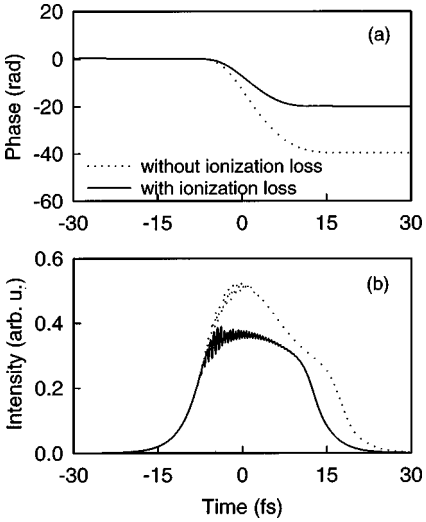

FIG. 28. A frequency-doubled Ti:sapphire laser pulse ($\lambda_0 = 0.4\,\mu$m) after a propagation distance of 8 mm in helium (500 Torr): (a) Phase; (b) intensity envelope for the following laser parameters: $I_0 = 2\times10^{15}$ W/cm^2, $\tau_p = 10$ fs. Dotted curve, the solution of the wave Eq. (31), in one space dimension without the ionization-loss term; solid curve, solution with the ionization-loss term. Ionization loss appears to have a strong influence on the evolution of a few-cycle laser pulse. Because more electrons are ionized at the peak of the pulse than in the pulse wings, the ionization loss leads to a stronger reduction of the pulse peak and hence, to lengthening of the pulse. As a result the nonlinear interaction saturates faster and the blue-shifting and spectral broadening of the pulse is reduced. The observed behavior has important implications for strong-field phenomena, such as a modification of the effective interaction length for x-ray lasing and high harmonic generation.

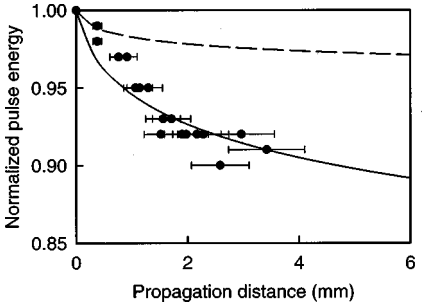

FIG. 29. Output pulse energy normalized to input pulse energy vs propagation distance for a laser pulse propagating in helium at a pressure of 500 Torr, showing the loss experienced by a laser pulse in a tunnel ionizing medium. ●, experimental values obtained with a laser pulse of $\tau_p \approx 5$ fs with $\lambda_0 = 0.8\,\mu$m and of $I_0 \approx 2\times10^{15}$ W/cm^2. The error bars relate to an estimated $\pm 20\%$ uncertainty in the measurement of the gas-interaction length. Solid and dashed curves, the theoretical values calculated from a solution of the first-order propagation wave equation [Eq. (31)] with and without the ionization loss term for peak intensites 2 and 3×10^{15} W/cm^2. Our analysis clearly reveals the necessity of the ionization loss term to account for the experimental data.

gations reveal that it also accurately accounts for the spatiotemporal dynamics of tightly focused femtosecond pulses (Fibich and Papanicolaou, 1997; Ranka and Gaeta, 1998; Zozulya *et al.*. 1999). Its simplest one-dimensional form (with $\alpha_m = 0$ for $m \geqslant 0$ and $\beta_m = 0$ for $m \geqslant 3$) is known as the nonlinear Schrödinger equation and has been widely used for modeling ultrashort pulse propagation in optical fibers (Agrawal, 1995).

B. The strong-field regime

A strikingly different approach must be taken in the strong-field regime. A glance at Eqs. (22) and (23) reveals that P_{nl} cannot be cast in the form given in Eq. (28), hence the ansatz (27) is not beneficial. On the other hand, P_{nl} originating from the electrons set free in the atomic ensemble is much larger than the contribution of the remaining bound electrons to the overall polarization response. As a consequence, linear dispersion is negligible as compared to that introduced by P_{nl}. Using the approximation $n(\omega) \approx 1 \rightarrow k(\omega) \approx \omega/c$, the combination of Eqs. (26) and (22) yields

$$\left(\partial_z + \frac{1}{c}\partial_t\right) E(\mathbf{r},t) = \frac{c}{2}\nabla_\perp^2 \int_{-\infty}^{t} dt' E - \frac{e^2}{2\varepsilon_0 mc}\int_{-\infty}^{t} dt' n_e E - \frac{W_b}{2\varepsilon_0 c}\frac{\partial_t n_e}{E}, \tag{31}$$

where $n_e(\mathbf{r},t)$ is connected to E by Eq. (23) and by the quasistatic optical-field ionization rate introduced in Sec. VI. In contrast with Eq. (29), this first-order propagation equation applies directly to the real electric field (Esarey *et al.*, 1991). In combination with the optical-field ionization rate, this equation provides a powerful tool for describing ultrashort-light-pulse propagation in a field-ionizing gas medium (Geissler *et al.*, 1999a). Like Eq. (29), this equation is valid within the frame of the slowly-evolving-wave approximation (Brabec and Krausz, 1997), which applies to good accuracy as long as the condition $\omega_p^2/\omega_0^2 \ll 1$ is fulfilled, where

$$\omega_p = \left(\frac{e^2 n_e}{m\varepsilon_0}\right)^{1/2} \tag{32}$$

is the plasma frequency of the ionized propagation medium. If the plasma frequency is much lower than the laser carrier frequency, Eq. (31) provides an accurate description of the interaction of intense femtosecond light pulses with an extended atomic gas target in the intensity range confined by $\gamma < 1$ and $\alpha_{rel} \ll 1$. As Eq. (31) depends on the electric field and no complex envelope was defined, it is valid for arbitrarily short pulse durations. Figure 28 shows the intensity envelope and phase of initially 5-fs pulses after propagation through ionizing helium, calculated using Eq. (31). The obtained

energy loss suffered by the laser pulse according to Eq. (24) is in good agreement with experimental observations (Fig. 29).

Equations (31) and (23) take proper account of nonlinear interactions in the strong-field regime where the use of intense few-cycle pulses pushes the nonlinear response of (ionizing) matter to unprecedented extremes. As a result, coherently generated harmonics of the driving laser radiation now exceed the 300th order. Modeling even predicts significant further improvement (in terms of both photon energy and conversion efficiency) in previously unaccessed parameter ranges and provides relevant guidelines for the experimenters (Sec. VII). This same theoretical framework also accounts for the fascinating temporal behavior of x-ray harmonic radiation (Sec. VII) as well as the dependence of strong-field processes on the carrier phase in few-cycle wave packets (Sec. VIII).

VI. OPTICAL-FIELD IONIZATION OF ATOMS

When matter is exposed to intense laser fields, a wealth of exciting phenomena can be observed, including high harmonic generation (Corkum, 1993), above-threshold ionization (Corkum *et al.*, 1989), atomic stabilization (Pont and Gavrila, 1990), x-ray lasing (Lemoff *et al.*, 1995; Hooker *et al.*, 1995), laser-induced damage of dielectrics (Du *et al.*, 1994; Stuart *et al.*, 1995; Lenzner *et al.*, 1998; Tien *et al.*, 1999) and molecular dissociation (Seidemann *et al.*, 1995; Chelkowski *et al.*, 1996). The key process triggering all of these strong-field phenomena is ionization. The theoretical investigation of these processes is significantly simplified by the analytic description of ionization that is available in the limiting cases characterized by $\gamma \gg 1$ and $\gamma \ll 1$ [see Eq. (21)]. The two limiting cases of multiphoton ionization and optical-field ionization are illustrated schematically in Figs. 30(a)–(c), respectively.

In what follows we shall restrict our discussion to the strong-field limit $\gamma \approx < 1$, for which significant ionization takes place. In this parameter range the quasistatic approximation is valid, which relies on the assumption that the perturbed electron wave function reaches a quasistatic state before the electric field changes significantly (Shakeshaft *et al.*, 1990). Then the fraction of electrons ionized in the laser field $E(t)$ as a function of time t may be calculated by Eq. (23). At the threshold for the detachment of the second (or higher) electrons, Eq. (23) must be generalized by calculating a sum over the individual ionization processes, $(1/n_a)\Sigma_i n_{ei}(t)$, determined by the ionization rates w_i for the ith electron. Furthermore, possible nonsequential ionization channels must be taken into account (Fittinghoff *et al.*, 1992; Corkum, 1993; Walker *et al.*, 1994; Augst *et al.*, 1995; Lablanquie *et al.*, 1995; Brabec *et al.*, 1996; Dorner *et al.*, 1998; Rosen *et al.*, 1999).

The power of the quasistatic approximation rests on the fact that ionization in time-varying laser fields may be calculated by using the static field ionization rate w. There exist two approaches for analytic calculation of

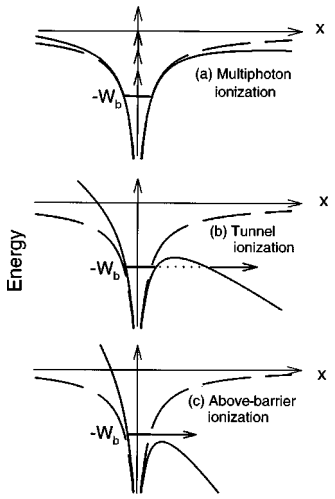

FIG. 30. Regimes of atomic ionization. Exposing an atom to an intense laser field will result in a modified potential (solid curve) composed of the Coulomb potential (dashed curve) and the time-dependent effective potential of the optical pulse. (a) At moderate intensities the resulting potential is close to the unperturbed Coulomb potential and an electron can be liberated only upon simultaneous absorption of N photons, resulting in multiphoton ionization. The multiphoton ionization rate scales with the Nth power of the intensity of the optical pulse. (b) At sufficiently high field strengths the Coulomb barrier becomes narrow, allowing optical tunneling ionization to take over and resulting in a tunneling current that follows adiabatically the variation of the resultant potential. (c) At very high field strengths, the electric field amplitude reaches values sufficient to suppress the Coulomb barrier below the energy level of the ground state, opening the way to above-barrier ionization.

static field ionization rates, namely, the Keldysh theory (Keldysh, 1965; Reiss, 1980) and the Ammosov-Delone-Krainov theory (Oppenheimer, 1928; Perelomov *et al.*, 1996; Ammosov *et al.*, 1986). In Fig. 31, the Ammosov-Delone-Krainov and Keldysh ionization rates for hydrogen and helium atoms exposed to a static electric field are compared with the rates obtained from an exact numerical solution of the time-independent Schrödinger

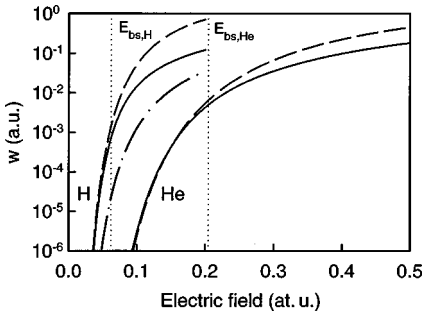

FIG. 31. Static field ionization rates in hydrogen and helium atoms vs the electric-field strength in atomic units: solid curve, numerical result; dashed curve, Ammosov-Delone-Krainov formula; dash-dotted curve, Keldysh theory for hydrogen. The dotted line denotes the barrier suppression field strength for H and He.

equation (Scrinzi *et al.*, 1999). The Keldysh theory predicts ionization rates that are smaller by 1–2 orders of magnitude. The reason for this discrepancy is the neglect of the Coulomb potential in the Keldysh theory.

By contrast, the Ammosov-Delone-Krainov rate is remarkably accurate in the tunneling regime characterized by $\gamma<1$ and $E<E_{bs}$. Here E_{bs} is the external field strength suppressing the peak of the binding potential to $-W_b$ along the direction of the electric field. For $E \geqslant E_{bs}$, the electron escapes "above the barrier" from its bound state (Augst *et al.*, 1989; Krainov, 1997) as illustrated in Fig. 30(c); therefore we refer to this process as above-barrier ionization. For $E \geqslant E_{bs}$, the Ammosov-Delone-Krainov theory increasingly overestimates the ionization rate and tends to lose its validity. In hydrogenlike atoms, the barrier supression field strength in atomic units is given by $E_{bs}=W_b^2/(4Z)$, where Z is the charge of the residual atom. Inserting the barrier supression field strength into the Keldysh parameter, we obtain $\gamma_{bs}=16\omega_0 Z/(2W_b)^{1.5}$. For a hydrogen atom and for a center wavelength $\lambda_0=0.8\,\mu$m, $\gamma_{bs}\approx 1$ so that tunneling does not take place. When the laser peak intensity is increased multiphoton ionization goes over directly into above-barrier ionization. Further, for the valence electrons of the noble gases and for the visible and near-infrared wavelength range, $\gamma_{bs}\approx 0.5$–2, showing the dominance of above-barrier ionization in this experimentally important parameter regime. Tunneling plays a dominant role only in the low-frequency limit that is realized for large λ_0 or W_b. For example, $\gamma_{bs}\approx 0.05$ for valence electrons of noble gases exposed to CO_2 laser radiation at $\lambda_0=10\,\mu$m.

It was shown recently that for $\gamma \approx < 1$ above-barrier ionization may also be calculated by using the quasistatic approximation (Scrinzi *et al.*, 1999). Therefore, in order to describe above-barrier ionization correctly, numerically determined, static ionization rates for a broad range of atoms are required. The exact static ionization rate of helium plotted in Fig. 31 was obtained by a solution of the two-electron Schrödinger equation (Scrinzi *et al.*, 1999). Currently, exact static rates $w(E)$ exist only for hydrogen and helium. It is hoped that $w(E)$ can be computed for more complex atoms by using, e.g., R-matrix techniques (Burke and Burke, 1997) in the near future.

Finally, we use Eq. (23) in combination with the computed $w(E)$ as given in Fig. 31 to investigate strong-field ionization induced by light pulses containing only a few field oscillation cycles. The laser pulse used in our calculation is defined by the vector potential

$$A(t)=-(E_0 c/\omega_0)\,\mathrm{sech}(t/\tau_0)\sin(\omega_0 t+\varphi_0), \qquad (33)$$

from which the electric field is determined by $E=-dA/dt$. Here, the normalization parameter τ_0 is related to the FWHM pulse duration by $\tau_p=1.76\tau_0$. The peak intensity of the laser pulse in Fig. 32 is $I_0=4\times 10^{15}\,\mathrm{W/cm^2}$. Finally, the center wavelength is $\lambda_0=0.8\,\mu$m ($\omega_0=0.057$ a.u.) and the initial phase is chosen as $\varphi_0=0$.

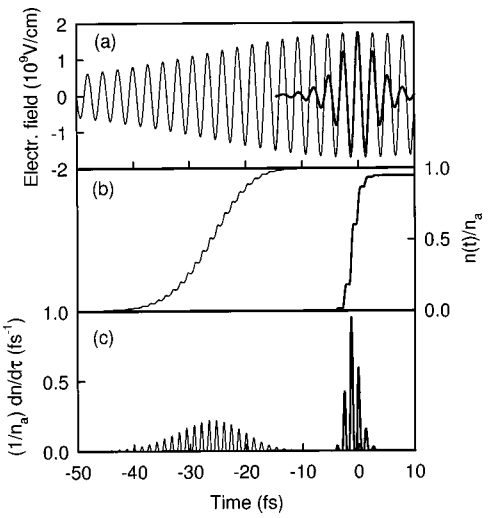

FIG. 32. Helium in the presence of a linearly polarized electric field of a laser pulse with $\lambda_0=0.8\,\mu$m and a peak intensity $I_0=4\times 10^{15}\,\mathrm{W/cm^2}$: (a) electric field; (b) fraction of ionized electrons; (c) instantaneous ionization rate. The thin and the heavy lines represent pulses of durations of $\tau_p=50$ fs and $\tau_p=5$ fs, respectively.

Figure 32 depicts ionization caused by a 50-fs and a 5-fs pulse in helium. In the multi-cycle regime, a number of ionized helium atoms can accumulate over many optical cycles. As a result, the ground state is depleted long before the peak of the laser pulse. For few-cycle pulses, saturation of ionization is shifted to considerably higher intensities. Consequently the ionization rate is enhanced and can even become comparable to the carrier frequency, $(dn_e/dt)/(n_a\omega_0)\approx 0.5$. The extreme ionization dynamics created by few-cycle pulses have important consequences for atomic and plasma physics, some of which which will be discussed in the following sections. In Sec. VII we shall analyze implications of few-cycle laser pulses for high harmonic generation, such as the role of nonadiabatic propagation effects, phase matching, and attosecond pulse generation. In Sec. VIII it will be shown that optical-field ionization, high harmonic generation, and other fundamental strong-field processes induced by few-cycle laser pulses become phase dependent, opening the way for control of atom-field interactions with phase-controlled laser fields.

VII. HIGH-ORDER HARMONIC GENERATION

The interaction of intense linearly polarized ultrashort laser pulses with atoms (McPherson *et al.*, 1987; Li *et al.*, 1989; Sarukura *et al.*, 1991; Crane *et al.*, 1992; Faldon *et al.*, 1992; Kondo *et al.*, 1993; L'Huillier and Balcou, 1993; Macklin *et al.*, 1993; Perry and Crane, 1993; Wahlström *et al.*, 1993; Tisch *et al.*, 1994; Myazaki and Takada, 1995), atom clusters (Donelly *et al.*, 1996; Hu and Xu, 1997), and molecules (Ivanov and Corkum, 1993; Liang *et al.*, 1994) results in the generation of high-order harmonic radiation in the extreme ultraviolet (xuv) and soft-x-ray spectral range. For recent reviews,

see the articles of Joachain *et al.* (2000) and of Salières *et al.* (1999). The moderate pump-energy requirements and the excellent coherence make high harmonic generation a promising approach to developing a compact bright laboratory short-wavelength source. Rapid progress in high harmonic generation over the last few years has already led to the first applications in core-level (Haight and Seidler, 1994) and plasma (Theobald *et al.*, 1996) spectroscopy and in x-ray fluorescence analysis (Schnürer, Streli, *et al.*, 1999). Unfortunately, the efficiency of high harmonic generation is still too low for many other potential applications. A major limitation arises from the fact that generation of high-order harmonics is inextricably linked to the generation of free electrons, which leads to a phase mismatch between the fundamental and the harmonic beams, limiting the maximum coherence length over which harmonic radiation can grow. As shorter wavelengths are generated in the presence of a higher free-electron density, the phase mismatch increases rapidly with the harmonic order, thus also setting a limit to the highest achievable harmonics. Resolution of this fundamental problem would pave the way towards a number of revolutionary applications, including laboratory x-ray microscopy, holography, and femtosecond time-resolved x-ray diffraction and absorption experiments.

Recently it was demonstrated that the phase mismatch can be drastically reduced by the use of ultrashort driver pulses (Zhou *et al.*, 1996; Schafer and Kulander, 1997), which improved conversion efficiency and extended the range of high harmonic generation into the water window (2.3–4.4 nm) for the first time (Chang *et al.*, 1997; Spielmann *et al.*, 1997; Schnürer *et al.*, 1998). In addition, theoretical analysis has predicted the possibility of generating attosecond pulses via few-cycle-driven high harmonic generation (Christov *et al.*, 1997; de Bohan *et al.*, 1998; Tempea *et al.*, 1999a). In this section we shall review the fundamentals of high harmonic generation with particular emphasis on its implementation with few-cycle driver pulses. We begin with the (microscopic) analysis of the strongly driven atomic dipole moment, then address (macroscopic) propagation effects and phase-matching issues, investigate the temporal structure of the emitted short-wavelength radiation, and briefly discuss possible applications. Atomic units are used for the study of the microscopic response, whereas SI units are preferred in the macroscopic analysis.

The theoretical results are compared with available experimental data, obtained with the sub-10-fs-laser-driven kHz-rate high-harmonic source developed at the Vienna University of Technology (Spielmann *et al.*, 1997; Schnürer *et al.*, 1998 1999b). The laser-atom interaction volume in this source is formed by a thin-wall nickel tube, in which holes are made by the pump laser beam; this tube can be squeezed to yield an effective interaction length as short as <0.2 mm (see Fig. 33). Spectral characterization of high harmonic radiation has traditionally been implemented by means of wavelength dispersive spectrometry based on a grating spectrograph

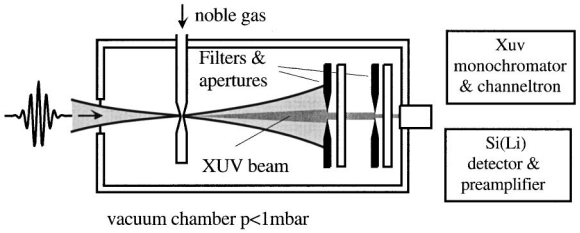

FIG. 33. Schematic of the experimental setup of a typical high harmonic generation experiment. The laser beam is focused into the target chamber. The target is formed by a tube, in whose walls are holes bored by the laser itself. The tube is continuously backed with some noble gas. The generated high harmonic radiation is measured either by wavelength-dispersive spectral analysis or by energy-dispersive x-ray spectrometry (courtesy of Ch. Spielmann).

all the way from vacuum ultraviolet to soft x-ray wavelengths. Alternatively, high pulse repetition rates ($\geqslant 1$ kHz) allow the use of energy dispersive spectrometry in the soft-x-ray regime ($\lambda < 10$ nm). Such a system consisting of a cooled semiconductor (e.g., lithium-drifted silicon) crystal detector and a multichannel pulse-height analyzer offers a significantly better signal-to-noise ratio and hence higher dynamic range in the x-ray regime (<10 nm) at the expense of lower resolution. In both cases, the driving laser beam and the low-order harmonics must be suppressed by apertures and filters in front of the spectrometer, as shown in Fig. 33.

A. Microscopic analysis: The single-atom dipole moment

Emission of harmonic radiation from a single atom or molecule is determined by the dipole acceleration, which in atomic units is $(d^2/dt^2)\langle\Psi|\mathbf{r}|\Psi\rangle$, where $\mathbf{r}$ is the space vector and Ψ is the electron wave function resulting from the solution of the nonrelativistic time-dependent Schrödinger equation.[3] The analysis of high harmonic generation can be considerably simplified by using the model of Lewenstein *et al.* (1994), which is based on two approximations first introduced by Keldysh for the calculation of strong-field ionization processes (Keldysh, 1965; Becker *et al.*, 1994); (i) In positive-energy (continuum) states the effect of the Coulomb potential is neglected so that the electron can be treated as a free particle. The main consequence of this approximation is that ionization is underestimated (see Fig. 31). We have corrected the Lewenstein model of high harmonic generation to remove this deficiency. (ii) The contribution of all other bound states except the ground state to the evolution of the system is neglected (Figueira *et al.*, 1998). This is fulfilled in the strong-field limit $\gamma < 1$, where excited bound states are smeared out beyond redemption due to enormous Stark shifts, and intermediate resonances do not affect the transition

[3]See, for example, (Eberly *et al.*, 1989a 1989b; Kulander and shore, 1989; Potvliege and Shakeshaft, 1989; Krause *et al.*, 1992; Xu, 1992; Ben-Tal *et al.*, 1993; Sanpera *et al.*, 1995; Zuo *et al.*, 1995; Bandrauk *et al.*, 1997; Moisey and Weinhold, 1997; Bandrauk and Yu, 1999).

from the ground state to positive-energy (continuum) states. Under the above assumptions (i) and (ii), the quantum-mechanical expectation value of the high-frequency part of the atomic dipole moment responsible for high harmonic generation is obtained as a product of three probability amplitudes:

$$\tilde{d}_h(\tau)=\sum_{\tau_b}\frac{1}{\sqrt{i}}a_{ion}(\tau_b)\tilde{a}_{pr}(\tau_b,\tau)a_{rec}(\tau). \tag{34}$$

Here the tilde again stands for complex quantities and we use a retarded frame of reference $\tau=t-z/c$ to ensure translational invariance of the dipole moment for the macroscopic analysis in the next subsection. The three probability amplitudes in Eq. (34) are given by

$$a_{ion}(\tau_b)=\sqrt{\frac{dn(\tau_b)}{d\tau}}, \tag{35}$$

$$\tilde{a}_{pr}(\tau_b,\tau)=\left(\frac{2\pi}{\tau-\tau_b}\right)^{3/2}\frac{(2W_b)^{1/4}}{E_l(\tau_b)}\exp[-iS],$$

$$S=\int_{\tau_b}^{\tau}d\tau'\{[p(\tau_b,\tau)-A_l(\tau')]^2+W_b\}, \tag{36}$$

$$a_{rec}(\tau)=\frac{p(\tau_b,\tau)-A_l(\tau)}{[W_b+\{p(\tau_b,\tau)-A_l(\tau)\}^2]^3}, \tag{37}$$

where $n(\tau)$ is the free-electron density as given by Eq. (23),

$$p(\tau_b,\tau)=\frac{1}{\tau-\tau_b}\int_{\tau_b}^{\tau}d\tau' A_l(\tau'), \tag{38}$$

and A_l is the vector potential of the fundamental laser field. The instant of birth τ_b as a function of the time τ is determined by solution of the algebraic equation

$$p(\tau_b,\tau)-A_l(\tau_b)=0. \tag{39}$$

The sum in Eq. (34) accounts for the fact that there exist several possible times of birth for the generation of a particular harmonic. Note that for the calculation of the single-atom dipole moment the full electric field of the laser pulse is used, i.e., the original model (Lewenstein *et al.*, 1994) is generalized to account for nonadiabatic effects. Further, the original model is also improved by replacing the Keldysh ionization rate with accurate static ionization rates and allowing for ground-state depletion in Eq. (35) (Ivanov *et al.*, 1996). The model presented here is limited to linearly polarized light, for which the center of gravity of the electron wave packet returns directly to the nucleus as long as the magnetic component of the Lorentz force can be neglected (Appendix C). Elliptic polarization of the driving field makes the center of the electron wave packet miss the parent ion on its return. This reduces overlap with the atomic ground state and hence the recombination probability amplitude $a_{rec}(\tau)$ in Eq. (34), which decreases the harmonic efficiency (Budil *et al.*, 1993; Dietrich *et al.*, 1994; Burnett *et al.*, 1995; Weihe *et al.*, 1995). An extension of the model of Lewenstein *et al.* (1994) to account for elliptic polarization can be found in the literature (Long *et al.*, 1995; Ivanov *et al.*, 1996).

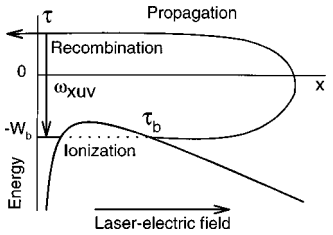

FIG. 34. Schematic illustration of the elementary processes responsible for high harmonic generation. A free electron is "born" at instant τ_b by tunnel ionization, is subsequently accelerated in the laser field, returns to the nucleus, and emits a high-energy extreme ultraviolet photon upon recombination to the ground state at the instant τ.

The probability amplitudes [Eqs. (35)–(37)] reflect the individual processes participating in high harmonic generation and can be interpreted in terms of a semiclassical model (Corkum, 1993; Kulander *et al.*, 1993; Lewenstein *et al.*, 1994) depicted graphically in Fig. 34. The electron wave packet is set free at an instant τ_b and a rate a_{ion} by tunnel ionization, then propagates in the strong laser field accounted for by $\tilde{a}_{pr}$, which brings it back to the nucleus approximately an oscillation period later at instant τ. It recombines to the ground state with probability a_{rec} upon releasing the energy it gained in the laser field plus W_b by emitting a high-energy photon. Due to quasiperiodic repetition of this process in a multicycle laser field, the resulting dipole emission spectrum is discrete, consisting of odd harmonics of the laser frequency ω_0. Figure 35 shows a typical high-order harmonic spectrum originating from Ne atoms irradiated by 30-fs pulses at $\lambda_0\approx 800$ nm, which exhibits well-resolved discrete harmonics. By contrast, the discrete structure is much less pronounced and even completely disappears in the cutoff region for a 7-fs driver. This is because for few-cycle pulses the highest harmonics are generated by a single-electron trajectory close to the peak, so that the periodicity of the high harmonic generation process is completely suppressed. In the time domain, the smooth

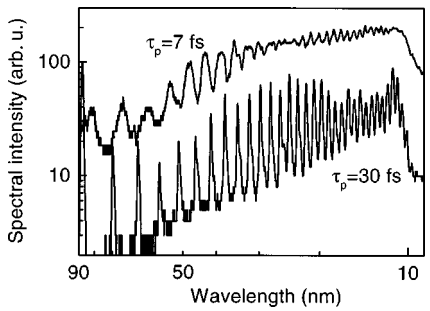

FIG. 35. Harmonic spectra generated in neon at a pressure of 250 Torr for Ti:sapphire laser pulses of 30 and 7 fs (FWHM) carried at $\lambda_0\approx 0.8\,\mu$m. The peak intensity of both pulses was $\approx 3\times 10^{14}$ W/cm^2. At the peak of the 30-fs pulse roughly 10% of the neon atoms are ionized, while at the peak of the 7-fs pulse 1% are ionized (courtesy of M. Schnürer).

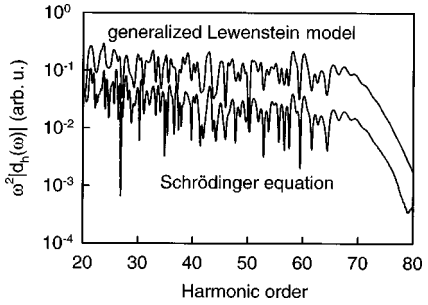

FIG. 36. Fourier transform of the single-atom dipole acceleration $\omega^2|\tilde{d}_h(\omega)|$ for high harmonic generation in hydrogen as determined by solving Eqs. (34)–(39) and the time-dependent nonrelativistic Schrödinger equation. The laser electric field is determined by Eq. (33) and the laser parameters are $I_0=5\times10^{14}$ W/cm^2, $\varphi_0=0$, $\lambda_0=0.8\,\mu$m, and $\tau_p=5$ fs.

spectrum at the cutoff was predicted to correspond to an isolated attosecond burst of radiation (Christov *et al.*, 1997), which will be discussed in more detail at the end of this section. Note that the smooth cutoff spectrum is currently the only (rather indirect) experimental evidence of the existence of subfemtosecond pulses.

The semiclassical picture predicts a cutoff in the harmonic spectrum at a harmonic photon energy (Krause *et al.*, 1992; Corkum, 1993; Kulander *et al.*, 1993; Lewenstein *et al.*, 1994; Milosevic and Starace, 1998, 1999) of

$$N_c\omega_0 = W_b + 3.17U_p(\tau), \tag{40}$$

where $U_p(\tau)$ is the ponderomotive potential, as defined in Sec. IV, to be inserted in atomic units in Eq. (40). If the ground state is not significantly depleted during the interaction, the fractional ionization is weak, which was the case in the experiments yielding the spectra in Fig. 35. In this limit, the cutoff harmonic N_c is determined by the ponderomotive potential at the pulse peak $U_p(0)$. As the pulses of different duration in Fig. 35 have the same peak intensity, the harmonic spectra are cut off at the same frequency, according to Eq. (40). In the limit of strong laser fields stripping the electron with a probability approaching one, well before the atoms are exposed to the pulse peak, N_c is no longer determined by the peak intensity, but by the laser intensity at which the ground state is depleted on the front edge of the pulse. As for shorter pulses, ground-state depletion is shifted to higher intensities (see Fig. 32), and the cutoff is shifted to higher harmonics (Christov *et al.*, 1996). In fact, the harmonic cutoff can be extended below 4.37 nm into the water window in neon by simply increasing the peak intensity of the 7-fs pulses. This could not be achieved with 30-fs pump pulses because of early depletion of the ground state.

In order to check the quality of the model drawing on Eqs. (34)–(39), we have compared the dipole moment for hydrogen as predicted by Eqs. (34)–(39) to that obtained from an exact solution of the Schrödinger equation for the electric field defined by Eq. (33) for various pulse durations and intensities. A typical result is depicted in Fig. 36. The model based on the theory of Lewenstein *et al.* (1994) overestimates the exact calculations by roughly one order of magnitude. The discrepancy is mainly due to the fact that for the chosen laser intensity, the electron is set free via above-barrier ionization and not via tunneling. Although the ionization rate in Eq. (35) is corrected to describe above-barrier ionization properly, the transverse distribution of the electron wave function at τ_b remains uncorrected and hence inaccurate. Nevertheless, aside from a quantitative difference, the structure of the exact harmonic spectrum is excellently reproduced by the model calculations for high photon energies near the cutoff. For low-order harmonics, the structural conincidence deteriorates due to the increasing influence of the Coulomb potential, which was neglected in the simplified model. Low-order harmonics are generated by electrons returning to the nucleus with low kinetic energies. The trajectory of these electrons is affected more strongly by the atomic Coulomb potential.

B. Macroscopic analysis: Propagation effects

Although many important features of high harmonic generation experiments can be understood from single-atom theory, for a detailed comparison with experiments a macroscopic theory including propagation effects, is required (L'Huillier *et al.*, 1990; 1991; L'Huillier, Lompré, *et al.*, 1992; Rae *et al.*, 1994; Kan *et al.*, 1997; Christov, Murnane, *et al.*, 1998; Tempea *et al.*, 1999a; 1999b). There are three important propagation effects, namely, (i) absorption, (ii) dephasing, and (iii) defocusing, setting a limit to the maximum achievable harmonic yield rate. These limitations are briefly discussed below.

(i) During propagation in the gas, the harmonic radiation can excite core electron states and be reabsorbed (Becker and Shirley, 1996). Numerical values of xuv/x-ray absorption coefficients can be found, for example, on the home page of the Center for X-ray Optics, Materials Sciences Division, Lawrence Berkeley National Laboratory (http://cindy.lbl.gov).

(ii) The difference between the phase velocities of the driving light wave and the high harmonic wave results in a phase mismatch between partial harmonic waves emitted at $z>0$ and $z=0$ in the gas medium. The propagation length at which the phase mismatch reaches π is referred to as the *coherence length*, indicating the propagation distance over which coherent growth of the macroscopic harmonic output tends to terminate. Three major effects contribute to the dephasing between fundamental and harmonic field:

(a) High harmonic generation is inextricably linked to ionization. The phase shift imposed by the free electrons on the laser pulse leads to dephasing because the effect of free electrons on the harmonic wave is negligible (Ditmire *et al.*, 1996; Shkolnikov *et al.*, 1996). The respective coherence length is given by

$$L_{fe}=\frac{2\pi c\omega_0}{\omega_p(\tau)^2 N}. \tag{41}$$

Here, $\omega_p(\tau)$ is the plasma frequency defined in Eq. (32), which is a function of the free-electron density at time τ where the Nth harmonic is generated (Kan *et al.*, 1997). For $n_a = 1.75\times10^{19}\,\mathrm{cm}^{-3}$ (500 Torr), $\lambda_0 = 800$ nm, $N = 100$, $n_e(\tau)/n_a = 0.1$, the plasma frequency $\omega_p^2 = 0.005\,57\,\mathrm{fs}^{-2}$, and Eq. (41) gives a coherence length of $L_{fe}\approx 8\ \mu$m.

(b) The curved wave front in the focused driving laser beam introduces a phase advance known as the Gouy phase shift, which is another "geometric" source of dephasing between fundamental and harmonic fields. A similar effect occurs in a hollow waveguide due to the wavelength dependence of the propagation constant. The related coherence length can be expressed as (L'Huillier *et al.*, 1991; L'Huillier, Lompré, *et al.*, 1992)

$$L_{g,fs}=\frac{\pi z_0}{N}=\frac{\pi^2 w_0^2}{N\lambda_0} \tag{42}$$

for propagation close to focus in free space, and as

$$L_{g,wg}=\frac{4\pi^2}{u_{11}^2}\frac{a^2}{N\lambda_0}, \tag{43}$$

where w_0 is the $1/e^2$ beam radius at focus, a is the bore radius, and $u_{11}=2.405$ (Marcatili and Schmeltzer, 1964). For optimum coupling, $w_0\approx(2/3)a$, which yields $L_{g,wg}\approx 1.56 L_{g,fs}$.

(c) The single-atom dipole moment for high harmonic generation depends on the pulse intensity, which is changed during propagation due to diffraction. As a result, the phase of the dipole moment decreases roughly linearly proportional to $-U_p/\omega_0$ with propagation, leading also to dephasing (Salières *et al.*, 1995). However, this contribution does not scale with the harmonic order and hence can usually be neglected for higher harmonics compared to the contributions (a) and (b).

(iii) During high harmonic generation, the laser pulse creates a free-electron density profile, in which the largest density is at the pulse peak and the density goes to zero at the pulse wings. Such a profile gives rise to defocusing, which reduces the laser pulse intensity, imposing a limitation on the effective interaction length over which a particular harmonic can be generated. For high harmonics, this effect is usually also weak compared to (iia) and (iib).

Limitations arising from geometric effects, such as dephasing by the Gouy phase shift (iib) and defocusing, depend on the confocal parameter and therefore can always be suppressed by increasing the pulse energy and the beam radius such that the peak intensity remains constant. These measures cannot remove free-electron-induced dephasing (iia) and absorption losses (i), which are more severe limitations. In what follows, we analyze the influence of these limiting effects on high harmonic generation by using a one-dimensional model (plane-wave propagation). The evolution of the laser field in an ionizing gas is described by

$$\partial_\xi E_l(\xi,\tau)=-\frac{1}{2c}\int_{-\infty}^{\tau}\omega_p^2(\xi,\tau')E_l(\xi,\tau')d\tau' - \frac{W_b}{2\varepsilon_0 c}\frac{\partial_\tau n_e(\xi,\tau)}{E_l(\xi,\tau)} \tag{44}$$

as it can be derived from Eq. (31). Here, we have introduced a coordinate frame moving at the speed of light in vacuum, $\tau=t-z/c$, $\xi=z$. The initial condition for solving Eq. (44) is assumed to be $E_l(0,\tau)=-dA_l/d\tau$, where $A_l(\tau)$ has the same form as given by Eq. (33). The wave equation for the generation and evolution of the harmonic field E_h,

$$\partial_\xi E_h(\xi,\tau)+\alpha_h E_h(\xi,\tau) = -\frac{1}{2\varepsilon_0 c}\partial_\tau \tilde{P}_h[E_l(\xi,\tau)]+\text{c.c.}, \tag{45}$$

is obtained from a derivation similar to that performed in Sec. V. Here, $\tilde{P}_h=kn_a\tilde{d}_h$ is the high-frequency part of the macroscopic nonlinear polarization, $\tilde{d}_h$ is given by Eq. (34), and $k=8.4773\times10^{-30}\,\mathrm{C\,m}$ (Coulomb-meters) is the conversion factor between atomic and SI units. Further, α_h is the xuv absorption coefficient, which is frequency dependent and must be evaluated in the frequency domain.

C. Absorption-limited xuv and dephasing-limited soft-x-ray harmonic generation

Recently, it was demonstrated that for moderate harmonic orders ($\lambda\geqslant 40$ nm) absorption limits the harmonic yield when using ultrashort, 40-fs driver pulses (Constant *et al.*, 1999). With a sub-10-fs driver absorption-limited high harmonic generation can be extended to the border of the soft-x-ray regime at ≈ 10 nm (Schnürer *et al.*, 1999b). In Fig. 37, the solid and dotted lines are obtained by solving Eqs. (44) and (45) including and neglecting xuv absorption, respectively. A comparison with experimental data (squares) provides conclusive evidence for the limiting role of absorption in few-cycle-driven high harmonic generation at the border of the xuv/soft-x-ray regime in neon. Owing to the steep front edge of the few-cycle driver, harmonics down to the 10–15-nm range can be produced at fractional ionization levels as low as $n_e(\tau_b)/n_a\approx 0.5\%$, resulting in a coherence length L_{fe} according to Eq. (41) that exceeds the xuv absorption length. A further conclusive demonstration of absorption-limited high harmonic generation is presented in Fig. 38 showing the harmonic intensity generated by 7-fs pulses in argon as a function of wavelength. Strong harmonic emission is confined to an area of 30 nm as a result of rapidly increasing absorption for longer wavelengths and increasing ionization for shorter wavelengths.

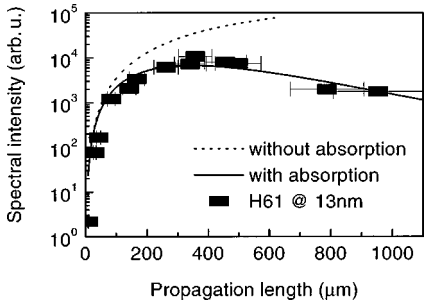

FIG. 37. Evolution of the 61st harmonic upon propagation of a few-cycle laser pulse in a neon target (300 Torr): ■, measured; solid curve, computed; dotted curve, result of the same calculation in the absence of absorption loss, $\alpha=0$. The laser parameters are $\lambda_0=0.8\,\mu$m, $I_0=5\times10^{14}$ W/cm^2, and $\tau_p=5$ fs. The error bars result from uncertainties in estimating effective interaction lengths and the pressure in the interaction region. The computed data are multiplied by a constant scaling parameter yielding best agreement between experiment and theory (Schnürer *et al.*, 1999b).

At sufficiently low ionization levels and for sufficiently large laser beam diameters, the phase advance of the driving laser radiation induced by free electrons and the Gouy phase shift (or waveguide phase shift), which lead to a finite L_{fe} and L_g, respectively, can be compensated for by the phase delay caused by the (positive) contribution of the neutral atoms to the refractive index. This compensation, which can be optimized by fine adjustment of the density n_a (i.e., pressure) of the atomic gas, results in a substantial (ideally infinite) enhancement of the coherence length over a limited fraction of the interaction time. This effect was first demonstrated at around 30 nm in an argon-filled hollow waveguide with 20-fs pump pulses carried at 800 nm (Rundquist *et al.*, 1998). More recently, it was also observed in the interaction of unguided (focused) 7-fs pulses with a neon gas jet, which led to absorption-limited harmonic emission down to 10–15 nm as reported above (Schnürer *et al.*, 1999). By extending the length of coherence growth to many times the xuv absorption length, this "pressure-tuned" phase-matching mechanism allows maximization of the yield (Constant *et al.*, 1999) in absorption-limited xuv harmonic generation with few-cycle laser pulses.

In Fig. 39, absolute measurements of the efficiency of few-cycle-driven high harmonic generation in Ar, Ne

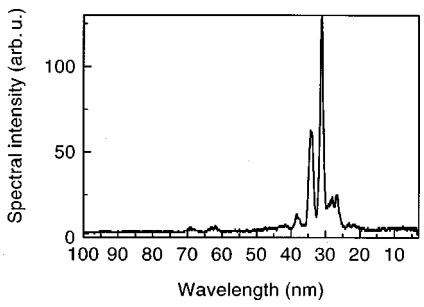

FIG. 38. Spectral harmonic intensity vs wavelength as generated in argon (300 Torr, interaction distance 2 mm). The laser parameters are $\lambda_0=0.8\,\mu$m, $I_0=5\times10^{14}$ W/cm^2, and $\tau_p=5$ fs.

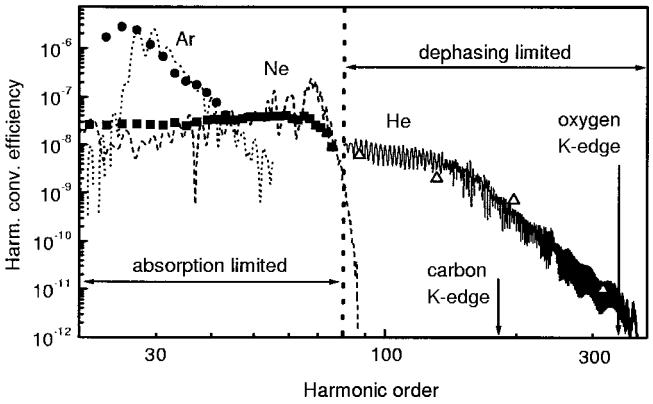

FIG. 39. Absolute measurement of the harmonic production efficiency in argon (225 Torr; effective gas length is 3 mm), in neon (300 Torr; effective gas length is 3 mm), and in helium (3000 Torr; effective gas length is 0.2 mm). The peak intensities in argon, neon, and helium are $I_0=5\times10^{14}$ W/cm^2, $I_0=2\times10^{15}$ W/cm^2, and $I_0=3\times10^{15}$ W/cm^2, respectively. The remaining pulse parameters are $\tau_p=7$ fs, $\lambda_0=0.8\,\mu$m (Ti:sapphire). Calculated spectra: dotted curve, argon; dashed curve, neon; solid curve, helium. For the calculations, a constant scaling factor was used to obtain optimum agreement between experiment and theory. The data obtained with Ar and Ne are accurate within a factor of 2, whereas those produced with He can be regarded as order-of-magnitude estimates (Schnürer *et al.*, 1999a).

and He, and a comparison with numerical simulations are presented. The efficiency of energy conversion into individual harmonics (within a bandwidth equal to twice the laser frequency) is plotted versus harmonic order (Schnürer *et al.*, 1999a; 1999b). Theoretical predictions from Eqs. (44) and (45) are found to be in reasonable agreement with experimental data. The numerical analysis also confirms that the maximum achievable harmonic yield in Ar and Ne is limited by xuv absorption. For few-cycle driver pulses absorption losses present the dominant limitation for wavelengths down to 10 nm. Within a 5% bandwidth, the few-cycle-driven neon harmonic source emits approximately 10^7 photons/pulse at 13.5 nm, a wavelength important for xuv lithography, and a repetition rate of 1 kHz within a time interval estimated as $\tau_x<3$ fs from the coalescence of discrete harmonics to a continuum in this wavelength range (Fig. 35). The enhanced photon yield together with its unprecedented temporal confinement results in peak powers on the order of 0.1 MW. These intense soft x-ray pulses are delivered in a near-diffraction-limited beam and hence should be focusable to peak intensities in excess of 10^{13} W/cm^2. These pulses are sufficiently intense to induce two-photon transitions in the x-ray regime, which may open the way to measuring the harmonic pulse duration. Such pulses will be discussed in Sec. VII E.

In the soft-x-ray regime ($\lambda\leqslant10$ nm) absorption rapidly increases with decreasing wavelength. As higher harmonics are generated in the presence of a larger free-electron density, according to Eqs. (23) and (40), dephasing increases with decreasing harmonic wave-

length. Hence in the wavelength region $\lambda < 10\,\mathrm{nm}$ dephasing becomes the dominant limitation. Because the coherence length given by Eq. (41) decreases rapidly with increasing order, the high harmonic yield rapidly drops below the detection limit at wavelengths below 10 nm when generated with pulses in the multicycle regime. At these wavelengths, the short rise time of the driver pulse is even more crucial than in the xuv range addressed above. In fact, the extremely steep intensity gradient on the pulse front of few-cycle drivers has allowed the generation of high-order harmonics at significantly reduced free-electron densities and hence increased coherence lengths, resulting in an extension of high harmonic generation at signal levels several orders of magnitude above detection limit into the water window (Chang *et al.*, 1997; Spielmann *et al.*, 1997; Schnürer *et al.*, 1998). Figure 39 plots a measured harmonic spectrum (open triangles) emitted by a helium gas target irradiated by sub-10-fs pulses at $\lambda_0 = 780\,\mathrm{nm}$ (Schnürer *et al.*, 1999a). Reasonable agreement with theoretical calculations is obtained. The propagated spectrum reveals a considerably stronger wavelength sensitivity than the single-atom dipole moment, which is introduced by the ionization-induced phase mismatch even for these extremely short driver pulses. The weak frequency dependence of the single-atom dipole radiation spectrum down to the water window offers the potential for substantially enhancing the harmonic conversion efficiencies in this wavelength range by devising techniques for making free-electron-induced dephasing less severe.

D. Phase matching of soft-x-ray harmonics

In the previous subsection we concluded that ionization-induced dephasing limits coherence growth of soft-x-ray laser harmonics even if the shortest (few-cycle) driver pulses are used for excitation. Due to this limitation, the efficiency of high harmonic generation is still too low for many important applications. During the last few years a number of phase-matching mechanisms have been proposed and demonstrated in the vuv-xuv range (Milchberg *et al.*, 1995; Kan *et al.*, 1996; Shkolnikov *et al.*, 1996; Peatross *et al.*, 1997; Christov, Kapteyn, *et al.*, 1998; Lange *et al.*, 1998; Rundquist *et al.*, 1998), but none of them could be extended into the x-ray regime. All the phase-matching schemes reported so far rely on the assumption that the phase of the harmonic wave emerging at a fixed position in the coordinate system moving at c grows linearly with propagation distance. In what follows, the phase-matching mechanisms relying on this linear growth are referred to as *adiabatic* (Geissler *et al.*, 1999b). Recent studies of propagation of few-cycle laser pulses in a field-ionizing atomic medium revealed distortions *within* an optical cycle, which can give rise to what we call *nonadiabatic phase matching* at wavelengths well below 10 nm (Tempea *et al.*, 1999b). On the other hand, nonadiabatic pulse shaping also sets a limit to adiabatic phase matching (Geissler *et al.*, 1999b). In what follows, we shall investigate how these effects can be exploited to substantially enhance the coherent growth of soft-x-ray laser harmonics.

All adiabatic phase-matching schemes rely on the approximation that the change in the free-electron density during one optical cycle may be neglected. Under this assumption the phase mismatch grows linearly with propagation distance and perfect phase matching may be achieved, as can be seen from an inspection of the spectral phase.

The spectral phase of a particular harmonic N at the frequency $N\omega_0$ is obtained by the Fourier transform of the second time derivative of the atomic dipole moment as given by Eq. (34), which yields

$$\phi_N = S(\tau_b, \tau_r) - N\omega_0\tau_r . \tag{46}$$

The primary change in ϕ_N during propagation results from the fact that the laser field experiences a phase shift in the presence of ionization that grows linearly with propagation distance, $\phi_l(\xi) = -\omega_p^2\xi/(2c\omega_0)$. In the frame propagating at the vacuum speed of light, which is comoving with the harmonic wave, this phase change shifts the local time τ_r, at which the harmonic is generated, as $\tau_r(\xi) = \tau_r(0) + \phi_l(\xi)/\omega_0$ with propagation distance. By virtue of Eq. (46), the shift of τ_r causes a change of the harmonic phase. In the adiabatic limit the change in the free-electron density during one laser cycle is negligible, hence $\Delta n_e = n_e(\tau_r) - n_e(\tau_b) \approx 0$. This implies that (i) τ_r and τ_b are shifted by the same amount and (ii) the laser electric field experienced by the electron between τ_b and τ_r remains unchanged, as illustrated in Fig. 40(a). As a consequence, the classical action integral S given by Eq. (36) remains constant. Inserting the resulting phase change into the condition $\phi_N(\xi) - \phi_N(0) = N\phi_l = \pi$ yields the coherence length L_{fe}, as given in Eq. (41). A similar procedure yields L_g if ϕ_l is dictated by the Gouy or waveguide phase shift.

The adiabatic solution is, strictly speaking, only valid as long as the laser pulse experiences a constant free-electron density. This is never the case, as high harmonic generation is inextricably linked to ionization. The *nonadiabatic* behavior originates from the variation of the free-electron density n_e [see Eq. (23)] during the interaction. The change in n_e within the optical cycle tends to slightly modify the laser electric-field evolution during the same time. As a result, the trajectory of the freed electrons is governed by slightly different electric-field evolutions at different positions in space during propagation, as illustrated in Fig. 40(b). As a result, the classical action S changes with ξ. This nonadiabatic contribution is opposite in sign to the above-discussed adiabatic contributions; therefore the (adiabatic) linear growth of the harmonic phase ϕ_N is reduced (Tempea *et al.*, 1999b). Nonadiabatic effects become increasingly significant as the pulse duration approaches and enters the few-cycle regime, which is revealed by the ionization rates depicted in Fig. 32. Subcycle modification of the laser electric field has two major impacts on high harmonic generation: (i) Adiabatic phase-matching mechanisms are adversely affected and ultimately limited by the nonadiabatically induced change in ϕ_N during

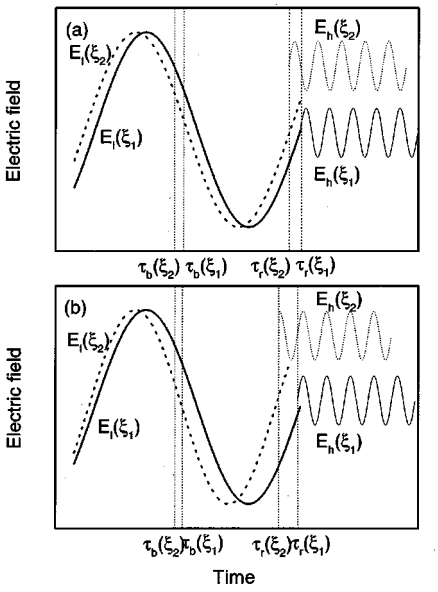

FIG. 40. Schematic of the laser field E_l and of the harmonic field E_h: solid curves, generated at ξ_1; dotted curves, generated at ξ_2, in the limit of (a) adiabatic evolution of a many-cycle laser pulse and (b) nonadiabatic evolution of a few-cycle laser pulse; the coordinate frame is moving with c, the approximate phase velocity of the harmonic wave. In this frame, the harmonic field remains unchanged with propagation and the laser field changes only due to the free-electron-induced phase mismatch. For comments see the text.

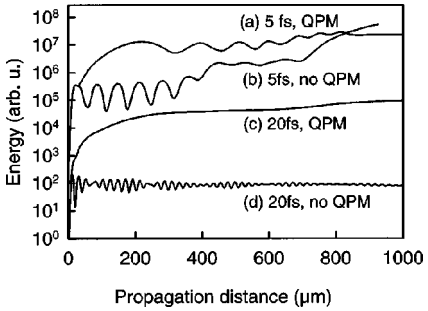

FIG. 41. Growth of the harmonic signal integrated between $N=430$ and $N=450$ vs propagation distance for the following parameters: $\lambda_0=0.8\,\mu$m for all plots; curves (c) and (d) the harmonic signal for $\tau_p=20$ fs, $I_0=3.5\times10^{15}$ W/cm^2 without and with quasiphase matching, respectively. For these parameters, the single-atom cutoff is at $N\approx445$. Curves (a) and (b) high harmonic generation for $\tau_p=5$ fs, $I_0=6.5\times10^{15}$ W/cm^2, without and with quasi-phase-matching (QPM), respectively. Both peak intensities were chosen to saturate ionization at the pulse peak. In order to make possible a comparison of calculations with and without QPM, the vacuum interaction distances were not plotted. Consequently the distance refers to the length propagated in the gas medium. The radius at the beam waist was assumed to be $w_0=0.5$ mm, corresponding to a confocal parameter of $z_0=98$ cm. The geometric coherence length of the harmonic $N=441$ is $L_g=7$ mm. To relax the pulse energy requirements, one could also use smaller confocal parameters for QPM. The helium gas density is 10 Torr, which corresponds to coherence lengths ($N=441$) of $L_{fe}=9.5\,\mu$m for $\tau_p=5$ fs and $L_{fe}=31.25\,\mu$m for $\tau_p=20$ fs, respectively.

propagation. (ii) The nonadiabatic contribution to the change in ϕ_N with ξ can become strong enough that few-cycle drivers can compensate for adiabatic change of the harmonic phase, which is shown in Fig. 40(b), giving rise to nonadiabatic self-phase-matching (Tempea *et al.*, 1999b).

Let us consider a representative adiabatic phase-matching scheme, namely, quasi-phase-matching. A periodic gas-vacuum structure is realized by using an array of gas jets. In order to achieve quasi-phase-matching, one must choose the length of each gas cell to be equal to $L_{fe}L_g/(L_{fe}+L_g)$, so that the harmonic signals at the entrance and end of the gas cell are out of phase by π. For the sake of simplicity, we assume the geometric coherence length $L_g \gg L_{fe}$, for which the length of the cell is $L_{fe}L_g/(L_{fe}+L_g)\approx L_{fe}$. When the vacuum length L_v is equal to L_g, the Gouy phase shift brings the laser and harmonic pulses into phase again, resulting in a continuation of coherent growth during the next gas cell. The Gouy shift accumulated during vacuum propagation is incorporated into our one-dimensional model by multiplying the laser pulse by a factor $\exp[i\tan^{-1}(L_v/z_0)]$ $\approx\exp[iL_v/z_0]$.

The limitations of quasi-phase-matching become apparent in Fig. 41, where the harmonic spectrum integrated over a band confined by $N=430$ and $N=450$ is plotted versus propagation distance for a 5-fs and for a 20-fs driver pulse. As anticipated, noadiabatic limitations become more severe for decreasing pulse duration. Whereas quasi-phase-matching with 20-fs pulses works properly over 35 gas-vacuum periods and enhances the harmonic yield by approximately three orders of magnitude, when 5-fs driver pulses are used quasi-phase-matched growth saturates after approximately seven periodic structures and the harmonic yield increases by a factor of ≈50. A comparison of plots (b) and (c) in Fig. 41 reveals that few-cycle pulses are able to produce soft-x-ray high harmonic radiation more efficiently even *without* phase matching than longer multicycle pulses *with* phase matching, owing to the significantly longer intrinsic coherence length L_{fe}, which results from the x-ray harmonic radiation emerging at a lower free-electron density. Adiabatic phase-matching schemes cannot compensate for the shortening of L_{fe} for longer pulses, due to the presence of nonadiabatic limitations (Geissler *et al.*, 1999b). From our investigations we may conclude that *x-ray laser harmonics can be most efficiently generated by few-cycle laser pulses even without having to rely on phase matching. This yield cannot be surpassed by applying an adiabatic phase-matching scheme based on a linear change of the harmonic phase.*

The reason for the sensitivity of nonadiabatic effects to the pulse duration becomes clear in Fig. 42, where the change in the free-electron density is plotted for the two pulse parameter sets of Fig. 41. The change between τ_b and τ_r for the harmonic $N=441$ for $\tau_p=5$ fs ($\Delta n_e\approx0.07$) is found to be larger by a factor of 5 than that for a 20-fs pulse ($\Delta n_e\approx0.015$). This explains the fact that in Fig. 41, quasi-phase-matching works for $\tau_p=20$ fs over a five times larger number of gas-vacuum periods than for a 5-fs pulse. Finally, Fig. 42 shows that quasi-phase-

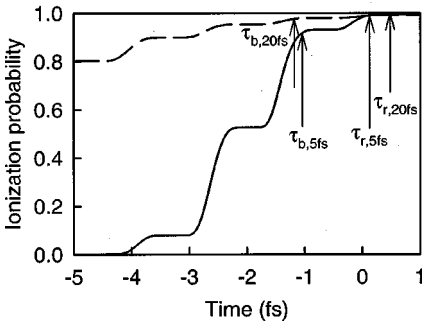

FIG. 42. Ionization profile for a 20-fs and 5-fs laser pulse and the parameters of Fig. 41. The arrows indicate the birth (τ_b) and recombination time (τ_r) of the electron, which generates the harmonic order $N=441$ close to the cutoff. Note that the harmonic $N=441$ is generated in several optical cycles. However, only the electron densities at the times τ_b and τ_r fulfill the quasi-phase-matching conditions chosen for the calculations in Fig. 41.

matching works best for cutoff harmonics produced in the vicinity of the laser pulse peak, where ionization saturates and Δn is small. For plateau harmonics Δn increases rapidly, which reduces the maximum gain achievable. In particular, for few-cycle laser pulses nonadiabatic limitations become so severe that adiabatic phase matching of plateau harmonics does not work at all.

As mentioned above, in the limit of high-intensity, few-cycle laser pulses, nonadiabatic effects can become strong enough to compensate for adiabatic dephasing, which makes nonadiabatic self-phase-matching possible. Nonadiabatic self-phase-matching already comes into play at the intensity level used in Fig. 41, as indicated by the growth of the harmonic signal [plot (b)] for $\xi > 300\,\mu$m. As a result, nonadiabatic self-phase-matching yields an output signal comparable to, or somewhat higher than, the output from the quasi-phase-matching scheme [plot (a)], because the former does not work in the presence of the latter. The performance of nonadiabatic self-phase matching becomes even more evident at somewhat higher intensities, $I_0 \approx 10^{16}\,\mathrm{W/cm^2}$. In Fig. 43, we have plotted the computed harmonic intensity spectra emerging from a He target at two peak intensity levels. For a peak intensity of $I_0 = 1.5\times10^{16}\,\mathrm{W/cm^2}$, an assessment of the influence of the magnetic component of the laser field on high harmonic generation is in order (see Appendix B). The harmonic yield is dramatically enhanced at harmonic orders higher than $N=400$ for the higher-intensity few-cycle pulse as a consequence of a more efficient nonadiabatic self-phase-matching. Owing to nonadiabatic self-phase-matching the spectrum remains nearly constant at the high-energy end, indicating that L_{fe} no longer determines the harmonic growth. A remarkable consequence of nonadiabatic self-phase-matching is that harmonics up to an order of $N=1200$ are predicted to emerge, corresponding to a photon energy in excess of 1.5 keV. The efficiency of high harmonic generation in the keV regime can be estimated by comparing calculations and experiments at lower laser intensities (Tempea *et al.*, 1999b). This suggests that $\approx 10^4$–10^5 photons/s in a 5% bandwidth at 1.5 keV are expected to be emitted from a He target pumped by 1-mJ sub-10-fs pulses at a 1-kHz repetition rate.

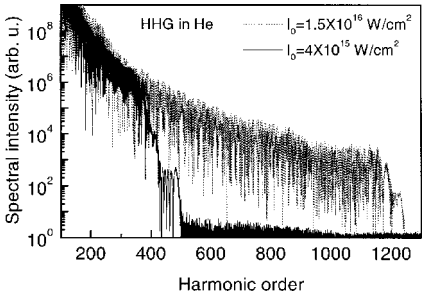

FIG. 43. Harmonic intensity spectra generated in a helium gas target at a gas pressure of 500 Torr after an interaction length of 125 μm for two different peak intensities: solid curves, $I_0 = 4\times10^{15}\,\mathrm{W/cm^2}$; dotted curve, $I_0 = 1.5\times10^{16}\,\mathrm{W/cm^2}$. The remaining laser pulse parameters are $\tau_p \approx 5$ fs and $\lambda_0 \approx 0.8\,\mu$m.

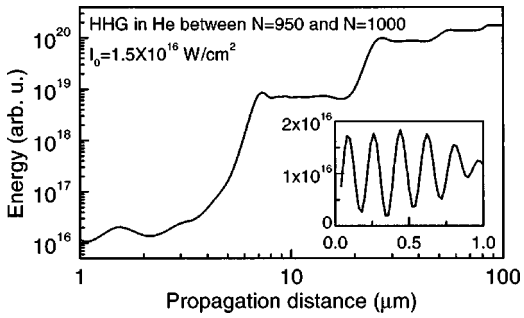

FIG. 44. Energy of the harmonic signal integrated between $N=950$ and $N=1000$ vs propagation distance for the parameters of Fig. 43 ($I_0 = 1.5\times10^{16}\,\mathrm{W/cm^2}$). The inset shows the growth of the harmonic over the first μm.

In Fig. 44 the growth of energy contained in the spectral window between the 950th and the 1000th harmonic is plotted versus interaction length for the parameters of Fig. 43. The harmonic signal grows over the coherence length $L_{fe} \approx 0.1\,\mu$m and oscillates for $\xi > L_{fe}$ over a limited propagation length, as shown in the inset. These oscillations originate from the interference between harmonic radiation generated at different positions along the propagation direction, in analogy to the Maker fringes in second-harmonic generation (Boyd, 1992). Note that the computed coherence length is a factor of 3 longer than the coherence length determined by Eq. (41). The increase in effective coherence length is related to the propagating pulse's being subject to significant modifications within one carrier oscillation cycle (nonadiabatic pulse shaping) as a consequence of the fractional ionization rate's becoming comparable to ω_0 (see Fig. 32) in intense few-cycle laser fields (Kan *et al.*, 1997). Another, even more striking, implication of nonadiabatic pulse evolution is the onset of nonadiabatic self-phase-matching for $\xi \gg L_f$. As a result, the Maker fringes disappear, and the harmonic signal exhibits a steplike increase, enhancing the energy converted into

harmonic radiation by some four orders of magnitude.

Future terawatt-scale sub-10-fs laser technology is expected to allow full exploitation of nonadiabatic self-phase-matching, which is out of reach at present. Once this technology becomes available, few-cycle-driven harmonic sources emitting coherent radiation at wavelengths of a few nanometers with high average brightness and high peak brightness may open up new fields of research. High average brightness may open the way to biological microscopy or interferometric testing of x-ray optics using a compact laboratory source. This is a relative value. The expected high peak brightness even promises to offer an absolute value: two-photon-induced transitions may become measurable, indicating the advent of nonlinear x-ray optics. Intriguing consequences may include the feasibility of time-resolved spectroscopy of inner-shell electron relaxation processes and the temporal characterization of few-cycle-driven harmonic x-ray pulses, which can be of subfemtosecond duration under specific conditions to be discussed in the next subsection. Once extended into the keV regime, few-cycle-driven harmonic sources may become a powerful tool for studying the ultrafast structural dynamics of molecules and solids by means of time-resolved x-ray diffraction or absorption (Rischel *et al.*, 1997; Barty, Ben-Nun *et al.*, 1998; Chin *et al.*, 1998; Jimenez *et al.*, 1998) with never-before-achieved resolution.

E. Attosecond x-ray pulse generation

In the time domain, harmonic emission is, within a laser oscillation period, confined to a small fraction of $T_o/2$ (within a limited frequency band near the cutoff), giving rise to a train of subfemtosecond or even attosecond bursts (1 as$=10^{-18}$ s) of short-wavelength radiation (Antoine *et al.*, 1996). This temporal structure was first proposed by Farkas and Toth (1992). Other proposals for pulse generation in this, thus far inaccessible, regime include Fourier synthesization (Hänsch, 1990) and stimulated Raman scattering (Yoshikawa and Imasaka, 1993; Kaplan, 1994; Harris and Sokolov, 1998). Although the conversion efficiency of high harmonic generation is lower than that of other schemes for attosecond pulse generation (Harris and Sokolov, 1998), the advantage of high harmonic generation is that there exist several possibilities for cutting a single attosecond pulse out of the pulse train, which are currently under intense investigation. The availability of single attosecond pulses will pave the way towards xuv/x-ray pump-probe experiments on a subfemtosecond time scale, the time scale in which, for example, inner-shell electron relaxation processes in medium- and high-Z atoms take place. Potential methods to isolate a single attosecond pulse include combining two perpendicularly polarized pulses with slightly different frequencies, known as the "atomic Pockels cell" (Corkum *et al.*, 1994; Corkum, 1996), and utilization of a time-dependent degree of ellipticity of the laser polarization (Antoine *et al.*, 1997).

A more direct method for the generation of a single-attosecond pulse is high harmonic generation with few-cycle laser pulses, as was revealed by the theoretical analysis of Christov *et al.* (1997). Under few-cycle excitation conditions, emission of the high-energy end of the harmonic spectrum can be confined to one half-oscillation period near the pulse peak, if the maximum ponderomotive potential U_p in Eq. (40) is reached for $\tau=0$. This is the case in the limit of weak ground-state depletion, resulting in the emission of a single x-ray pulse of attosecond duration within a 10% spectral window near the cutoff, as shown in Fig. 45. By contrast, in the regime of nonadiabatic self-phase-matching the emergence of a single-attosecond pulse is predicted to be feasible also in the plateau region of the harmonic spectrum.

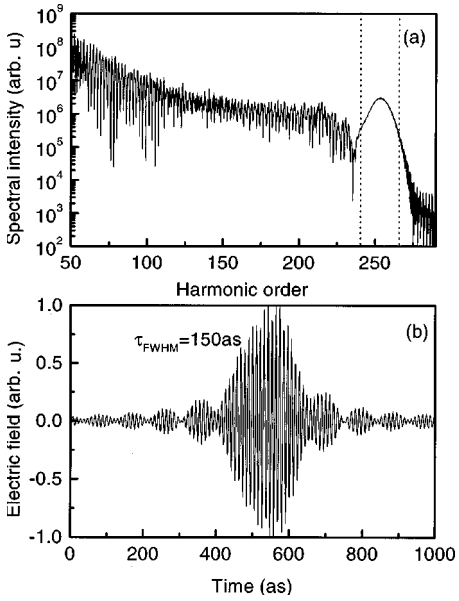

FIG. 45. Harmonic spectrum in helium (500 Torr) after a propagation distance of 9 μm for $\lambda_0=0.8\,\mu$m, $\tau_p=5$ fs, $I_0=2\times10^{15}$ W/cm^2, and $\varphi_0=0$. (a) Computed harmonic spectrum; dotted lines, harmonic orders $N=240$ and $N=265$; (b) Fourier transform of the spectral band between $N=240$ and $N=265$.

So far the only experimental indication (there is no real evidence!) for the possible emergence of xuv emission on a subfemtosecond time scale is the coalescence of harmonics in the xuv spectrum of Ne driven by 7-fs pulses, as revealed by Fig. 35. Clearly, before exciting applications such as inner-shell spectroscopy can be tackled, more reliable techniques for the temporal characterization of these ultrashort x-ray pulses need to be developed. Cross-correlation techniques based on ionization by a harmonic photon in the presence of a strong laser field (Kálmán *et al.*, 1993) have been successful in the sub-100-fs range (Glover *et al.*, 1996; Schins *et al.*, 1996) and more recently in the sub-10-fs range (Murnane and Kapteyn, 1999). However, the resolution of this method is limited by the fundamental pulse duration to a few femtoseconds. This limitation does not appear in autocorrelation measurements utilizing two-photon ionization of atoms, which was demonstrated for the ninth harmonic of the Ti:sapphire laser at around 90 nm (Kobayashi *et al.*, 1998). Unfortunately, the two-photon

transition cross section scales with λ^6 (Faisal, 1986; Kálmán, 1989), making implementation of this technique even more difficult for shorter wavelengths.

Recently, it was shown that few-cycle-driven harmonics may extend nonlinear autocorrelation techniques to the border of the soft-x-ray regime (Schnürer *et al.*, 1999b). The harmonic peak intensity predicted from the measured conversion efficiency in Fig. 39 for $\lambda \approx 13.4$ nm should be sufficient to create *K*-shell vacancies in boron by two-photon-induced photoemission. Before autocorrelation measurements on subfemtosecond xuv/x-ray pulses can be tackled, precise control of the the transverse beam profile of the driving laser pulse will be required. This is because the position and the phase of the attosecond harmonic burst within a selected frequency band is subject to variation across the pump laser beam, impairing the quality and duration of the focused harmonic pulse. Creating a near-flat-top laser beam profile in the interaction volume is one possible solution to this problem. Finally, the spectrum and hence the temporal structure of radiation emitted by a few-cycle-driven harmonic source depends sensitively on the absolute phase of the laser pulse φ_0 [see Eq. (14)]. The random variation of φ_0 translates into a timing jitter and fluctuations of the energy and duration of the harmonic pulse. Hence stable subfemtosecond x-ray harmonic pulse generation, like any other strong-field light-atom interaction process, calls for access to and control of φ_0 in few-cycle wave packets, a problem which is addressed in the next section.

VIII. PHASE SENSITIVITY OF STRONG-FIELD PHENOMENA

This section will show that the phase sensitivity of strong-field processes offers routes to measuring and subsequently controlling the absolute phase φ_0 of light pulses. The interactions to be addressed require intensities of the order of 10^{14} W/cm^2 or higher. Until recently, this intensity range was out of the reach of cw mode-locked laser oscillators. Advances in femtosecond technology reviewed in Sec. III have recently made it possible to focus the output of a 1-MW, sub-10-fs MDC KLM Ti:sapphire oscillator to peak intensities in excess of 5×10^{13} W/cm^2 (Xu *et al.*, 1998). An improved version of this system now delivers sub-10-fs pulses with peak powers approaching 3 MW (Poppe, Lenzner *et al.*, 1999), which should be focusable to intensities beyond the 10^{14}-W/cm^2 level. These intensities are sufficient for triggering the phase-sensitive strong-field processes discussed below, opening up ways to measure and eventually control the phase of few-cycle light pulses delivered by mode-locked laser oscillators.

A. Is few-cycle pulse evolution phase sensitive?

Before we address the influence of φ_0 on nonlinear interactions, let us consider the principal question for the design of few-cycle pulse experiments: how does the pulse phase behave during (linear) propagation? A few-cycle pulse envelope with a cosine carrier can have a finite spectral dc component, whereas the dc component of a sine wave carrying a symmetric amplitude envelope must be zero for reasons of symmetry. As the dc component does not constitute a solution to the wave equation, i.e., it cannot propagate, it is important to know which kind of pulses are capable of interacting with an extended medium without suffering significant distortions due to linear propagation. In order to answer this question, we have calculated the evolution of few-cycle pulses in vacuum, which is most conveniently described by Eq. (26) in the frequency domain and in a coordinate system moving at the speed of light in vacuum:

$$\partial_\xi \tilde{E}(r,\xi,\omega) = \frac{ic}{2\omega}\nabla_\perp^2 \tilde{E}(r,\xi,\omega). \tag{47}$$

Equation (47) is solved by starting from a Gaussian initial spatial pulse profile

$$\tilde{E}(r,\xi=0,\omega) = E_0 \exp\left[-\left(\frac{r}{a}\right)^2\right]\tilde{F}(\omega). \tag{48}$$

Here, E_0 is the peak electric-field amplitude, $\tilde{F}$ denotes the complex Fourier spectrum of a pulse of arbitrary temporal shape, a is the radius at the beam waist, and $r=|\mathbf{r}_\perp|=\sqrt{x^2+y^2}$ is the radial coordinate, assuming cylindrical symmetry.

At the beam center $r=0$ and at propagation distances $\xi/z_0 \gg 1$, where $z_0=\pi a^2/\lambda_0$ is the confocal parameter, Eq. (47) can be solved analytically, yielding

$$\tilde{E}(\xi,\omega,r=0) = \frac{\omega a^2}{2ic\xi}\tilde{F}(\omega). \tag{49}$$

Choosing the initial electric field in the time domain to be $E(\xi=0,\tau)=E_0\,\mathrm{sech}(\tau/\tau_p)\cos(\omega_0\tau+\varphi_0)$, we obtain from a Fourier transform of Eq. (49)

$$E(\xi,\tau,r=0) \approx \frac{z_0}{\xi}\sqrt{1+\frac{1}{(\omega_0\tau_0)^2}\tanh^2\left(\frac{\tau}{\tau_p}\right)} \times \mathrm{sech}\left(\frac{\tau}{\tau_p}\right)\cos[\omega_0\tau+\varphi(\tau)], \tag{50}$$

where the phase is given by

$$\varphi(\tau) = \varphi_0 - \frac{\pi}{2} + \frac{1}{\omega_0\tau_p}\tanh\left(\frac{\tau}{\tau_p}\right) \tag{51}$$

and $\varphi_0=\varphi(\tau=0,\xi=0)$ is the initial pulse phase at the pulse center. Our analysis reveals that during propagation the pulse envelope remains symmetric, so that the pulse center remains at $\tau=0$. As the pulse center does not change in the far field, the pulse phase can be determined at $\tau=0$. The pulse phase in the far field, $\varphi(\tau=0)=\varphi_0-\pi/2$, undergoes a phase shift which comes from the Gouy phase shift $\lim_{\xi\to\infty}-\tan^{-1}(\xi/z_0)\to-\pi/2$.

Note that the Guoy phase shift and all the other changes experienced by the pulse during propagation do not depend on the initial pulse phase. Therefore it can be concluded that the evolution of few-cycle pulses is independent of the initial carrier phase φ_0. The low-

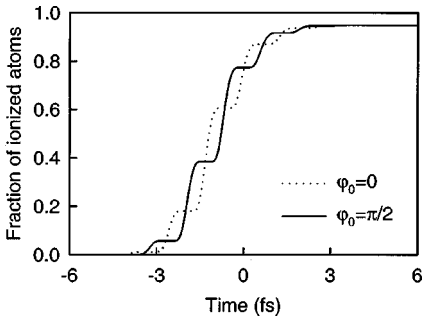

FIG. 46. Fraction of ionized helium atoms vs time. The laser pulse parameters are $\tau_p=5$ fs, $I_0=4\times10^{15}$ W/cm^2, and $\lambda_0=0.8\,\mu$m. Dotted lines, pulse phase $\varphi_0=0$; solid line, $\varphi_0=\pi/2$. These fundamental phases correspond approximately to a cosine and a sine carrier wave, respectively. The electric field is defined by Eq. (33).

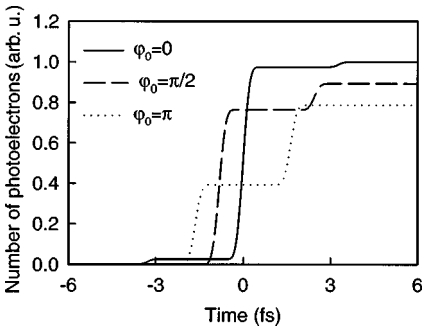

FIG. 47. Number of electrons ionized from a gold surface ($W_b=4.9$ eV) for a pulse impinging at an angle of incidence of 45°. The pulse parameters are $\lambda_0=0.8\,\mu$m, $I_0\approx2\times10^{13}$ W/cm^2, and $\tau_p=5$ fs. Pulse phases: solid curve, $\varphi_0=0$; dashed curve, $\varphi_0=\pi/2$; dotted curve, $\varphi_0=\pi$.

frequency (dc) components of the pulse spectrum are suppressed by diffraction, which manifests itself mathematically in a multiplication of the laser spectrum with ω in Eq. (49). This distorts the pulse envelope; however, the pulse phase φ_0, which is defined at the pulse center, is invariant during free-space vacuum pulse propagation. This suggests that there must exist a class of envelopes that do not have a dc component irrespective of the initial phase. This class of pulses is obtained by defining the electric field via the vector potential, $E=-\partial A/\partial t$ [see, for example, Eq. (33)]. The temporal derivative corresponds to a multiplication with ω in the frequency domain and ensures that the spectrum contains no dc components. A thorough treatment of pulse propagation in the single-cycle regime was recently presented by Shvartsburg (1996).

B. Phase sensitivity of optical field ionization

The quasistatic ionization rate $w(E)$ depends on the instantaneous electric-field strength [see Eq. (23)]. As the electric field of a few-cycle pulse depends on its phase, strong-field ionization becomes phase dependent. In Fig. 46, the ionization profile in He is depicted for the linearly polarized pulses of $\tau_p=5fs$ with $\varphi_0=0$ and $\varphi_0=\pi/2$. Ionization was calculated by using Eq. (23) together with the exact static ionization rates of helium. Whereas the ionization profile is phase sensitive, the final fraction of ionized atoms is, somewhat surprisingly, independent of φ_0. This is a general feature of strong-field ionization in the gaseous phase, as long as ionization is calculated in the quasistatic approximation. Recently, a full numerical solution of the time dependent Schrödinger equation showed some phase sensitivity (Christov, 1999).

Alternatively, there exist various other routes that provide access to φ_0 in few-cycle light pulses. Tunnel ionization at the surface of a solid occurs only during positive or negative half cycles. This symmetry breaking makes the total number of photoelectrons released by a p-polarized laser pulse impinging at oblique incidence on the photocathode phase dependent. Figure 47 shows the number of photoelectrons emitted upon irradiation of a gold photocathode with 5-fs pulses of various phases (Poppe, Fürbach, *et al.*, 1999). The ionization rate in Fig. 47 was calculated using the quasistatic ionization theory for metal surfaces (Sommerfeld, 1967). The predicted variation of the photoelectron yield versus φ_0 should be easily detectable. Another approach to determining φ_0 is the measurement of the angular distribution of electrons set free by circularly polarized light (Dietrich *et al.*, 1999), which also varies with φ_0.

C. Phase effects in high harmonic generation

Because the high-frequency atomic dipole moment $\tilde{d}_h$ given by Eq. (34), which is responsible for high harmonic generation, is also driven directly by the electric field, the emission characteristics exhibit a pronounced dependence on the phase of a few-cycle driver pulse (de Bohan *et al.*, 1998; Krausz *et al.*, 1998; Salières *et al.*, 1998; Tempea *et al.*, 1999a). This can be seen in Fig. 48, where the harmonic intensity spectra emitted from He pumped by 5-fs pulses of different phases, $\varphi_0=0$ (dotted line) and $\varphi_0=\pi/2$ (solid line), are plotted for various propagation distances. Figure 48(a) shows the harmonic spectrum after a short interaction length, reflecting the single-atom dipole response. In the cutoff region, a pulse with a cosine carrier yields a significantly stronger signal and the cutoff is shifted towards shorter wavelengths as compared to that obtained with a sine-carrier pulse.

A reliable deduction of φ_0 from high harmonic generation experiments calls for phase-dependent characteristics invariant to propagation. Figures 48(b)–(d) show the evolution of the harmonic radiation over distances comparable to the coherence length. The coherence length at the cutoff ($N=255$) is $\approx11\,\mu$m. The phase dependence of plateau harmonics is subject to strong variations with propagation. By contrast, the qualitative behavior in the cutoff region, as found in graph (a), is preserved for longer propagation distances. Hence the detection of cutoff harmonics may offer another route to measuring the phase of few-cycle light pulses.

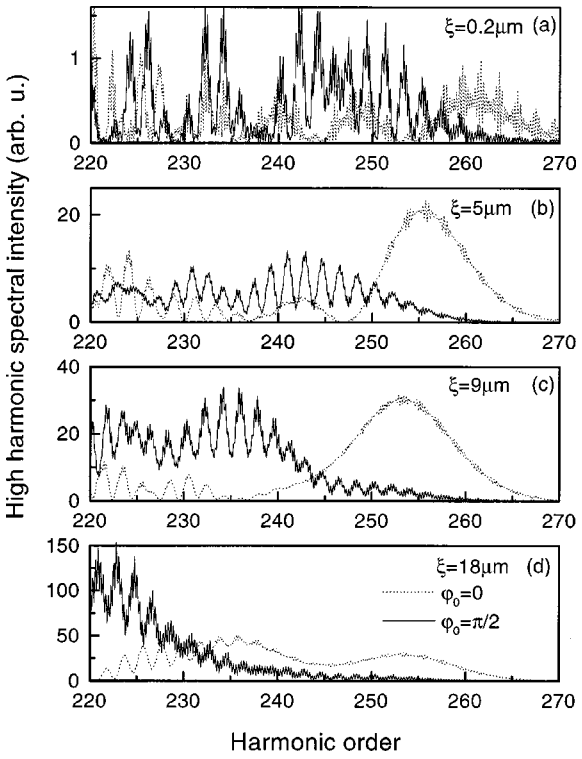

FIG. 48. Spectral intensity of the harmonic radiation in helium at a pressure of 500 Torr for the fundamental pulse phases: dotted curve, $\varphi_0=0$; solid curve, $\varphi_0=\pi/2$, after propagation distances of (a) 0.2, (b) 5, (c) 9, and (d) 18 μm. The laser parameters are $I_0=2\times10^{15}$ W/cm^2, $\lambda_0=0.8\,\mu$m, and $\tau_p=5$ fs. The electric field is defined by Eq. (33).

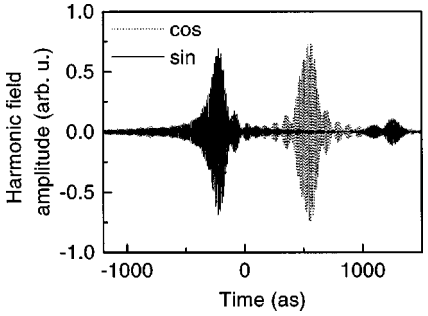

FIG. 49. Fourier transform of the harmonic amplitude spectrum between the orders 230 and 260 for the parameters of Fig. 48(c). Pulse phases: dotted line, $\varphi_0=0$; solid line, $\varphi_0=\pi/2$.

The origin of the characteristic phase dependence near the cutoff becomes clear by inspection of the cutoff harmonic signal in the time domain. Figure 49 shows the evolution of the temporal harmonic signal as obtained by an inverse Fourier transform of the harmonic spectra depicted in Fig. 48(c) transmitted through a bandpass between the 230th and the 260th harmonic order. For $\varphi_0=0$, the cutoff harmonics are generated at a single instant during the 5-fs driver pulse, whereas for $\varphi_0=\pi/2$ they emerge at two instants approximately half a cycle apart, resulting in a couple of x-ray bursts during the driver pulse.

The single attosecond pulse for $\varphi_0=0$ has a duration of approximately 160 as and presents a promising tool for time-resolved attosecond x-ray experiments. However, it is obvious that the timing jitter and the intensity fluctuations introduced by the phase sensitivity of few-cycle-driven harmonic emission impairs the utility of such a source for pump-probe experiments. Therefore the birth of attosecond science is closely linked to the development of techniques for measuring and controlling the phase of few-cycle light pulses.

IX. OUTLOOK

Intense few-cycle light pulses open up never-before-accessed parameter ranges in high-field physics. Strong-field processes induced by few-cycle laser fields hold out the promise of gaining access to the phase of the carrier wave and hence to the light fields for the first time. Presumably only a few of the many implications can be assessed at the present time. The investigations presented in this work suggest that phase-controlled light pulses will allow control of high-intensity light-matter interactions on a subcycle time scale. Consequences include the injection of an electron jet into a plasma with a subfemtosecond rise time and timing precision as well as the generation of single, well-controlled x-ray bursts of less than 100 attoseconds in duration. These pulse durations approach the atomic time scale and may allow the tracing of quantum dynamics in bound states characterized by low principal quantum numbers for the first time.

Beyond these long-term prospects, intense few-cycle laser pulses are likely to become the most efficient pump sources of ultrashort-pulsed short-wavelength radiation all the way from the xuv to the hard-x-ray regime, which may be produced at practically useful photon flux levels in the foreseeable future. At xuv and soft x-ray wavelengths few-cycle-driven high harmonics have been demonstrated to reach peak brightness levels that may allow two-photon excitations to be detected. Once achieved, nonlinear x-ray optics will become reality, with numerous intriguing implications including the autocorrelation measurement of subfemtosecond or attosecond xuv/x-ray pulses. When focused to relativistic intensities, few-cycle pulses will create ponderomotive forces as high as 0.1 MeV/μm at moderate (few-millijoule) energy levels, promising efficient conversion of light energy into kinetic energy of a collimated relativistic electron jet (Gahn *et al.*, 1999) with a duration comparable to that of the driver pulse. This electron jet could produce characteristic or channeling radiation (Kálmán, 1993, 1994), giving rise to hard x rays with similar pulse durations.

The search for laser-driven ultrafast x-ray sources is motivated by a number of important processes in the microscopic world that are very hard to gain insight into by conventional spectroscopy. Figure 50 depicts the relevant time scales for some important physical, chemical, and biological processes taking place in the microcosm. Whereas relaxation processes of weakly bound (outer-shell or valence-band) electrons can be accessed directly by pump-probe laser spectroscopy, only indirect and in

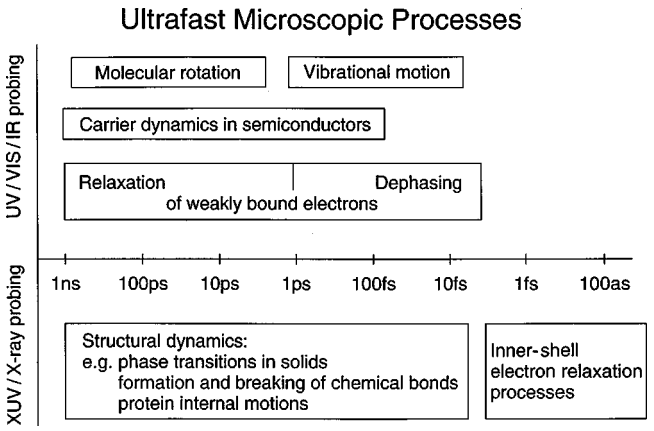

FIG. 50. Characteristic time scales of some elementary atomic, molecular, and collective processes. The boundaries of the presented time range are not intended to imply upper or lower limits on some of the processes.

many cases insufficient information about the motion of nuclei and the dynamics of inner-shell electronic transitions can be obtained by conventional ultrafast laser spectroscopy. Laser-produced x-ray pulses of a few femtoseconds or less in duration will allow the tracing of nuclear motion in a wide range of phenomena including phase transitions in the solid phase, the formation and breaking of chemical bonds in the gaseous and liquid phases, and biological processes as important as protein unfolding by means of time-resolved x-ray diffraction or absorption. Also, the wavelength and duration of these pulses will open the way to probing inner-shell atomic electron relaxation processes directly in the time domain.

In conclusion, ultrafast optics and high-field physics are likely to continue rapidly evolving over the coming years. Approaching the light oscillation cycle in intense ultrashort pulse generation issues new challenges to the research community but also promises great rewards, e.g., access to the electric and magnetic fields of light or the birth of attosecond metrology. The expected significant impact on numerous fields provides the major driving force for further progress.

ACKNOWLEDGMENTS

This review is dedicated to Professor A. J. Schmidt, who directed the authors' attention to this fascinating field. The authors are deeply indebted to Z. Cheng, M. Geissler, M. Hentschel, A. Poppe, M. Schnürer, A. Scrinzi, Ch. Spielmann, and G. Tempea for making their experimental and numerical data available for this work, as well as for fruitful discussions. We thank U. Keller for providing the data in Fig. 17. This work was sponsored by the Austrian Science Fund, Grant Nos. P-12631-PHY, Y44-PHY, and the special research program F016.

APPENDIX A: CONVERSION BETWEEN ATOMIC AND SI UNITS

Atomic units are used for convenience in quantum mechanics (Bethe and Salpeter, 1997), as by setting the fundamental constants $\hbar = m = e^2 = 1$ calculations are simplified substantially. In the following, conversion factors between atomic units and SI units are given.

(1) 1 atomic charge unit = charge of the electron = 1.602×10^{-19} C
(2) 1 atomic mass unit = mass of the electron = 9.109×10^{-31} kg
(3) 1 atomic length unit = radius of the first Bohr orbit = 5.2917×10^{-11} m
(4) 1 atomic velocity unit = electron velocity in the first Bohr orbit = 2.1877×10^{6} m/s
(5) 1 atomic momentum unit = electron momentum in the first Bohr orbit = 1.9926×10^{-24} kg m/s
(6) 1 atomic energy unit = twice the ionization potential of hydrogen = 4.359×10^{-18} J
(7) 1 atomic time unit = 2.4189×10^{-17} s
(8) 1 atomic frequency unit = 4.1341×10^{16} s^{-1}
(9) 1 atomic unit of electric potential = 27.210 V
(10) 1 atomic unit of electric-field strength = 5.142×10^{11} V/m.

APPENDIX B: DERIVATION OF THE FIRST-ORDER PROPAGATION EQUATION

The derivation of the first-order propagation equation starts from the scalar wave equation in the frequency domain

$$[\partial_z^2 + \nabla_\perp^2 + k^2(\omega)]E(\mathbf{r},\omega) = \frac{\omega^2}{\varepsilon_0 c^2}\hat{F}[P_{nl}(\mathbf{r},t)], \qquad \text{(B1)}$$

which can be obtained from the time-domain scalar wave equation by replacing the operations ∂_t and $\int dt$ by multiplications with $-i\omega$ and i/ω in the frequency domain. The scalar wave equation is appropriate as long as the electric field and the induced polarization in the transversal dimensions (x,y) exhibit little variation over a distance comparable to the center wavelength λ_0 (Yariv and Yeh, 1984). The derivation of the first-order propagation equation for the full electric field is performed by choosing the ansatz $\tilde{E} = \tilde{U}\exp[ik(\omega)z]$. Inserting this into Eq. (B1), we obtain

$$[2ik(\omega)\partial_z + \nabla_\perp^2]\tilde{U}(\omega) = \frac{\omega^2}{\varepsilon_0 c^2}\exp[-ik(\omega)z]\hat{F}[P_{nl}], \qquad \text{(B2)}$$

where the second space derivative is neglected. This approximation has been termed the slowly-evolving-wave approximation (Brabec and Krausz, 1997) and is applicable as long as changes in the electric field induced by the polarization of the medium over a distance comparable to one center wavelength λ_0 are small, i.e., $|\partial_z \tilde{E}| \ll \beta_0 \tilde{E}$, with $\beta_0 = k(\omega_0) = 2\pi/\lambda_0$. Transforming back to $\tilde{E}$ yields

$$[\partial_z - ik(\omega)]\tilde{E}(\omega) = \frac{i}{2k(\omega)}\nabla_\perp^2 \tilde{E}(\omega) - \frac{i\omega}{2\varepsilon_0 n(\omega) c}\hat{F}[P_{nl}]. \qquad \text{(B3)}$$

Although this equation is not directly usable, it is the starting point for the derivation of first-order propagation equations governing the evolution of laser pulses in various nonlinear media. A detailed analysis is given in Sec. V.

APPENDIX C: INFLUENCE OF THE LORENTZ FORCE ON HIGH HARMONIC GENERATION

Our model of high-order harmonic generation Eqs. (34)–(39), does not take into account the $\mathbf{v}\times\mathbf{B}$ (Lorentz) force that tends to become significant at high laser intensities. Here, $\mathbf{v}$ is the velocity of the electron and $\mathbf{B}$ is the magnetic field of the laser pulse. The Lorentz force shifts the electron trajectory in the direction of the laser wave vector, which presents a potential limitation to high harmonic generation. To estimate its effect on our predictions presented in Sec. VII, the electron trajectory in the laser field was calculated by solving the classical equation of motion. For an intensity of $I \approx 10^{16}\,\mathrm{W/cm^2}$, we find that the electron is offset by $z_o \approx 1\,\mathrm{nm}$ when it returns to the nucleus in the linearly polarized field. This shift must be compared to the transversal width of the returning electron wave function, $z_r = v_b(\tau_r - \tau_b)$, in order to determine the influence on high harmonic generation. Here, $\tau_r - \tau_b \approx 2.2\,\mathrm{fs}$ is the interval between the birth and the return time of the electron and v_b is the width of the velocity distribution of the electron wave packet at its birth. As for the intensities under consideration, the electrons are set free by above-barrier ionization, and the width of the spatial distribution of the electron wave packet at its birth, x_b, cannot be determined by tunneling theory relying on the presence of a barrier (Delone and Krainov, 1991). Therefore, to estimate a lower limit for x_r, it is assumed that the initial spatial distribution is equal to the Bohr radius, $a_B \approx = 5.3\times 10^{-9}\,\mathrm{cm/s}$. By virtue of the uncertainty relation $[a_B v_b \geqslant \hbar/(2m)]$ we obtain $v_b \approx 1.1\,\mathrm{nm/fs}$. This leads to $z_r \geqslant 2.5\,\mathrm{nm}$, i.e., the extension of the electron wave packet is expected to be larger than the offset z_r. This justifies neglect of the Lorentz force in our calculations.

REFERENCES

Agnesi, A., 1995, IEEE J. Quantum Electron. **30**, 1115.

Agostini, P., F. Fabre, G. Mainfray, G. Petite, and N. K. Rahman, 1979, Phys. Rev. Lett. **42**, 1127.

Agrawal, G. P., 1995, *Nonlinear Fiber Optics*, 2nd ed. (Academic, San Diego).

Akhmanov, S. A., V. A. Vysloukh, and A. S. Chirkin, 1992, *Optics of Femtosecond Laser Pulses* (American Institute of Physics, New York).

Alfano, R. R., and S. L. Shapiro, 1970, Phys. Rev. Lett. **24**, 592.

Ammosov, M. V., N. B. Delone, and V. P. Krainov, 1986, Zh. Eksp. Teor. Fiz. [Sov. Phys. JETP **64**, 1191 1986].

Antoine, P., A. L'Huillier, and M. Lewenstein, 1996, Phys. Rev. Lett. **77**, 1234.

Antoine, P., D. B. Milosevic, A. L'Huillier, M. B. Gaarde, P. Salières, and M. Lewenstein, 1997, Phys. Rev. A **56**, 4960.

Armstrong, J. A., 1967, Appl. Phys. Lett. **10**, 16.

Asaki, M. T., C.-P. Huang, D. Garvey, J. Zhou, H. C. Kapteyn, and M. M. Murnane, 1993, Opt. Lett. **18**, 977.

Augst, S., D. Strickland, D. D. Meyerhofer, S. L. Chin, and J. H. Eberly, 1989, Phys. Rev. Lett. **63**, 2212.

Augst, S., A. Talebpour, S. L. Chin, Y. Beaudoin, and M. Chaker, 1995, Phys. Rev. A **52**, R917.

Backus, S., C. G. Durfee III, G. Mourou, H. C. Kapteyn, and M. M. Murnane, 1997, Opt. Lett. **22**, 1256.

Backus, S., C. G. Durfee III, M. M. Murnane, and H. C. Kapteyn, 1998, Rev. Sci. Instrum. **69**, 1207.

Baltuska, A., Z. Wei, M. S. Pshenichnikov, and D. A. Wiersma, 1997a, Opt. Lett. **22**, 102.

Baltuska, A., Z. Wei, R. Szipöcs, M. S. Pshenichnikov, and D. A. Wiersma, 1997b, Appl. Phys. B: Lasers Opt. **65**, 175.

Bandrauk, A. D., S. Chelkowski, and H. Yu, 1997, Phys. Rev. A **56**, R2537.

Bandrauk, A. D., and H. Yu, 1999, Phys. Rev. A **59**, 539.

Barbara, P. F., J. G. Fujimoto, W. H. Knox, and W. Zinth, 1996, Eds., *Ultrafast Phenomena X* (Springer, Berlin).

Barbara, P. F., W. H. Knox, G. A. Mourou, and A. H. Zewail, 1994, Eds., *Ultrafast Phenomena IX* (Springer, Berlin).

Barr, J. R. M., D. C. Hanna, and D. W. Hughes, 1991, *Digest of Conference on Lasers and Electro-optics* (Optical Society of America, Washington, DC), Paper FQ5.

Barty, C. P. J., M. Ben-Nun, T. Guo, F. Raksi, Ch. Rose-Petruck, J. Squier, K. R. Wilson, V. V. Yakovlev, P. M. Weber, Z. Jiang, A. Ikhlef, and J. C. Kieffer, 1998, in *Time-Resolved X-Ray Diffraction*, edited by J. Helliwell and P. M. Rentzepis (Oxford University, New York), Chap. 2.

Barty, C. P. J., C. L. Gordon III, and B. E. Lemoff, 1994, Opt. Lett. **19**, 1442.

Barty, C. P. J., T. Guo, C. Le Blanc, F. Raksi, C. Rose-Petruck, J. Squier, K. R. Wilson, V. V. Yakovlev, and K. Yamakawa, 1996, Opt. Lett. **21**, 668.

Barty, C. P. J., W. White, W. Sibbett, and R. Trebino, 1998, Eds., *Ultrafast Optics*, IEEE J. Sel. Top. Quantum Electron. **4**, p. 157.

Beaud, P., M. Richardson, E. J. Miesak, and B. H. T. Chai, 1993, Opt. Lett. **18**, 1550.

Becker, U., and D. A. Shirley, 1996, *Vacuum uv and Soft X-Ray Photoionization* (Plenum, New York).

Becker, W., S. Long, and J. K. McIver, 1994, Phys. Rev. A **50**, 1540.

Beddard, T., W. Sibbett, D. T. Reid, J. Garduno-Mejia, N. Jamasbi, and M. Mohebi, 1999, Opt. Lett. **24**, 163.

Ben-Tal, N., N. Moiseyev, R. Kosloff, and C. Cerjan, 1993, J. Phys. B **26**, 1445.

Bethe, H. A., and E. E. Salpeter, 1977, *Quantum Mechanics of One- and Two-Electron Atoms* (Plenum, New York).

Blanchot, N., C. Rouyer, C. Sauteret, and A. Migus, 1995, Opt. Lett. **20**, 395.

Bloembergen, N., 1965, *Nonlinear Optics* (Addison-Wesley, Reading, MA).

Blow, K. J., and B. P. Nelson, 1988, Opt. Lett. **13**, 1026.

Blow, K. J., and D. Wood, 1988, J. Opt. Soc. Am. B **5**, 629.

Borodin, N. L., A. G. Okrimchuk, and A. V. Shestakov, 1992, in *OSA Proceedings on Advanced Solid-State Lasers*, Vol. 13, edited by Lloyd L. Chase and Albert A. Pinto (Optical Society of America, Washington, DC), p. 42.

Boyd, R. W., 1992, *Nonlinear Optics* (Academic, San Diego).

Brabec, T., M. Yu. Ivanov, and P. Corkum, 1996, Phys. Rev. A **54**, R2551.

Brabec, T., S. M. J. Kelly, and F. Krausz, 1995, in *Compact Sources of Ultrashort Pulses*, edited by I. N. Duling III (Cambridge University, Cambridge, England), p. 57.
Brabec, T., and F. Krausz, 1997, Phys. Rev. Lett. **78**, 3282.
Brabec, T., Ch. Spielmann, P. F. Curley, and F. Krausz, 1992, Opt. Lett. **17**, 1292.
Brabec, T., Ch. Spielmann, and F. Krausz, 1991, Opt. Lett. **16**, 1961.
Brabec, T., Ch. Spielmann, and F. Krausz, 1992, Opt. Lett. **17**, 748.
Bradley, D. J., and G. H. C. New, 1974, Proc. IEEE **62**, 313.
Braun, A., G. Korn, X. Liu, D. Du, J. Squier, and G. Mourou, 1995, Opt. Lett. **20**, 73.
Brunel, F., 1990, J. Opt. Soc. Am. B **7**, 521.
Budil, K. S., P. Salières, A. L'Huillier, T. Ditmire, and M. D. Perry, 1993, Phys. Rev. A **48**, R3437.
Burke, P. G., and V. M. Burke, 1997, J. Phys. B **30**, L383.
Burnett, N. H., C. Kan, and P. B. Corkum, 1995, Phys. Rev. A **51**, R3418.
Campillo, A. J., S. L. Shapiro, and B. R. Suydam, 1973, Appl. Phys. Lett. **23**, 628.
Cerullo, G., S. De Silvestri, V. Magni, and L. Pallaro, 1994, Opt. Lett. **19**, 807.
Chambaret, J. P., C. Le Blanc, G. Cheriaux, P. Curley, G. Darpentigny, P. Rousseau, G. Hamoniaux, A. Antonetti, and F. Salin, 1996, Opt. Lett. **21**, 1921.
Chang, Z., A. Rundquist, H. Wang, M. Murnane, and H. C. Kapteyn, 1997, Phys. Rev. Lett. **79**, 2967.
Chelkowski, S., A. Conjusteau, T. Zuo, and A. D. Bandrauk, 1996, Phys. Rev. A **54**, 3235.
Chen, S., A. Maksimchuk, and D. Umstadter, 1998, Nature (London) **396**, 653.
Cheng, Z., A. Fürbach, S. Sartania, M. Lenzner, Ch. Spielmann, and F. Krausz, 1999, Opt. Lett. **24**, 247.
Cheng, Z., G. Tempea, T. Brabec, K. Ferencz, C. Spielmann, and F. Krausz, 1998, in *Ultrafast Phenomena XI*, edited by T. Elsässer, J. G. Fujimoto, D. A. Wiersma, and W. Zinth (Springer, Berlin), p. 8.
Cheriaux, G., P. Rousseau, F. Salin, J. Chambaret, B. Walker, and L. Dimauro, 1996, Opt. Lett. **21**, 414.
Chilla, J. L. A., and O. E. Martinez, 1993, J. Opt. Soc. Am. B **10**, 638.
Chin, A. H., R. W. Schoenlein, T. E. Glover, P. Balling, W. P. Leemans, and C. V. Shank, 1998, in *Ultrafast Phenomena XI*, edited by T. Elsässer, J. G. Fujimoto, D. A. Wiersma, and W. Zinth (Springer, Berlin), p. 401.
Cho, S. H., B. E. Bouma, E. P. Ippen, and J. G. Fujimoto, 1999, Opt. Lett. **24**, 417.
Christov, I. P., 1999, Opt. Lett. **24**, 1425.
Christov, I. P., H. C. Kapteyn, and M. M. Murnane, 1998, Opt. Express **3**, 360.
Christov, I. P., M. M. Murnane, and H. C. Kapteyn, 1997, Phys. Rev. Lett. **78**, 1251.
Christov, I. P., M. M. Murnane, and H. C. Kapteyn, 1998, Phys. Rev. A **57**, R2285.
Christov, I. P., J. Zhou, J. Peatross, A. Rundquist, M. M. Murnane, and H. C. Kapteyn, 1996, Phys. Rev. Lett. **77**, 1743.
Constant, E., D. Garzella, P. Breger, E. Mevel, C. Dorrer, C. Le Blanc, F. Salin, and P. Agostini, 1999, Phys. Rev. Lett. **82**, 1668.
Corkum, P. B., N. H. Burnett, and F. Brunel, 1989, Phys. Rev. Lett. **62**, 1259.
Corkum, P. B., 1993, Phys. Rev. Lett. **71**, 1994.
Corkum, P. B., 1996, Nature (London) **384**, 118.
Corkum, P. B., N. H. Burnett, and M. Yu. Ivanov, 1994, Opt. Lett. **19**, 1870.
Crane, J. K., M. D. Perry, S. Hermann, and R. W. Falcone, 1992, Opt. Lett. **17**, 1256.
Curley, P. F., Ch. Spielmann, T. Brabec, F. Krausz, E. Wintner, and A. J. Schmidt, 1993, Opt. Lett. **18**, 54.
Dahlström, L., 1972, Opt. Commun. **5**, 157.
de Bohan, A., P. Antoine, D. B. Milosevic, and B. Piraux, 1998, Phys. Rev. Lett. **81**, 1837.
de Groot, S., W. van Leeuwen, and C. van Weert, 1980, *Relativistic Kinetic Theory, Principles and Applications* (North-Holland, Amsterdam).
Delone, N. B., and V. P. Krainov, 1991, J. Opt. Soc. Am. B **8**, 1207.
DeMaria, A. J., W. H. Glenn, M. J. Brienza, and M. E. Mack, 1969, Proc. IEEE **57**, 2.
DeMaria, A. J., D. A. Stetser, and H. Heynau, 1966, Appl. Phys. Lett. **8**, 174.
De Silvestri, S., P. Laporta, and O. Svelto, 1984, IEEE J. Quantum Electron. **20**, 533.
Deutsch, T., 1965, Appl. Phys. Lett. **7**, 80.
DiDomenico, M., 1964, J. Appl. Phys. **35**, 2870.
DiDomenico, M., H. M. Marcos, J. E. Geusic, and R. E. Smith, 1966, Appl. Phys. Lett. **8**, 180.
Diels, J.-C., W. Dietel, J. J. Fontaine, W. Rudolph, and B. Wilhelmi, 1985, J. Opt. Soc. Am. B **2**, 680.
Diels, J.-C., J. J. Fontaine, I. C. McMichael, and F. Simoni, 1985, Appl. Opt. **24**, 1270.
Diels, J.-C., and W. Rudolph, 1996, *Ultrashort Laser Pulse Phenomena* (Academic, New York).
Diels, J.-C., E. Van Stryland, and G. Benedict, 1978, Opt. Commun. **25**, 93.
Dietrich, P., N. H. Burnett, M. Ivanov, and P. B. Corkum, 1994, Phys. Rev. A **50**, R3583.
Dietrich, P., F. Krausz, and P. B. Corkum, 1999, "Determining the absolute carrier phase of a few-cycle laser pulse," in press.
Ditmire, T., J. K. Crane, H. Nguyen, L. B. DaSilva, and M. D. Perry, 1995, Phys. Rev. A **51**, R902.
Ditmire, T., K. Kulander, J. K. Crane, H. Nguyen, and M. D. Perry, 1996, J. Opt. Soc. Am. B **13**, 406.
Ditmire, T., and M. D. Perry, 1993, Opt. Lett. **18**, 426.
Donelly, T. D., T. Ditmire, K. Neumann, M. D. Perry, and R. W. Falcone, 1996, Phys. Rev. Lett. **76**, 2472.
Dorner, R., H. Brauning, O. Jagutzki, V. Mergel, M. Achler, R. Moshammer, J. M. Feagin, T. Osipor, A. Brauning-Demain, L. Spielberger, T. M. McGuire, M. M. Prior, N. Berrah, J. D. Bozek, C. L. Cocke, H. Schmidt-Böcking, 1998, Phys Rev. Lett. **81**, 5776.
Du, D., X. Liu, G. Korn, J. Squier, and G. Mourou, 1994, Appl. Phys. Lett. **64**, 3071.
Duling, I. N. III, 1991, Opt. Lett. **16**, 539.
Duling III, I. N., and M. L. Dennis, 1995, in *Compact Sources of Ultrashort Pulses*, edited by I. N. Duling III (Cambridge University, Cambridge, England), p. 140.
Durfee, C. G. III, S. Backus, M. M. Murnane, and H. C. Kapteyn, 1998, IEEE J. Sel. Top. Quantum Electron. **4**, 395.
Eberly, J. H., Q. Su, and J. Javanainen, 1989a, Phys. Rev. Lett. **62**, 881.
Eberly, J. H., Q. Su, and J. Javanainen, 1989, J. Opt. Soc. Am. B **6**, 1289.

Elsässer, T., J. G. Fujimoto, D. A. Wiersma, and W. Zinth, 1998, Eds., *Ultrafast Phenomena XI* (Springer, Berlin).
Esarey, E., G. Joyce, and P. Sprangle, 1991, Phys. Rev. A **44**, 3908.
Faisal, F. H. M., 1986, *Theory of Multiphoton Processes* (Plenum, New York).
Faldon, M. E., M. H. R. Hutchinson, J. P. Marangos, J. E. Muffett, R. A. Smith, J. W. G. Tisch, and C. G. Wahlström, 1992, J. Opt. Soc. Am. B **9**, 2094.
Farkas, Gy. and Cs. Toth, 1992, Phys. Lett. A **168**, 447.
Feldmann, J., J. Sacher, and E. Göbel, 1991, Opt. Lett. **16**, 241.
Fermann, M. E., 1995, in *Compact Sources of Ultrashort Pulses*, edited by I. N. Duling III (Cambridge University, Cambridge, England), p. 179.
Fermann, M. E., L. M. Yang, M. L. Stock, and M. J. Andrejco, 1994, Opt. Lett. **19**, 43.
Feurer, T., and R. Sauerbrey, 1997, in *Atomic, Molecular, and Optical Physics: Electromagnetic Radiation; Experimental Methods in the Physical Sciences, Vol. 29*, edited by F. B. Dunning and R. G. Hulet (Academic, New York), p. 193.
Fibich, G. and G. C. Papanicolaou, 1997, Opt. Lett. **18**, 1379.
Figueria-de-Morisson-Faria, C., M. Dörr, and W. Sandner, 1998, Phys. Rev. A **58**, 2990.
Fisher, R. A., P. L. Kelly, and T. K. Gustafson, 1969, Appl. Phys. Lett. **14**, 140.
Fittinghoff, D. N., P. R. Bolton, B. Chang, and K. C. Kulander, 1992, Phys. Rev. Lett. **69**, 2642.
Fork, R. L., C. H. Cruz, P. C. Becker, and C. V. Shank, 1987, Opt. Lett. **12**, 483.
Fork, R. L., B. I. Greene, and C. V. Shank, 1981, Appl. Phys. Lett. **38**, 71.
Fork, R. L., O. E. Martinez, and J. P. Gordon, 1984, Opt. Lett. **9**, 150.
Fork, R. L., C. V. Shank, and R. Yen, 1982, Appl. Phys. Lett. **41**, 223.
Fork, R. L., C. V. Shank, R. Yen, and C. A. Hirlimann, 1983, IEEE J. Quantum Electron. **19**, 500.
Freeman, R. R., P. H. Bucksbaum, W. E. Cooke, G. Gibson, T. J. McIlrath, and L. D. Van Woerkom, 1992, in *Atoms in Intense Laser Fields*, edited by M. Gavrila (Academic, San Diego), p. 43.
French, P. M., 1985, Rep. Prog. Phys. **58**, 169.
French, P. M. W., 1996, Contemp. Phys. **37**, 283.
French, P. M., M. M. Opalinska, and J. R. Taylor, 1989, Opt. Lett. **14**, 217.
French, P. M., and J. R. Taylor, 1988, Opt. Lett. **13**, 470.
French, P. M., J. A. R. Williams, and J. R. Taylor, 1987, Opt. Lett. **12**, 684.
French, P. M., J. A. R. Williams, and J. R. Taylor, 1989, Opt. Lett. **14**, 686.
Gahn, C., G. D. Tsakiris, A. Pukhov, J. Meyer-ter-Vehn, G. Pretzler, P. Thirolf, D. Habs, and K. J. Witte, 1999, Phys. Rev. Lett. **83** (in press).
Gallmann, L., D. H. Sutter, N. Matuschek, G. Steinmeyer, U. Keller, C. Iaconis, and I. A. Walmsley, 1999, Opt. Lett. **24**, 1314.
Geissler, M., G. Tempea, M. Schnürer, F. Krausz, and T. Brabec, 1999a, Phys. Rev. Lett. **83**, 2930.
Geissler, M., G. Tempea, and T. Brabec, 1999b, ''Quasi-phase-matching of high harmonic generation,'' submitted to Phys. Rev. A.
Georgiev, D., J. Herrmann, and U. Stamm, 1992, Opt. Commun. **92**, 368.
Gildenburg, V. B., A. V. Kim, and A. M. Sergeev, 1990, Pis'ma Zh. Eksp. Teor. Fiz. [JETP Lett. **51**, 104 1990].
Gildenburg, V. B., T. A. Petrova, and A. D. Yunakovsky, 1995, Physica D **87**, 335.
Glover, T. E., R. W. Schoenlein, A. H. Chin, and C. V. Shank, 1996, Phys. Rev. Lett. **76**, 2468.
Glownia, J. H., J. Misewich, and P. P. Sorokin, 1987, J. Opt. Soc. Am. B **4**, 1061.
Greenhow, R. C., and A. J. Schmidt, 1974, in *Advances in Quantum Electronics Vol. 2*, edited by D. W. Goodwin (Academic, London), p. 158.
Grischkowski, D., and A. C. Balant, 1981, Appl. Phys. Lett. **41**, 1.
Haight, R. and P. F. Seidler, 1994, Appl. Phys. Lett. **65**, 517.
Hargrove, L. E., R. L. Fork, and M. A. Pollack, 1964, Appl. Phys. Lett. **5**, 4.
Harris, S. E. and A. V. Sokolov, 1998, Phys. Rev. Lett. **81**, 2894.
Haus, H. A., 1975a, IEEE J. Quantum Electron. **11**, 736.
Haus, H. A., 1975b, J. Appl. Phys. **46**, 3049.
Haus, H. A., 1976, IEEE J. Quantum Electron. **12**, 169.
Haus, H. A., 1984, *Waves and Fields in Optoelectronics* (Prentice-Hall, Englewood Cliffs, NJ), p. 99.
Haus, H. A., J. G. Fujimoto, and E. P. Ippen, 1991, J. Opt. Soc. Am. B **8**, 2068.
Haus, H. A., J. G. Fujimoto, and E. P. Ippen, 1992, IEEE J. Quantum Electron. **28**, 2086.
Hänsch, T. W., 1990, Opt. Commun. **80**, 71.
Heinz, P., and A. Lauberau, 1989, J. Opt. Soc. Am. B **6**, 1574.
Heritage, J. P., and M. Nuss, 1992, Eds., *Special Issue on Ultrafast Optics and Electronics*, IEEE J. Quantum Electron. **28**, p. 2084.
Herrmann, J., 1994, J. Opt. Soc. Am. B **11**, 498.
Hofer, M., M. E. Fermann, F. Haberl, M. H. Ober, and A. J. Schmidt, 1991, Opt. Lett. **16**, 502.
Hofer, M., M. H. Ober, F. Haberl, and M. E. Fermann, 1992, IEEE J. Quantum Electron. **28**, 720.
Hooker, S. M., and S. E. Harris, 1995, Opt. Lett. **20**, 1994.
Hu, S. X., and Z. Z. Xu, 1997, Appl. Phys. Lett. **71**, 2605.
Hunsche, S., S. Feng, H. G. Winful, A. Leitenstorfer, M. C. Nuss, and E. P. Ippen, 1999, J. Opt. Soc. Am. A **16**, 2025.
Iaconis, C., and I. Walmsley, 1998, Opt. Lett. **23**, 792.
Ippen, E. P., H. A. Haus, and L. Y. Liu, 1989, J. Opt. Soc. Am. B **6**, 1736.
Ippen, E. P., L. Y. Liu, and H. A. Haus, 1990, Opt. Lett. **15**, 183.
Ippen, E. P., C. V. Shank, and A. Dienes, 1972, Appl. Phys. Lett. **21**, 348.
Ivanov, M. Y., T. Brabec, and N. Burnett, 1996, Phys. Rev. A **54**, 742.
Ivanov, M. Y., and P. B. Corkum, 1993, Phys. Rev. A **48**, 580.
Jasapara, J., and W. Rudolph, 1999, Opt. Lett. **24**, 777.
Jimenez, R., C. Rose-Petruck, T. Guo, K. R. Wilson, and C. P. J. Barty, 1998, in *Ultrafast Phenomena XI*, edited by T. Elsässer, J. G. Fujimoto, D. A. Wiersma, and W. Zinth (Springer, Berlin), p. 404.
Joachain, C. J., M. Dörr, and N. J. Kylstra, 2000, Adv. At., Mol., Opt. Phys. **42**, 225.
Johnson, A. M., W. M. Simpson, and R. H. Stolen, 1984, Appl. Phys. Lett. **44**, 729.
Kálmán, P., 1989, Phys. Rev. A **39**, 3200.
Kálmán, P., 1993, Phys. Rev. A **48**, R42.
Kálmán, P., 1994, Phys. Rev. A **49**, 620.

Kálmán, P., F. Krausz, and E. Wintner, 1993, Phys. Rev. A **47**, 729.
Kalosha, V. P., M. Müller, J. Herrmann, and S. Gatz, 1998, J. Opt. Soc. Am. B **15**, 535.
Kan, C., N. H. Burnett, C. Capjack, and R. Rankin, 1997, Phys. Rev. Lett. **79**, 2971.
Kan, C., C. E. Capjack, R. Rankin, T. Brabec, and N. H. Burnett, 1996, Phys. Rev. A **54**, R1026.
Kane, D. J., and R. Trebino, 1993, IEEE J. Quantum Electron. **29**, 571.
Kaplan, A. E., 1994, Phys. Rev. Lett. **73**, 1243.
Kärtner, F. X., I. D. Jung, and U. Keller, 1996, IEEE J. Sel. Top. Quantum Electron. **2**, 540.
Kärtner, F. X., and U. Keller, 1995, Opt. Lett. **20**, 16.
Kärtner, F. X., N. Matuschek, T. Schibli, U. Keller, H. A. Haus, C. Heine, R. Morf, V. Scheuer, M. Tilsch, and T. Tschudi, 1997, Opt. Lett. **22**, 831.
Kasper, A., and K. J. Witte, 1996, Opt. Lett. **21**, 360.
Kean, P. N., X. Zhu, D. W. Crust, R. S. Grant, N. Langford, and W. Sibbett, 1989, Opt. Lett. **14**, 39.
Keldysh, L. V., 1965, Zh. Eksp. Teor. Fiz. [Sov. Phys. JETP **20**, 1307 1965].
Keller, U., 1994, Appl. Phys. B: Lasers Opt. **58**, 347.
Keller, U., 1997, Ed., *Special Issue on Ultrafast Lasers*, Appl. Phys. B: Lasers Opt. **65**, 2.
Keller, U., 1999, in *Nonlinear Optics in Semiconductors*, edited by A. Kost and E. Garmire (Academic, Boston), Vol. 59, p. 211.
Keller, U., W. H. Knox, and H. Roskos, 1990, Opt. Lett. **15**, 1377.
Keller, U., W. H. Knox, and G. W. 't Hooft, 1992, IEEE J. Quantum Electron. **28**, 2123.
Keller, U., D. A. B. Miller, G. D. Boyd, T. H. Chiu, J. F. Ferguson, and M. T. Asom, 1992, Opt. Lett. **17**, 505.
Keller, U., G. W. 't Hooft, W. H. Knox, and J. E. Cunningham, 1991, Opt. Lett. **16**, 1022.
Keller, U., K. J. Weingarten, F. X. Kärtner, D. Kopf, B. Braun, I. D. Jung, R. Fluck, C. Hönninger, N. Matuschek, and J. Aus der Au, 1996, IEEE J. Sel. Top. Quantum Electron. **2**, 435.
Kim, D.-E., Cs. Tóth, and C. P. J. Barty, 1999, Phys. Rev. A **59**, R4129.
Knox, W. H., 1988, IEEE J. Quantum Electron. **24**, 388.
Knox, W. H., M. C. Downer, R. L. Fork, and C. V. Shank, 1985, Opt. Lett. **9**, 552.
Kobayashi, Y., T. Seikikawa, Y. Nabekawa, and S. Watanabe, 1998, Opt. Lett. **23**, 64.
Koechner, W., 1996, *Solid-State Laser Engineering* (Springer, Berlin).
Kogelnik, H. W., E. P. Ippen, A. Dienes, and C. V. Shank, 1972, IEEE J. Quantum Electron. **8**, 373.
Kondo, K., N. Sarukura, K. Sajiki, and S. Watanabe, 1993, Phys. Rev. A **47**, R2480.
Koroshilov, E. V., I. V. Kryukov, P. G. Kryukov, and A. V. Sharkov, 1984, in *Ultrafast Phenomena VI*, edited by T. Yajima, K. Yoshihara, C. B. Harris, and S. Shionoya (Springer, Berlin), p. 22.
Krainov, V. P., 1997, J. Opt. Soc. Am. B **14**, 425.
Krause, J. L., K. J. Schafer, and K. C. Kulander, 1992, Phys. Rev. Lett. **68**, 3535.
Krausz, F., T. Brabec, M. Schnürer, and C. Spielmann, 1998, Opt. Photonics News **9**, 46.
Krausz, F., T. Brabec, and Ch. Spielmann, 1991, Opt. Lett. **16**, 235.
Krausz, F., M. E. Fermann, T. Brabec, P. F. Curley, M. Hofer, M. H. Ober, Ch. Spielmann, E. Wintner, and A. J. Schmidt, 1992, IEEE J. Quantum Electron. **28**, 2097.
Krausz, F., and E. Wintner, 1994, Eds., *Special Issue on Ultrashort Pulse Generation*, Appl. Phys. B: Lasers Opt. **58**, 3.
Kühlke, D., W. Rudolph, and B. Wilhelmi, 1983, IEEE J. Quantum Electron. **19**, 526.
Kuizenga, D. J., and A. E. Siegman, 1970a, IEEE J. Quantum Electron. **QE-6**, 694.
Kuizenga, D. J., and A. E. Siegman, 1970b, IEEE J. Quantum Electron. **QE-6**, 709.
Kulander, K. C., K. J. Schafer, and J. L. Krause, 1992, in *Atoms in Intense Laser Fields*, edited by M. Gavrila (Academic, San Diego), p. 247.
Kulander, K. C., K. J. Schafer, and J. L. Krause, 1993, in *Proceedings of the Workshop on Super Intense Laser Atom Physics (SILAP III)*, edited by B. Piraux (Plenum Press, New York), Vol. 316, p. 95.
Kulander, K. C., and B. W. Shore, 1989, Phys. Rev. Lett. **63**, 524.
Lablanquie, P., J. Mazeau, L. Andric, P. Selles, and A. Huetz, 1995, Phys. Rev. Lett. **74**, 2192.
Landau, L. D., and E. M. Lifshitz, 1977, *Quantum Mechanics* (Pergamon, Oxford).
Lange, H. R., A. Chrion, J.-F. Ripoche, A. Mysyrewicz, P. Breger, and P. Agostini, 1998, Phys. Rev. Lett. **81**, 1611.
Laporta, P., and V. Magni, 1985, Appl. Opt. **24**, 2014.
Laubereau, A., 1969, Phys. Lett. **29A**, 539.
Laubereau, A., and D. von der Linde, 1970, Z. Naturforsch. A **25a**, 1626.
Lemoff, B. E., and C. P. J. Barty, 1993a, Opt. Lett. **18**, 57.
Lemoff, B. E., and C. P. J. Barty, 1993b, Opt. Lett. **18**, 1651.
Lemoff, B. E., G. Y. Yin, C. L. Gordon III, C. P. J. Barty, and S. E. Harris, 1995, Phys. Rev. Lett. **74**, 1574.
Lenzner, M., J. Krüger, S. Sartania, Z. Cheng, Ch. Spielmann, G. Mourou, W. Kautek, and F. Krausz, 1998, Phys. Rev. Lett. **80**, 4076.
Lewenstein, M., Ph. Balcou, M. Yu. Ivanov, A. L'Huillier, and P. B. Corkum, 1994, Phys. Rev. A **49**, 2117.
L'Huillier, A., and P. Balcou, 1993, Phys. Rev. Lett. **70**, 774.
L'Huillier, A., P. Balcou, S. Candel, K. J. Schafer, and K. C. Kulander, 1992, Phys. Rev. A **46**, 2778.
L'Huillier, A., X. F. Li, and L. A. Lompré, 1990, J. Opt. Soc. Am. B **7**, 527.
L'Huillier, A., L.-A. Lompré, G. Mainfray, and C. Manus, 1992, in *Atoms in Intense Laser Fields*, edited by M. Gavrila (Academic, New York), p. 139.
L'Huillier, A., K. J. Schafer, and K. C. Kulander, 1991, Phys. Rev. Lett. **66**, 2200.
Li, X. F., A. L'Huillier, M. Ferray, L. A. Lompré, and G. Mainfray, 1989, Phys. Rev. A **39**, 5751.
Liang, Y., S. August, S. L. Chin, Y. Beaudoin, and M. Chaker, 1994, J. Phys. B **27**, 5119.
Libertun, A. R., R. Shelton, H. C. Kapteyn, and M. Murnane, 1999, in *Conference on Lasers and Electro-Optics*, OSA Technical Digest (Optical Society of America, Washington, DC), p. 469.
Lin, K.-H., Y. Lai, and W.-F. Hsieh, 1995, J. Opt. Soc. Am. B **12**, 468.
Long, S., W. Becker, and J. K. McIver, 1995, Phys. Rev. A **52**, 2262.
Macklin, J. J., J. D. Kmetec, and C. L. Gordon III, 1993, Phys. Rev. Lett. **70**, 766.

Maier, M., W. Kaiser, and J. A. Giordmaine, 1966, Phys. Rev. Lett. **17**, 1275.
Maine, P., D. Strickland, P. Bado, M. Pessot, and G. Mourou, 1988, IEEE J. Quantum Electron. **24**, 398.
Marburger, J. H., 1975, Prog. Quantum Electron. **4**, 35.
Marcatili, E. A. J., and R. A. Schmeltzer, 1964, Bell Syst. Tech. J. **43**, 1783.
Mark, J., L. Y. Liu, K. L. Hall, H. A. Haus, and E. P. Ippen, 1989, Opt. Lett. **14**, 48.
Martin, J.-L. A. Migus, G. A. Mourou, and A. H. Zewail, 1993, Eds., *Ultrafast Phenomena VIII* (Springer, Berlin).
Martinez, O. E., 1987, IEEE J. Quantum Electron. **23**, 1385.
Martinez, O. E., R. L. Fork, and J. P. Gordon, 1984b, Opt. Lett. **9**, 156.
Martinez, O. E., R. L. Fork, and J. P. Gordon, 1985, J. Opt. Soc. Am. B **2**, 753.
Martinez, O. E., J. P. Gordon, and R. L. Fork, 1984, J. Opt. Soc. Am. A **1**, 1003.
Matuschek, N., F. X. Kärtner, and U. Keller, 1998, IEEE J. Sel. Top. Quantum Electron. **4**, 414.
McPherson, A., G. Gibson, H. Jara, U. Johann, T. S. Luk, I. A. McIntyre, K. Boyer, and C. K. Rhodes, 1987, J. Opt. Soc. Am. B **4**, 595.
Milchberg, H. M., C. G. Durfee III, and T. J. McIlrath, 1995, Phys. Rev. Lett. **75**, 2494.
Milosevic, D. B., and A. F. Starace, 1998, Phys. Rev. Lett. **81**, 5097.
Milosevic, D. B., and A. F. Starace, 1999, Phys. Rev. A **60**, 3943.
Milosevic, N., G. Tempea, and T. Brabec, 1999, "Optical pulse compression: bulk media versus hollow waveguides," in press.
Mitschke, F. M., and L. F. Mollenauer, 1986, IEEE J. Quantum Electron. **22**, 2242.
Mitschke, F. M., and L. F. Mollenauer, 1987, Opt. Lett. **12**, 407.
Mocker, H. W., and R. J. Collins, 1965, Appl. Phys. Lett. **7**, 270.
Modena, A., Z. Najmudin, A. E. Dangor, C. E. Clayton, K. A. Marsh, C. Joshi, V. Malka, C. B. Darrow, C. Danson, D. Neely, and F. N. Walsh, 1995, Nature (London) **377**, 606.
Moiseyev, N., and F. Weinhold, 1997, Phys. Rev. Lett. **78**, 2100.
Mollenauer, L. F., and R. H. Stolen, 1984, Opt. Lett. **9**, 13.
Morgner, U., F. X. Kärtner, S. H. Cho, Y. Chen, H. A. Haus, J. G. Fujimoto, E. P. Ippen, V. Scheuer, G. Angelow, and T. Tschudi, 1999, Opt. Lett. **24**, 411.
Morin, M., and M. Piché, 1990, Opt. Lett. **14**, 1119.
Mossavi, K., Th. Hoffmann, F. K. Tittel, and G. Szabó, 1993, Appl. Phys. Lett. **62**, 1203.
Moulton, P. F., 1982, Opt. News **8**, 9.
Moulton, P. F., 1986, J. Opt. Soc. Am. B **3**, 125.
Mourou, G., 1997, Appl. Phys. B: Lasers Opt. **65**, 205.
Muller, H. G., P. Agostini, and G. Petite, 1992, in *Atoms in Intense Laser Fields*, edited by M. Gavrila (Academic, San Diego), p. 1.
Murnane, M., and H. C. Kapteyn, 1999, private communication.
Myazaki, K., and H. Takada, 1995, Phys. Rev. A **52**, 3007.
Nabekawa, Y., Y. Kuramoto, T. Togashi, T. Sekikawa, and S. Watanabe, 1998, Opt. Lett. **23**, 1384.
Nees, J., S. Biswal, F. Druon, J. Faure, M. Nantel, G. A. Mourou, A. Nishimura, H. Takuma, J. Itatani, J.-C. Chanteloup, and C. Hönninger, 1998, IEEE J. Sel. Top. Quantum Electron. **4**, 376.
New, G. H. C., 1972, Opt. Commun. **6**, 188.
New, G. H. C., 1974, IEEE J. Quantum Electron. **10**, 115.
Nibbering, E. T., P. F. Curley, G. Grillon, B. S. Prade, M. A. Franco, F. Salin, and A. Mysyrowicz, 1996, Opt. Lett. **21**, 62.
Nibbering, E. T., J. O. Duhr, and G. Korn, 1997, Opt. Lett. **22**, 1355.
Nisoli, M., S. De Silvestri, and O. Svelto, 1996, Appl. Phys. Lett. **68**, 2793.
Nisoli, M., S. De Silvestri, O. Svelto, R. Szipöcs, K. Ferencz, Ch. Spielmann, S. Sartania, and F. Krausz, 1997, Opt. Lett. **22**, 522.
Nisoli, M., S. Stagira, S. De Silvestri, O. Svelto, S. Sartania, Z. Cheng, M. Lenzner, Ch. Spielmann, and F. Krausz, 1997, Appl. Phys. B: Lasers Opt. **65**, 175.
Nisoli, M., S. Stagira, S. De Silvestri, O. Svelto, S. Sartania, Z. Cheng, G. Tempea, Ch. Spielmann, and F. Krausz, 1998, IEEE J. Sel. Top. Quantum Electron. **4**, 414.
Nuss, M. C., R. Leonhart, and W. Zinth, 1985, Opt. Lett. **10**, 16.
Oppenheimer, J. R., 1928, Phys. Rev. **13**, 66.
Osterink, L. M., and J. D. Foster, 1968, J. Appl. Phys. **39**, 4163.
Ouellette, F., and M. Piché, 1986, Opt. Commun. **60**, 99.
Patterson, F., J. Bonlie, D. Price, B. White, and P. Springer, 1999, in *Conference on Lasers and Electro-Optics*, OSA Technical Digest (Optical Society of America, Washington, DC) Post-Deadline Paper CPD6.
Patterson, F. G., and M. D. Perry, 1991, J. Opt. Soc. Am. B **8**, 2384.
Peatross, J., S. Voronov, and I. Prokopovich, 1997, Opt. Express **1**, 114.
Perelomov, A. M., V. S. Popov, and M. V. Terent'ev, 1966, Zh. Eksp. Teor. Fiz. [Sov. Phys. JETP **23**, 924 1966].
Perry, M. D., and J. K. Crane, 1993, Phys. Rev. A **48**, R4051.
Perry, M. D., and G. Mourou, 1994, Science **264**, 917.
Perry, M. D., D. Pennington, B. C. Stuart, G. Tietbohl, J. A. Britten, C. Brown, S. Herman, B. Golick, M. Kartz, J. Miller, H. T. Powell, M. Vergino, and V. Yanovski, 1999, Opt. Lett. **24**, 160.
Peterson, O. G., S. A. Tuccio, and B. B. Snavely, 1970, Appl. Phys. Lett. **17**, 245.
Petricevic, V., S. K. Gayen, and R. R. Alfano, 1989, Opt. Lett. **14**, 612.
Piché, M., 1991, Opt. Commun. **86**, 156.
Pont, M., and M. Gavrila, 1990, Phys. Rev. Lett. **65**, 2362.
Poppe, A., A. Fürbach, Ch. Spielmann, and F. Krausz, 1999, "Electronic on the time scale of the light oscillation period?" in *Ultrafast Electronics and Optoelectronics*, Trends in Optics and Photonics No. 28, edited by John E. Bowers and Wayne H. Knox (Optical Society of America, Washington, D.C.), p. 31.
Poppe, A., M. Lenzner, F. Krausz, and Ch. Spielmann, 1999, "A sub-10fs 2.5-MW Ti:sapphire oscillator," *Technical Digest of the Ultrafast Optics Conference*, to be published.
Poppe, A., L. Xu, F. Krausz, and Ch. Spielmann, 1998, IEEE J. Sel. Top. Quantum Electron. **4**, 179.
Potvliege, R. M., and R. Shakeshaft, 1989, Phys. Rev. A **40**, 3061.
Potvliege, R. M., and R. Shakeshaft, 1992, in *Atoms in Intense Laser Fields*, edited by M. Gavrila (Academic, San Diego), p. 373.
Proctor, B., and F. Wise, 1993, Appl. Phys. Lett. **62**, 470.

Pshenichnikov, M. S., A. Baltuska, R. Szipöcs, and D. A. Wiersma, 1998, in *Ultrafast Phenomena XI*, edited by T. Elsässer, J. G. Fujimoto, D. A. Wiersma, and W. Zinth (Springer, Berlin), p. 3.
Pshenichnikov, M. S., W. P. de Boeij, and D. A. Wiersma, 1994, Opt. Lett. **19**, 572.
Pukhov, A., and J. Meyer-ter-Vehn, 1996, Phys. Rev. Lett. **76**, 3975.
Rae, S. C., K. Burnett, and J. Cooper, 1994, Phys. Rev. A **50**, 3438.
Ramaswamy, M., M. Ulman, J. Paye, and J. G. Fujimoto, 1993, Opt. Lett. **18**, 1822.
Ranka, J. K., and A. L. Gaeta, 1998, Opt. Lett. **23**, 534.
Reichert, J., R. Holzwarth, Th. Udem, and T. W. Hänsch, 1999, ''Measuring the frequency of light with mode-locked lasers,'' Opt. Commun. (in press).
Reiss, H. R., 1980, Phys. Rev. A **22**, 1786.
Reiss, H. R., 1992, Prog. Quantum Electron. **16**, 1.
Richardson, D. J., R. I. Laming, D. N. Payne, V. Matsas, and M. W. Phillips, 1991, Electron. Lett. **27**, 542.
Rischel, Ch., A. Rousse, I. Uschmann, P. A. Albouy, J. P. Geindre, P. Audebert, J. C. Gauthier, E. Förster, J. L. Martin, and A. Antonetti, 1997, Nature (London) **390**, 490.
Rizvi, N. H., P. M. W. French, J. R. Taylor, P. J. Delfyett, and L. T. Florez, 1993, Opt. Lett. **18**, 983.
Rolland, C., and P. B. Corkum, 1988, J. Opt. Soc. Am. B **5**, 641.
Rosen, C., M. Dörr, U. Eichmann, and W. Sandner, 1999, Phys. Rev. Lett. **83**, 4514.
Rouyer, C., E. Mazataud, I. Allais, A. Pierre, S. Seznec, C. Sauteret, G. Mourou, and A. Migus, 1993, Opt. Lett. **18**, 214.
Ruddock, I. S., and D. J. Bradley, 1976, Appl. Phys. Lett. **29**, 296.
Rundquist, A., C. G. Durfee III, Z. Cheng, C. Herne, S. Backus, M. M. Murnane, and H. C. Kapteyn, 1998, Science **280**, 1412.
Sala, K., M. C. Richardson, and N. R. Isenor, 1977, IEEE J. Quantum Electron. **13**, 915.
Salières, P., A. l'Huillier, P. Antoine, and M. Lewenstein, 1999, Adv. At., Mol., Opt. Phys. **41**, 83.
Salières, P., P. Antoine, A. de Bohan, and M. Lewenstein, 1998, Phys. Rev. Lett. **81**, 5544.
Salières, P., A. L'Huillier, and M. Lewenstein, 1995, Phys. Rev. Lett. **74**, 3776.
Salin, F., P. Grangier, P. Georges, and A. Brun, 1990, Opt. Lett. **15**, 1374.
Salin, F., J. Squier, and M. Piché, 1991, Opt. Lett. **16**, 1674.
Sanpera, A., P. Jönsson, J. B. Watson, and K. Burnett, 1995, Phys. Rev. A **51**, 3148.
Sarachick, E., and G. Schappert, 1970, Phys. Rev. D **1**, 2738.
Sartania, S., Z. Cheng, M. Lenzner, G. Tempea, Ch. Spielmann, F. Krausz, and K. Ferencz, 1997, Opt. Lett. **22**, 1562.
Sarukura, N., K. Hata, T. Adachi, R. Nodomi, M. Watanabe, and S. Watanabe, 1991, Phys. Rev. A **43**, 1669.
Sauteret, C., D. Husson, G. Thiell, S. Seznec, G. Gray, A. Migus, and G. Mourou, 1991, Opt. Lett. **16**, 238.
Schäfer, F. P., F. P. W. Schmidt, and J. Volze, 1966, Appl. Phys. Lett. **9**, 306.
Schafer, K. J., and K. C. Kulander, 1997, Phys. Rev. Lett. **78**, 638.
Schins, J. M., P. Breger, P. Agostini, R. C. Constantinescu, H. G. Muller, A. Bouhal, G. Grillon, A. Antonetti, and A. Mysyrowicz, 1996, J. Opt. Soc. Am. B **13**, 197.
Schnürer, M., Z. Cheng, M. Hentschel, F. Krausz, T. Wilhein, D. Hambach, G. Schmahl, M. Drescher, Y. Lim, U. Heinzmann, 1999a, ''Few-cycle-drìven XUV harmonics: generation and focusing,'' Appl. Phys. B. (in press).
Schnürer, M., Z. Cheng, M. Hentschel, G. Tempea, P. Kalman, T. Brabec, and F. Krausz, 1999b, Phys. Rev. Lett. **83**, 722.
Schnürer, M., Ch. Spielmann, P. Wobrauschek, C. Streli, N. H. Burnett, C. Kan, K. Ferencz, R. Koppitsch, Z. Cheng, T. Brabec, and F. Krausz, 1998, Phys. Rev. Lett. **80**, 3236.
Schnürer, M., C. Streli, P. Wobrauschek, M. Hentschel, R. Kienberger, Ch. Spielmann, and F. Krausz, 1999, ''Femtosecond X-ray fluorescence,'' submitted for publication.
Schoenlein, R. W., W. P. Leemans, A. H. Chin, P. Volfbeyn, T. E. Glover, P. Balling, M. Zolotorev, K.-J. Kim, S. Chattopadhay, and C. V. Shank, 1996, Science **274**, 236.
Scrinzi, A., M. Geissler, and T. Brabec, 1999, Phys. Rev. Lett. **83**, 706.
Seidemann, T., M. Yu. Ivanov, and P. B. Corkum, 1995, Phys. Rev. Lett. **75**, 2819.
Shakeshaft, R., R. M. Potvliege, M. Dörr, and W. E. Cooke, 1990, Phys. Rev. A **42**, 1656.
Sheik-Bahae, M., A. A. Said, D. J. Hagan, M. J. Soileau, and W. W. Stryland, 1984, Opt. Eng. (Bellingham) **30**, 1228.
Shank, C. V., 1988, in *Ulrashort Laser Pulses and Applications*, Topics in Applied Physics No. 60, edited by W. Kaiser (Springer, New York), p. 5.
Shen, Y. R., 1984, *The Principles of Nonlinear Optics* (Wiley, New York).
Shimizu, F., 1967, Phys. Rev. Lett. **19**, 1097.
Shirakawa, A., I. Sakane, M. Takasaka, and T. Kobayashi, 1999, Appl. Phys. Lett. **74**, 2268.
Shkolnikov, P. L., A. E. Kaplan, and A. Lago, 1996, J. Opt. Soc. Am. B **13**, 412.
Shvartsburg, A. B., 1996, *Time-Domain Optics of Ultrashort Waveforms* (Clarendon, Oxford).
Sizer, T. II, J. D. Kafka, I. N. Duling III, C. W. Gabel, and G. A. Mourou, 1983, IEEE J. Quantum Electron. **19**, 506.
Smith, L. K., S. A. Payne, W. L. Kway, L. L. Chase, and B. H. T. Chai, 1992, IEEE J. Quantum Electron. **28**, 2612.
Smith, P. W., M. A. Duguay, and E. P. Ippen, 1974, Prog. Quantum Electron. **3**, 109.
Sommerfeld, A., 1967, *Elektronentheorie der Metalle* (Springer, Berlin), p. 109.
Sorokin, P. P., and J. R. Lankard, 1966, IBM J. Res. Dev. **10**, 162.
Spence, D. E., P. N. Kean, and W. Sibbett, 1991, Opt. Lett. **16**, 42.
Spielmann, Ch., N. H. Burnett, S. Sartania, R. Koppitsch, M. Schnürer, C. Kan, M. Lenzner, P. Wobrauschek, and F. Krausz, 1997, Science **278**, 661.
Spielmann, Ch., P. F. Curley, T. Brabec, and F. Krausz, 1994, IEEE J. Quantum Electron. **30**, 1100.
Spielmann, Ch., C. Kan, N. H. Burnett, T. Brabec, M. Geissler, A. Scrinzi, M. Schnürer, and F. Krausz, 1998, IEEE J. Sel. Top Quantum Electron. **4**, 249.
Spinelli, L., B. Couillaud, N. Goldblatt, and D. K. Negus, 1991, in *Conference on Lasers and Electro-Optics* (Optical Society of America, Washington, D.C.), Paper CPDP7.
Stankov, K. A., and J. Jethwa, 1988, Opt. Commun. **66**, 41.
Stingl, A., M. Lenzner, Ch. Spielmann, F. Krausz, and R. Szipöcs, 1995, Opt. Lett. **20**, 602.
Stix, M. S., and E. P. Ippen, 1983, IEEE J. Quantum Electron. **19**, 520.

Strickland, D., and G. Mourou, 1985, Opt. Commun. **56**, 219.
Stuart, B. C., M. D. Feit, A. M. Rubenchik, B. W. Shore, and M. D. Perry, 1995, Phys. Rev. Lett. **74**, 2248.
Sullivan, A., H. Hamster, H. C. Kapteyn, S. Gordon, W. White, H. Nathel, R. J. Blair, and R. W. Falcone, 1991, Opt. Lett. **16**, 1406.
Sutter, D. H., G. Steinmeyer, L. Gallmann, N. Matuschek, F. Morier-Genoud, U. Keller, V. Scheuer, G. Angelow, and T. Tschudi, 1999, Opt. Lett. **24**, 631.
Szatmári, S., 1994, Appl. Phys. B: Lasers Opt. **58**, 211.
Szatmári, S., B. Rácz, and F. P. Schäfer, 1987, Opt. Commun. **62**, 271.
Szipöcs, R., K. Ferencz, Ch. Spielmann, and F. Krausz, 1994, Opt. Lett. **19**, 201.
Szipöcs, R., A. Stingl, Ch. Spielmann, and F. Krausz, 1995, Opt. Photonics News **6**, 16.
Tamura, K., J. Jacobson, E. P. Ippen, H. A. Haus, and J. G. Fujimoto, 1993, Opt. Lett. **18**, 220.
Taylor, A. J., T. R. Gosnell, and J. P. Roberts, 1990, Opt. Lett. **15**, 39.
Telle, H. R., G. Steinmeyer, A. E. Dunlop, J. Stenger, D. H. Sutter, and U. Keller, 1999, Appl. Phys. B: Lasers Opt. **69**, 327.
Tempea, G., and T. Brabec, 1998a, Opt. Lett. **23**, 762.
Tempea, G., and T. Brabec, 1998b, Opt. Lett. **23**, 1286.
Tempea, G., M. Geissler, and T. Brabec, 1999a, J. Opt. Soc. Am. B **16**, 669.
Tempea, G., M. Geissler, and T. Brabec, 1999b, "Self-phase-matched high harmonic generation," Phys. Rev. Lett., in press.
Tempea, G., F. Krausz, Ch. Spielmann, and K. Ferencz, 1998, IEEE J. Sel. Top. Quantum Electron. **4**, 193.
Theobald, W., R. Häßner, C. Wülker, and R. Sauerbrey, 1996, Phys. Rev. Lett. **77**, 298.
Tien, A. C., S. Backus, H. Kapteyn, and M. Murnane, 1999, Phys. Rev. Lett. **82**, 3883.
Tisch, J. W. G., R. A. Smith, J. E. Muffett, M. Ciarrocca, J. P. Marangos, and M. H. R. Hutchinson, 1994, Phys. Rev. A **49**, R28.
Tomlinson, W. J., R. H. Stolen, and C. V. Shank, 1984, J. Opt. Soc. Am. B **1**, 139.
Toth, Cs., G. Farkas, and K. L. Vodopyanov, 1991, Appl. Phys. B: Photophys. Laser Chem. **53**, 221.
Treacy, E. B., 1969, Phys. Lett. **28A**, 34.
Trebino, R., K. W. DeLong, D. N. Fittinghoff, J. N. Sweetser, M. A. Krumbügel, B. A. Richman, and D. J. Kane, 1997, Rev. Sci. Instrum. **68**, 3277.
Tsuda, S., W. H. Knox, S. T. Cundiff, W. Y. Jan, and J. E. Cunningham, 1996, IEEE J. Sel. Top. Quantum Electron. **2**, 435.
Tsuda, S., W. H. Knox, E. A. de Souza, W. Y. Jan, and J. E. Cunningham, 1995, Opt. Lett. **20**, 1406.
Udem, Th., J. Reichert, R. Holzwarth, and T. W. Hänsch, 1999a, Phys. Rev. Lett. **82**, 3568.
Udem, Th., J. Reichert, R. Holzwarth, and T. W. Hänsch, 1999b, Opt. Lett. **24**, 881.
Umstadter, D., S.-Y. Chen, A. Maksimchuk, G. Mourou, and R. Wagner, 1996, Science **273**, 472.
Valdmanis, J. A., and R. L. Fork, 1986, IEEE J. Quantum Electron. **22**, 112.
Valdmanis, J. A., R. L. Fork, and J. P. Gordon, 1985, Opt. Lett. **10**, 131.
Wahlström, C. G., J. Larsson, A. Persson, T. Starczewski, S. Svanberg, P. Salières, Ph. Balcou, and A. L'Huillier, 1993, Phys. Rev. A **48**, 4709.
Walker, B., B. Sheehy, L. F. DiMauro, P. Agostini, K. J. Schafer, and K. C. Kulander, 1994, Phys. Rev. Lett. **73**, 1227.
Walmsley, I., and V. Wong, 1996, J. Opt. Soc. Am. B **13**, 2453.
Watanabe, S., A. Endoh, M. Watanabe, and N. Sakura, 1988, Opt. Lett. **13**, 580.
Weber, H. P., 1967, J. Appl. Phys. **38**, 2231.
Weihe, F. A., S. K. Dutta, G. Korn, D. Du, P. H. Bucksbaum, and P. L. Shkolnikov, 1995, Phys. Rev. A **51**, R3433.
Wood, Wm. M., C. W. Siders, and M. C. Downer, 1991, Phys. Rev. Lett. **67**, 3523.
Wöste, L., C. Wedekind, H. Wille, P. Rairoux, B. Stein, S. Nikolov, C. Werner, S. Niedermeier, F. Ronneberger, H. Schillinger, and R. Sauerbrey, 1997, *Laser Optoelektron.* **29**, 51 (October issue).
Xu, H., X. Tang, and P. Lambropoulos, 1992, Phys. Rev. A **46**, R2225.
Xu, L., Ch. Spielmann, A. Poppe, T. Brabec, F. Krausz, and T. Hánsch, 1996, Opt. Lett. **21**, 2008.
Xu, L., G. Tempea, A. Poppe, M. Lenzner, Ch. Spielmann, F. Krausz, A. Stingl, and K. Ferencz, 1997, Appl. Phys. B: Lasers Opt. **65**, 151.
Xu, L., G. Tempea, Ch. Spielmann, F. Krausz, A. Stingl, K. Ferencz, and S. Takano, 1998, Opt. Lett. **23**, 789.
Yamakawa, K., H. Siraga, Y. Kato, and C. P. J. Barty, 1991, Opt. Lett. **16**, 1593.
Yamakawa, K., M. Aoyama, S. Matsuoka, H. Takuma, C. P. J. Barty, and D. Fittinghoff, 1998a, Opt. Lett. **23**, 525.
Yamakawa, K., M. Aoyama, S. Matsuoka, T. Kase, Y. Akahane, H. Takuma, D. Fittinghoff, and C. P. J. Barty, 1998b, in *Ultrafast Phenomena XI*, edited by T. Elsässer, J. G. Fujimoto, D. A. Wiersma, and W. Zinth (Springer, Berlin), p. 44.
Yariv, A., 1965, J. Appl. Phys. **36**, 388.
Yariv, A., and P. Yeh, 1984, *Optical Waves in Crystals* (Academic, New York).
Yoshikawa, S. and T. Imasaka, 1993, Opt. Commun. **96**, 94.
Zakharov, V. E., and A. B. Shabat, 1972, Zh. Eksp. Teor. Fiz. [Sov. Phys. JETP **34**, 62 (1972)].
Zhang, X.-C., B. H. Kolner, and K. Leo, 1996, Eds., *Ultrafast Electronics, Photonics, and Optoelectronics*, IEEE J. Sel. Top. Quantum Electron. **2**, p. 433.
Zhou, J. P., C. P. Huang, M. M. Murnane, and H. C. Kapteyn, 1995, Opt. Lett. **20**, 64.
Zhou, J., J. Peatross, M. M. Murnane, H. C. Kapteyn, and I. P. Christov, 1996, Phys. Rev. Lett. **76**, 752.
Zhou, J., G. Taft, C. P. Huang, M. M. Murnane, H. C. Kapteyn, and I. Christov, 1994, Opt. Lett. **19**, 1149.
Ziolkowski, R. W., and J. B. Judkins, 1993, J. Opt. Soc. Am. B **10**, 186.
Zozulya, A. A., S. A. Diddams, A. G. Van Engen, and T. S. Clement, 1999, Phys. Rev. Lett. **82**, 1430.
Zuo, T., A. D. Bandrauk, M. Ivanov, and P. B. Corkum, 1995, Phys. Rev. A **51**, 3991.